CARDIFF UNIVERSITY
SCHOOL OF ENGINEERING

Development of Convection in High-Temperature Coil Annealing Furnaces Using Rotating Cylinders Technique

By
Oula M. Hadawi Fatla

A Thesis Submitted To Cardiff University
For The Degree of Doctor of Philosophy
In Mechanical Engineering

May 2019

DECLARATION

This work has not been submitted in substance for any other degree or award at this or any other university or place of learning, nor is being submitted concurrently in candidature for any degree or other award.

Signed ……  …… (Oula Fatla) Date 10/07/2019

STATEMENT 1

This thesis is being submitted in partial fulfilment of the requirements for the degree of PhD

Signed ……  …… (Oula Fatla) Date 10/07/2019

STATEMENT 2

This thesis is the result of my own independent work/investigation, except where otherwise stated, and the thesis has not been edited by a third party beyond what is permitted by Cardiff University's Policy on the Use of Third Party Editors by Research Degree Students. Other sources are acknowledged by explicit references. The views expressed are my own.

Signed ……  …… (Oula Fatla) Date 10/07/2019

STATEMENT 3

I hereby give consent for my thesis, if accepted, to be available online in the University's Open Access repository and for inter-library loan, and for the title and summary to be made available to outside organisations.

Signed ……  …… (Oula Fatla) Date 10/07/2019

ACKNOWLEDGEMENTS

I would like to express my very great appreciation to my supervisors ***Prof Phil Bowen*** *and* ***Dr Agustin Valera-Medina*** *for their excellent guidance and continuous support throughout my PhD study. Their guidance helped me in all the time of research and writing of this thesis.*

I would like to thank Cogent Power Ltd and in particular ***Dr Fiona Robinson*** *for answering all my questions and her assistance in keeping my progress on schedule. I also would like to thank* ***Dr Nathan Beynon*** *for his assistance and guidance during the data collection in Chapter 4.*

I would like to take the opportunity to thank ***Dr Allan Mason-Jones*** *for his help and guidance during the numerical work in this thesis.*

My great thanks also extended to all my friends and colleagues in Cardiff especially those who helped and inspired me, ***Zayneb****,* ***Nadia, Sally, Hua****,* ***Fares, Osama Al-Hussaini, Hesham and Irving****. Their advice and good spirits have greatly helped me.*

I would like to extend my thanks to the ***Iraqi Government*** *for sponsoring my PhD study, and many thanks to the staff of the* ***Iraqi Cultural Attaché in London*** *for their help during my stay in the UK.*

I would like to show my deepest appreciation to ***Al- Qadisiya University*** *for awarding me the scholarship. I am particularly grateful to* ***Dr Baqer Gurji Al-Joubory, Dr Abbas Alwi Al-Jeebori, Dr Batol Al- Joubory, Dr Abdulazem A. Kaddum, Mr Abbas A. Lafta*** *and* ***Mr Salam Alawi,*** *for their help and support.*

My final thanks go to my ***parents****,* ***brothers,*** *and* ***sister*** *for their constant love and support throughout my life.*

ABSTRACT

The formation of hotspots in HTCA furnaces presents significant engineering challenges. The problem occurs due to lack of fluid recirculation to distribute the heat inside the furnace uniformly. The problem exaggerates when the hotspots cause electrical failure in the heating elements leading to a long process duration and high energy consumption to compensate the thermal deficiency. Therefore, it is important to investigate opportunities for improving fluid mixing in the HTCA furnace to eliminate the formation of hotspots.

The main objective of this thesis is to investigate generating fluid flow inside the HTCA furnace. With generating fluid recirculation, the advantages are twofold: it enhances fluid mixing and promotes convection. In this study, a rotating cylinders technique was proposed to generate the fluid recirculation inside the furnace during the annealing process of the grain-oriented electrical steel. The thesis begins with a survey of the energy consumption in the HTCA furnace to set the energy benchmarks. The survey revealed that an annealing process with electrical failure consumed about 8000 kWh extra higher than that of a standard annealing process.

The thesis also presents an experimental investigation which was designed to test the validity of the proposed technique on controlling the flow around it when it is placed in a cross flow. The results confirmed that the technique is quite capable of generating flow instabilities around them.

A numerical investigation was conducted to simulate the rotating cylinder during the annealing cycle. Six different cylinder arrangements were tested to select the configuration that can offer the best fluid recirculation inside the furnace. Four different rotational rates were used 100, 150, 200, and 250 rad/sec. The results show that a turbulent flow can be generated due to cylinder rotation and its intensity proportional to the cylinder's rotational rate.

The optimal cylinder layout was then tested using a transient model created for this process to examine the effect of the proposed technique on the cycle duration. It was

found that the optimal cylinder configuration can save the process at least one hour of the heating-up segment.

PUBLICATIONS

[1] Oula M. H. Fatla, Agustin Valera-Medina, Fiona Robinson, Mark Cichuta, Nathan Beynon, 2018. Development of convection in high-temperature coil annealing furnaces using rotating cylinder technique. Applied Thermal Engineering, 129, 1392-1402, ISNB 1359-4311.

[2] Ghassan. F. Smaism, O. M. H. Fatla, A. Valera-Medina, A.M. Rageb, N. Syred, 2016. Investigation of heat transfer and fluid mechanics across a heated rotating circular cylinder in crossflow. 54th American Institute Aeronautics and Astronautics (AIAA), Aerospace Science Meeting, 2016-0494.

[3] Oula M. H. Fatla, Ghassan F. Smaisim, Agustin Valera-Medina, A.M. Rageb, N. Syred, 2015. Experimental and numerical investigation of heat transfer and fluid mechanics across a rotating circular cylinder dissipating uniform heat flux by cross flow. 10th Pacific Symposium on Flow Visualisation and Image Processing, Naples, Italy, 15-18 June.

[4] Ghassan. F. Smaism, Oula M. H. Fatla, A. Valera-Medina, A.M. Rageb, N. Syred, 2016 Experimental and theoretical investigation of the effect of rotating circular cylinder speed on the lift and drag forces. International Journal of Energy and Environment, 7, 23-36.

TABLE OF CONTENTS

LIST OF FIGURES

LIST OF TABLES

NOMENCLATURE

Alphabetic Symbols

B_g	In plane magnetic flux flow through the gap	Tesla
B_{sat}	Saturation induction of the material	Tesla
Re	Reynolds number	[-]
U_o	Flow mean velocity	[m/s]
Q	Heat transfer rate	[watt]
q'_x	Heat flux	[w/m^2]
k	Thermal conductivity	[w/m. k]
h	Convection heat transfer coefficient	[w/(m^2.k)]
A	Surface area	[m^2]
T	Temperature	[k]
Nu_L	Nusselt number over plate length (L)	[-]
D	Cylinder diameter	[m]
U_∞	Incoming free stream velocity	[m/s]
H	Height	[m]
L	Length	[m]
f_D	Doppler frequency	[Hz]
d $_{fringe}$	Distance between the fringes	[nm]
u	Velocity component on x direction	[m/s]
v	Velocity component on y direction	[m/s]
w	Velocity component on z direction	[m/s]
t	Time	[s]
p	Pressure	[N/m^2]
E	Energy	Joule
R^2	Correlation coefficient	[-]
m	Mass	Kg
C_p	Specific heat capacity	[J/kg. k]
Q_l	Electrical power	[watt. h]
P	Active power	[watt]
V	Resultant velocity	[m/s]
St	Strouhal number	[-]
f	Vortex frequency	[Hz]
x_i	Mass fraction	[%]

Greek symbols

ρ	Fluid density	[kg/m^3]
δ	Characteristic length	[m]
μ	Fluid dynamic viscosity	[(N.s)/m^2]
σ	Stefan-Boltzman constant	W/(m^2 K^4)
ε	Surface emissivity	[-]
κ	Kinetic energy of turbulence	[m^2/s^2]
ϵ	Rate of dissipation of turbulent kinetic energy	[m^2/s^3]
ω	Specific rate of dissipation of turbulent kinetic energy	[1/s]
Ω	Angular velocity	[rpm]
α	Non-dimensional ratio	[-]
ν	Kinematic viscosity	[m^2/s]
τ	The viscous stress	[N/m2]
λ	Volumetric deformation	[-]
ϕ	Gas property	[-]

Acronyms

GOES	Grain-Oriented Electrical Steel
CGO	Convectional Grain-Oriented
HGO	High-permeability Grain-Oriented
HTCA	High-Temperature Coil Annealing
Hi-B	High permeability
MnS	Manganese Sulphide
MgO	Magnesium Oxide
NHx	Nitrogen with 3% hydrogen and other rare gasses
LDV	Laser-Doppler Velocimetry
LDA	Laser Doppler Anemometry
CFD	Computational Fluid Dynamics
CV	Control Volume
FVM	Finite Volume Method
RANS	Reynolds-Averaged Navier–Stokes
RSM	Reynolds Stress Model
RMS	Root-Mean Square
FFT	Fast Fourier Transforms
LPF	Low-Pass Filter
IFFT	Inverse Fast Fourier Transforms
TI	Turbulence Intensity
H_2	Hydrogen
N_2	Nitrogen

CHAPTER 1:

INTRODUCTION

Chapter 1

Introduction

1.1 Electrical Steel

Electricity is indispensable to our modern life and is far superior to other energy sources with respect to convenience of use, cleanliness and safety. Since the demand for electric power is high, the improvement of efficiency of electrical equipment becomes very important. This includes transferring the electrical energy. The term *"electrical steel"* covers the soft ferromagnetic materials that form the cores of a large range of electrical machines. The performance of such machines depends largely upon the core materials used.

All electricity produced will pass, at some stage during transmission and distribution, through a transformer and about 5% of the energy will be lost in the form of heat [1]. Core losses in transformers comprises, basically, of hysteresis loss (Watt) and eddy current loss (W/kg), both depend upon magnetic properties of the material used to construct the core of the transformer and its design [2, 3]. So these losses are fixed and do not depend upon the load current [4].

Steel is a very good ferromagnetic material. This kind of material is very sensitive to being magnetised. This means, whenever magnetic flux would pass through, it will behave like a magnet. Ferromagnetic substances have numbers of domains in their structure. Domains are very small regions in the material structure, where all the dipoles are paralleled to the same direction. In other words, the domains are like small permanent magnets situated randomly in the structure of the substance. Because these domains are arranged inside the material structure in such a random manner, the net resultant magnetic field of the material is zero. Whenever an external magnetic field or magnetomotive force (mmf) is applied to the substance, these randomly directed domains begin to align themselves parallel to the axis of applied (mmf). After removing the external field, most domains return to random positions, but some of

them remain in their changed position. Because of these unchanged domains, the substance becomes slightly magnetised permanently [4].

In transformers, the core is magnetised under the influence of the Alternative Current (AC) condition. This alternating current produces alternating magnetising flux in the core. Because of the alternating flux, local electromagnetic fields (emf) would be induced in this part of the transformer. For every cycle due to this domain reversal, hysteresis loss, there will be extra work done and power losses occur, such losses known as the eddy current losses. Core loss in electrical equipment, especially in transformers, is undesirable as it represents a continuing economic loss to the user of the equipment. To minimise these energy losses, it is essential that the electrical steel is very efficient by using the appropriate core material.

Typically, the performance of such materials is measured by permeability, that is, the ability for the material to support the formation of a magnetic field within itself, and the low core loss. The core loss depends on the ease at which the material is magnetised and demagnetised. The more permeability the steel can have, the more efficient the transformer and the lower the core loss. The main factor affecting permeability is the closeness of orientation of the grains to the ideal texture [5, 6]. The core loss and permeability dictate the grade and hence the price of the fully finished product.

The grains in a non-processed steel, however, are normally randomly oriented. To achieve maximum permeability and saturation of magnetisation, it is desirable to produce steel whose individual crystals are all oriented in the same way.

The use of electrical or silicon steel replaced high quality wrought iron cores after the work of Robert Hadfield [4] in 1900, who found the addition of silicon could reduce magnetic losses by a factor of four. With the addition of silicon to the steel, the advantages are twofold: it increases the electrical resistivity, therefore reducing the core loss, and it improves the material's stability with age.

One of the important improvements made to the silicon steel was in the process of the cold rolling, grain-oriented. The production came about during the 1930's when N. P. Goss [7] combined metallurgical changes incurred during cold rolling and subsequent heat treatment to produce grain-oriented electrical steel with the easy magnetisation direction of the grains aligned predominantly in the rolling direction. The structure of such material is symmetrical with cubic crystals that are all arranged in the direction in which the steel plate has been rolled. This is called the Goss texture.
The superior magnetic properties of the grain-oriented electrical steel are closely related to the sharpness of the Goss texture, which develops due to a discontinuous or abnormal Goss grain growth during high-temperature heat treatment at the end of the process route [6]. The grain-oriented steel has anisotropic magnetic property to the rolling direction. Hence it is mainly used in static machinery which requires unidirectional magnetization such as transformers [8].

Non-oriented is another structure of electrical steel that the cubic crystals are randomly oriented. Non-oriented electrical steel has isotropic magnetic property in all direction and it is used in applications of rotating machineries which require multidirectional magnetization such as stator cores, generators, and alternators [9, 10].

1.2 Grain-Oriented Electrical Steel (GOES) Markets

In general, there are two basics types of grain oriented material that are commercially produced; these are conventional grain-oriented (CGO) and high permeability grain-oriented electrical steel (HGO). The HGO is more difficult to be produced than the CGO as the orientation of the grains is closer to the optimum direction. Table 1.1 show the magnetic properties of these two types of GO

The HGO has a more preferred grade because of lower core losses. Of the 16 global producers of GOES, only eight of these can currently manufacture HGO.

- North America – AK Steel and Allegheny
- Brazil- Aperam
- India- TKSE
- Russia-NLMK

- China- Wisco, Baosteel, Shougang, Anshan and Maanshan
- Korea- Posco
- Japan- NSSMC and JFE
- Europe- TKES, AMFM, Stalprodukt and Tata Cogent

In Cogent Power, part of Tata steels, at Newport, the production of silicon alloyed sheet flourished in the early years of the 20th century [11]. Nowadays it provides about 10% of the HGO production to the UK market. The rest is exported to other countries. The transformer market in the UK is relatively small because the transformers are imported as integrated units from other countries. As a result, there are very few transformer manufacturers in the UK, for instant some major companies are Melrose plc, Allam Marine Ltd and Cummins Generator Technologies Ltd [12].

Because of the high electricity prices, natural gas prices and various legislative costs in the UK, Cogent is finding it difficult to keep profit margins in a market where GOES can be bought from countries like China at very low prices. The plant has invested in new equipment in order to remain competitive. This, however, has come at the cost of a large number of people being made redundant. The only other alternative to buying new, expensive equipment such as new effective furnaces, while at the same time remain competitive in the market, is to invest in enhancing the HGO production processes. Table 1.1 shows some values of enhanced HGO in comparison with conventional electrical steel.

Table 1.1: Typical magnetic properties of CGO and HGO [13]

	CGO	**HGO**	
B_g	1.830	1.905	Tesla
$W_{17/50}$ *	1.25	1.02	W/Kg
B_{sat}	2.00	2.03	Tesla
Density	7650	7650	Kg/m^3
Thickness	0.3	0.3	mm
Resistivity	0.48	0.48	$\mu\Omega\,.m$

* Core loss at magnetic flux density, 1.7 Tesla, 50 Hz

1.3 Grain- Oriented Electrical Steel Production

The production of the GO steel consists of subjecting the steel sheet of hot-rolled silicon steel to a series of cold-rolling and annealing operations to set the sheet thickness to the commercial standards. The steel sheet with the desired thickness is subjected to decarburising annealing in a wet hydrogen atmosphere, followed by applying final high-temperature annealing at more than 1100 C for more than 10 hours to obtain the abnormal grain-growth in a process known as the "secondary recrystallisation".

The excellent electrical steel properties such as low core loss can be secured only by the appropriate level of secondary recrystallisation [14]. Steel sheets that are attaining the appropriate level of secondary recrystallization are characterised by higher magnetic flux density.

The development of the magnetic properties of the electrical steel is achieved during the high-temperature coil annealing process. It is a crucial stage in the GO production, which requires careful control of heating rates and gas composition. The high-temperature annealing process is performed after cold working to release final residual stresses in the steel strip due to thickness reduction and the changes in the crystalline structure of the metal [15].

During the high-temperature annealing process, the deformed microstructures of the cold rolled sheets are recovered, and recrystallisation takes place. Recrystallization improves strip mechanical properties because of grain size and shape, which are themselves affected by temperature, near or about the recrystallisation temperature, and the holding time at this temperature.

At Cogent, the annealing process of the HGO is carried out in electrical multi-stack furnaces Figure 1.16, where the steel coils are heat treated at ~1200 ^{o}C with an inert gas atmosphere to prevent oxidation of the steel strip.

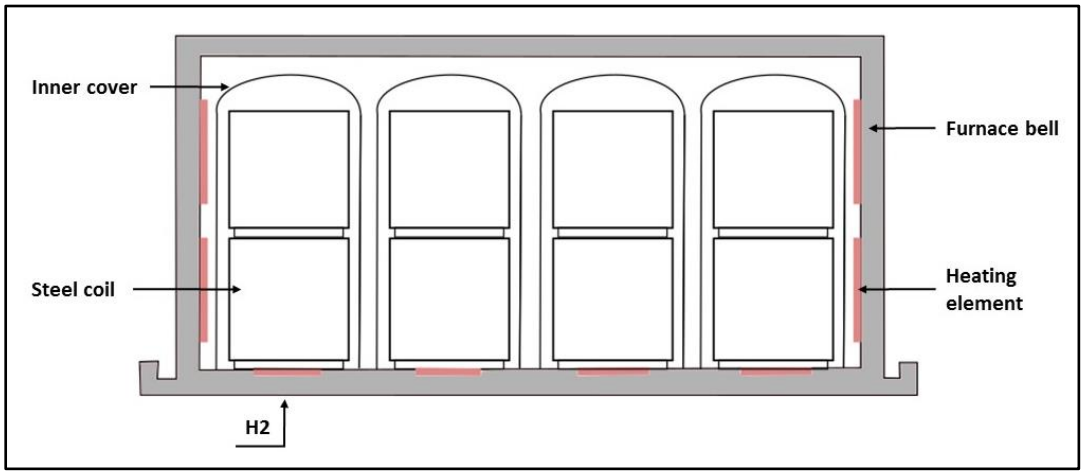

Figure 1.1: Schematic diagram of a section of multi-stack annealing furnace

Due to lack of convection and long operation conditions as well as the extreme high annealing temperature, the process becomes static, and some issues result:

- Thermal inefficiencies, due to the formation of hot spots and temperature differentials in areas of higher exposure ratio to the heating elements.
- Failure of equipment, particularly the deformations of covers.
- The issues exaggerate in the case of electrical element breakage as the remaining elements have to work harder to maintain the set-point, thus leading to parts of steel coils being over-heated while other parts suffer under-heating or have incorrect annealing time. Over-heating the coil affects the final product appearance as well as the total power consumption to complete the annealing treatment.

1.4 Aim and Objectives

The aim of the present study is to appraise a method to enhance the performance of the HTCA process. The focus of this research is on generating fluid recirculation inside the high-temperature coil annealing furnace during the annealing process of the electrical steel, in order to promote fluid mixing thus developing forced convection heat transfer during the process. This is by using rotating cylinder techniques to be inserted into the furnace to generate fluid flow within the furnace cavity. The validity of the technique will be tested numerically by a CFD approach using ANSYS Fluent software.

1.5 Thesis structure

Chapter 1, covers the current energy and environmental situation, with some closer look to the power situation in the UK. The conception of the electrical steel and its use is also presented. Manufacturing and marketing of the Grain-oriented electrical steel in the UK are stated.

Chapter 2, presents the fundamentals of vortex generators and particularly the rotating cylinder technique. It also presents a literature review on the production of the grain-oriented electrical steel.

Chapter 3, describes the experimental part of this thesis, the basic theories used, the CFD codes used, the processing analysis, basic equations and turbulence modelling.

Chapter 4, presents an energy analysis of the HTCA furnaces. The parameters that affect the energy consumption were investigated.

Chapter 5, investigates experimentally the effect of the rotating and non-rotating cylinder on a flow structure. Results of velocity profiles, turbulence intensity and Strouhal number are presented in this chapter.

Chapter 6, presents numerical investigation on using the rotating cylinder technique in HTCA furnace for flow generation.

Chapter 7, presents a transient model of the heating-up segment of the annealing process when using the rotating cylinders technique.

Chapter 8, presents general discussions of all the results in order to guide future works.

Chapter 9, provides some conclusions and suggestions for future work.

CHAPTER 2:

LITERATURE REVIEW

Chapter 2

Literature Review

2.1 Introduction

The literature review on the topics related to this research is presented in this chapter. A brief review of turbulence and its related phenomena, as well as the heat transfer mechanism, is given first. Subsequently, methods of enhancing heat transfer mechanism with emphasize on vortex generator techniques are presented in the following sections. The high-temperature annealing technology is also presented in this chapter.

2.2 Principles of Fluid Flow

The convection heat transfer rates strongly depend on the fluid boundary layer whether it is laminar or turbulent [16]. Therefore, to determine the heat transfer coefficient, the equations of motion of fluid must be combined with those of convective heat transfer.

In the laminar boundary layer, the fluid motion is classified to be predictable and ordered (i.e. not random or unstable) [17]. In contrast, fluid motion in turbulent boundary layers is irregular and characterised by velocity fluctuations. These fluctuations mix the fluid and enhance the transfers of energy. The fundamental assumption of the boundary layer approximation is the no-slip condition of the flow, at which fluid immediately adjacent to the boundary surface is at rest relative to the body, the physical mechanism responsible is viscosity [18]. As a brief explanation, fluid viscosity is a measure of fluid resistance to the flow, and it is a strong function of temperature. The concept of the boundary layer is of importance in all of the viscous fluid dynamics and the theory of heat transfer.

The boundary layer is initially laminar, but at some distance from the leading edge (x_{cr}), Figure 2.1, small disturbances begin to grow, and a transition or turbulent flow begins to occur. Fluctuations develop in a transition region before the flow becomes completely turbulent.

The immediate layer next to the surface is a laminar sublayer, in which molecular diffusion dominates transport. Moving away from the surface and adjoining to the sublayer is a buffer region in which diffusional and turbulent mixing are comparable. Next to the buffer layer is a turbulent region where transport occurs by turbulent mixing.

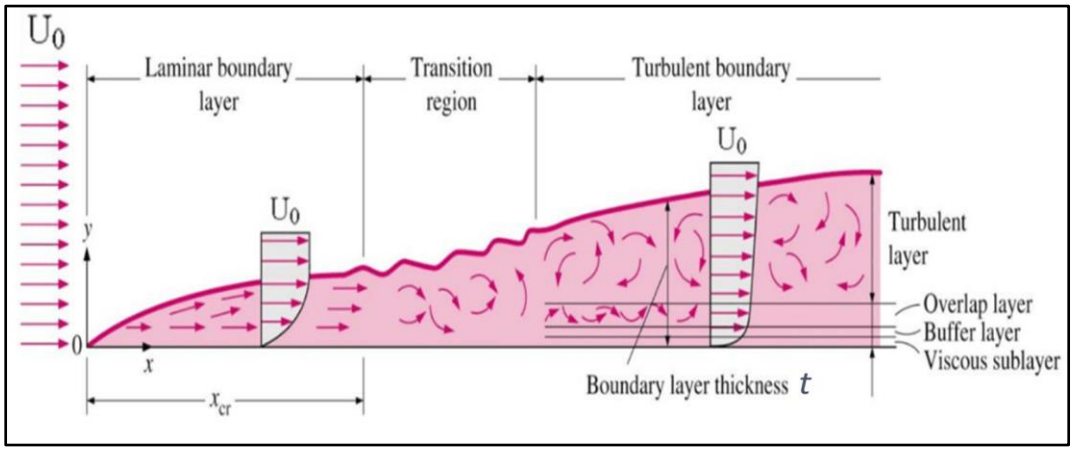

Figure 2.1: Development of boundary over a flat plate [19]

Osborn Reynolds was the first to distinguish laminar from turbulent. He observed the behaviour of a streamline of dye in water inside a glass tube under different velocities. The flow of an incompressible fluid is subjected to inertial forces and viscous forces, the ratio between inertia and viscous forces was developed by Reynolds, and known as the Reynolds number, Re. It is used to determine whether a flow is laminar or turbulent in fluid or gases [20].

$$Re = \frac{inertia\ forces}{viscous\ forces} = \frac{\rho\, U_o\, \delta}{\mu} \qquad 2.1$$

where δ is the characteristic length, i.e. Diameter, D, for the tube and length, L, for the plate, U_o is the flow mean velocity, ρ is the fluid density, and μ the fluid viscosity.

Reynolds number at which the flow becomes turbulent is called the critical Reynolds number. For flow passing a flat plate, it is estimated that the turbulence starts if Re > 5* 10^5, and Re > 2000 in pipes. At higher Re numbers, the inertia forces, which are proportional to the density and the velocity of the fluid, are large relative to the viscous

forces; thus, the viscous forces cannot prevent the random and rapid fluctuation of the turbulent flow.

2.3 The Concept of Turbulence and Its Mechanism

Turbulence is the most complicated state of fluid motion, making even its definition difficult. In engineering practice, flow is nearly always turbulent. Fluid motion is described as turbulent if it is rotational, intermittent, highly disordered, diffusive and dissipative. Its main characteristic is random and chaotic three-dimensional vorticity. Turbulent flow is the result of the combined effect of viscosity and shear stresses near the surfaces, which both cause the formation of small eddies of varying speeds. Some of these eddies transport in random directions and merge with other eddies to form large ones [17]. At any point in the three-dimensional vorticity, the velocity magnitudes of the particles fluctuate with respect to space and time. Figure 2.2 shows typical chart recording of fully turbulent flow.

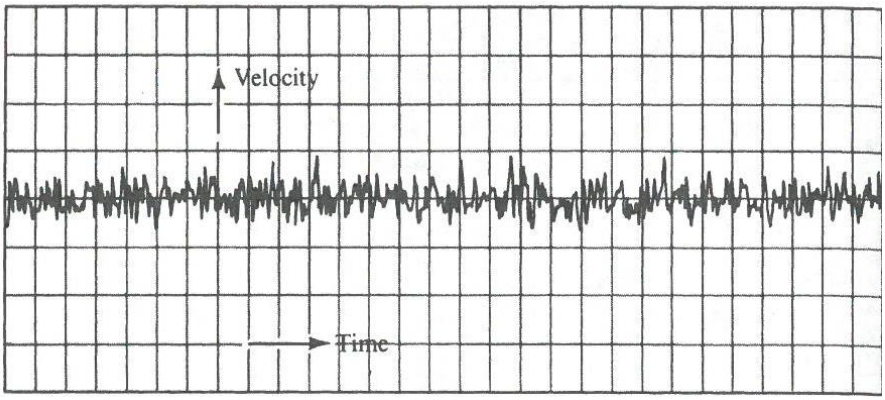

Figure 2.2: Typical velocity fluctuation chart in a turbulent flow [17]

Turbulence in fluid flow usually dominates the entire fluid domain and results in an enhancement of fluid mixing and energy transfer quality due to its high degree of diffusivity. Turbulent flow can be desired on parts of the gas turbine blade, internal cooling, surface of an aircraft wing or in industrial applications such as heat exchangers and the mixing of fluids.

The complexity of the turbulent flow has made the task of solving the problem quite difficult and has posed a great challenge for researchers for decades. This is because

there is no rigid mathematical analysis of turbulent flow because of the unpredictable motion of the fluid particles [20]. However, theories and models have been developed through the decades to predict and estimate the turbulence impacts on various conditions and applications.

2.3.1 Turbulence modelling

For decades, understanding and modelling the turbulent flow motion has stimulated the creativity of scientists, engineers, and applied mathematicians. Often the aim is to develop theories and models to predict the flow field of devices or processes [21]. The goal of turbulence theories and models is to describe turbulent motion by computational methods. Computational models are devised that can be solved in computational fluid dynamics (CFD) codes.

A turbulence model is a computational procedure, which closes the system with mean flow equations so that a wide variety of flow problems can be calculated. In the 1940s turbulence was treated by statistical theories [17]. In this approach, the turbulence models are meant to bypass the chaotic details and to predict statistics of turbulent flows directly. Nowadays almost all turbulence models are based on this statistical techniques.

However, there is no turbulence model seems to be universally applicable to a wide variety of applications. A model that can be described a very good fit for solving one certain case may fail to solve another. Therefore, it is important to choose a suitable turbulence model for the problem under consideration.

The choice of turbulence model will depend on some considerations such as physics surrounding the flow, the level of accuracy required and the availability of computational resources considering the amount of time available for the simulation. To obtain the most appropriate choice of model for a specific application, it is necessary to understand the capabilities and limitations of various options.

As the use of turbulence models in computational fluid dynamics increases, more sophisticated models will be needed to simulate the range of phenomena that arise.

The most common turbulent models are classical models, which are based on the Reynolds time-averaged equations presented as (i) a zero-equation model (eddy viscosity and mixing length), (ii) a one equation model (Spalart –Allmaras), (iii) a two-equation model k-epsilon, (k- ϵ), model and k-omega, (k-ω), model, (iv) the Reynolds stress equation model, and (v) an algebraic stress model.

The momentum in turbulent flow is exchanged by small-scale fluctuations. The resolution of these fluctuations requires a computer system with large enough memory and speed, which even the modern computer system, cannot offer. Therefore, to compensate the deficiency of the hardware resources, in quantitative work one is obliged to use turbulence models based on using averaged Navier-Stoks (NS) equations [22].

2.3.2 Mixing mechanism in turbulent flows

Mixing is a physical process that aims at reducing non-uniformities in fluids by eliminating gradients of temperature and other properties. The process is of importance to some applications such as blending, heat and mass transfer and for homogeneous liquid phase reactions [23]. In such applications, mixing is achieved by, together, increasing fluid velocity and generating turbulence. In a turbulent flow, the fluid particles are transported to all regions of the fluid domain by bulk circulation currents usually called eddies. Eddies interactions are the key mechanism of the mixing process. However, when eddies can no longer sustain rotational motion, their kinetic energy is dissipated, and mixing becomes slow as it depends only on the molecular diffusion of the fluid [24].

2.4 Heat Transfer Mechanism

Whenever a temperature difference exists in a medium or between media, heat transfer must occur. When a temperature gradient exists in a stationary medium, which may be solid or fluid, the term used to describe the mode of heat transfer is conduction. In contrast, convective heat transfer will occur when fluid and solid are in contact and moving relative to one another and are at different temperatures. The final mode of heat transfer is thermal radiation or the emission of the electromagnetic waves from surfaces of infinite temperature.

2.4.1 Conduction

Conduction is the process by which heat flows from an area of higher temperature to one of lower temperature within a single medium- solid, liquid or gas-in an attempt to equalize the thermal differences in the substance. It is also used to describe heat transfer between media that are in direct physical contact such as two touching solids. The physical mechanism is that of molecular activity.

For heat conduction, the rate equation is known as Fourier's law.

$$\acute{q_x} = -k\frac{dT}{dx} \qquad 2.2$$

The heat flux,$\acute{q_x}$, is the heat transfer rate in the x direction per unit area perpendicular to the direction of transfer, dx is the length over which the temperature difference is measured.

The proportionality constant, k, is a transport property known as the thermal conductivity and is a characteristic of the material through which the heat is passing. This transport property provides an indication of the rate of energy at which the material is capable of transferring. In general, the thermal conductivity of solids is larger than that of liquids, which is larger than that of gases.

2.4.2 Radiation

Radiation heat transfer results when thermal energy in the form of electromagnetic waves is emitted from a body due to its high temperature. Emission and absorption are determined by the temperature and surface conditions of the radiating source, and the temperature of the surrounding environment.

The Stefan-Boltzmann law gives the maximum flux at which radiation may be emitted from a real surface.

$$\acute{q} = \sigma\, \varepsilon\, {T_s}^4 \qquad 2.3$$

Where T_s is the absolute temperature of the surface and σ is the Stefan-Boltzmann constant. The emissivity, ε, of the surface is a radiative property of the material, whose value is in the range $0 < \varepsilon < 1$. Emissivity is the ratio of a surface's ability to emit radiant energy compared with the ability of a perfect ideal body of the same area at the same temperature. Generally, engineering materials do not behave as ideal radiators. If the bodies are not ideal radiators then:

$$q = \sigma A_1 \varepsilon F_{12} (T_1^4 - T_2^4) \quad 2.4$$

The portion of radiation exchanged between two differently oriented surfaces has to be defined by a geometric function known as view factor, which depends only on the geometry of the body.

2.4.3 Convection

In convection heat transfer, energy transfers by two mechanisms: diffusion and bulk motion of the fluid. Near the surface, the fluid velocity is low, due to shear stresses and the formation of the boundary layer, and diffusion mechanism dominates. Away from the surface, the fluid bulk motion is high, and its mechanism dominates. The convective heat transfer mode is sustained by both the diffusivity of the fluid molecular and the bulk motion. The convective heat transfer is usually presented as in Equation 2.5:

$$Q = h A (T_1 - T_2) \quad 2.5$$

Where h, is a convective coefficient for the heat transfer between the surface and the fluid body.

Fluid motion, in the presence of temperature gradient, contributes significantly to heat transfer [16]. Therefore, convection heat transfer can be classified, depending on how the fluid motion is initiated, to natural convection and forced convection.

2.4.3.1 Natural convection

Natural or free convection is induced by buoyancy forces, which arise from density differences caused by temperature variations in the fluid. At heating, the fluid experiences an increase in temperature and hence a reduction in density. Since it is now lighter than the surrounding flow, buoyancy forces induce a vertical motion for which warm air is ascending from the boards and replaced by an inflow of cooler ambient air under the effect of the gravity. Thus no external forces other than gravity, need to be applied to move the energy in the form of heat [16].

Natural convection heat transfer is extensively used in some engineering applications such as heating of houses by electric baseboard heaters, cooling of commercial high voltage electrical power transformers and electronic devices (chips, transistors). However, in the most industrial application, it is more economical to speed up the convection process by artificially generating a current by the use of a pump, agitator, or some other mechanical device. This procedure is referred as forced convection.

2.4.3.2 Forced convection

Forced or assisted convection, is when an external source such as a fan is used to actuate a fluid flow, in order to increase the convective heat transfer rate. The mechanism has a wide range of applications in everyday life, including central heating, air conditioning, etc. It can be considered as one of the main methods of useful heat transfer as a significant amount of heat energy can be transported very efficiently.

Experience shows that convection heat transfer strongly depends on the fluid properties such as viscosity, thermal conductivity, density as well as the fluid velocity. It also depends on the geometry and the surface roughness as well as the type of fluid flow, whether it is laminar or turbulent [25, 26].

The fluid motion enhances heat transfer, since it brings hotter and cooler layers of fluid into contact, initiating higher rates of conduction between fluid layers at a greater number of sites in a fluid. The type of flow also contributes to heat transfer quality, for an instant, in turbulent flow, the interaction among the eddies of various scales passes energy sequentially from the larger eddies gradually to the smaller ones [26].

In convection, it is a common practice to non-dimensionalise the governing equations and combine the variables which group together into dimensionless numbers. The most recognised number in this regard is the Nusselt number. This parameter provides a measure of convection heat transfer occurring at the surface, hence it represents the ratio of convective to conductive heat transfer across the boundary layer, Equation 2.6.

$$Nu_L = \frac{hL}{k} \tag{2.6}$$

2.5 Methods for Heat Transfer Enhancement

This subject of enhanced heat transfer has become much more important to industry with progressing time. Energy and material savings considerations, as well as economic incentives, have led to efforts to investigate methods to enhance the energy transfer rate.

Enhancing heat transfer performance within the system or process of interest means increasing the energy transfer rates. Due to the dependency of convective heat transfer on fluid mechanics, attempts at increasing rate of heat transfer can include but not limited to [27]:

a) Increasing the fluid thermal properties such as thermal conductivity. (e.g. by choice of an alternative fluid or utilising the nanoparticle technology [28]).
b) Increasing fluid velocity thus delaying the development of the boundary layer.
c) Fluid redistribution. Etc.

According to Bergles [29], these techniques of enhancing heat transfer can be classified as active and passive methods. Those that required applying external power to maintain the enhancement are the active methods. On the other hand, the passive enhancement methods are those that do not require external power to sustain the enhancements' characteristics. A large enhancement would possibly be achieved when two or more of the passive and active techniques are utilised simultaneously, see Table 2.1.

These methods are commonly used in areas such as process industries, heating and cooling in evaporators, thermal power plants, air conditioning equipment, refrigerators, radiators for space vehicles, automobiles, etc.[30] .

The costs involved, and the problems that are associated with vibration and acoustic noise as well as difficulty to provide external power, have made the active techniques less preferable than the passive techniques. However, active methods are used when there are some limitations of using the passive ones, such as the requirements dictated by the application.

Table 2.1: Classification of convection enhancement technique [31, 32]

Passive Techniques	**Active Technique**
Treated surfaces	Mechanical aids
Rough surfaces	Surface vibration
Extended surfaces	Fluid vibration
Displaced enhancement devices	Electrostatic fields
Swirl flow devices	Suction or injection
Coiled tubes	Jet impingement
Surface tension devices	Additives for fluid
	Rotation
Compound Enhancement	
Rough surface with twisted-tape swirl flow device, for example	

Most of the techniques presented in Table 2.1 are based on flow control mechanism to improve the heat transfer performance of a system or a process. The mechanism is of great interest to researchers and has been intensively studied recently [33]. The intent of flow control is manipulating a flow field, which may be accomplished by delay/enhance transition, suppress/enhance turbulence, or prevent/promote separation [34].

The passive techniques that are usually used for controlling the flows employ special surface geometries such as fins and winglets [35, 36], whereas, the active techniques utilise mechanical devices for fluid stirring such as fan and jets [37].

The mechanical aids are used to promote flow unsteadiness via stirring the fluid or by rotating the surface. The concept of this approach is the induction of secondary flows and restarting the boundary layer. A possible flow control mechanism is through promoting turbulence via special techniques such as turbulence promoters or vortex generator [38]. This technique allows fluid mixing and thus enhances the heat transfer.

2.5.1 Vortex generator mechanism for turbulence production

The term *vortex/eddy* is commonly used to describe a region of concentrated rotation in the flow. It usually occurs when an aerodynamic device extracts energy from the flow and generates this rotation within the flow. Rotating fluids occur in a wide variety of technical contexts, such as a rigid-body rotation, and in geophysics, particularly in the atmosphere and the oceans [39]. Rotating flows are common in turbomachinery, mixing tanks and a variety of other applications.

The forces that hold the particles together in a fluid are much weaker, in comparison to those in a solid, which gives rise to their more complex behaviour. Fluid does not offer lasting resistance to displacement of one layer of particles over another. If a fluid experiences a shear force, the fluid particles will move in response to a permanent change in their relative position, even when the force is removed. By comparison, a solid will adopt its previous shape when the force is removed [18].

2.6 Rotating Cylinder Technique – A Turbulence Promoter

External flow over a bluff body is a common phenomenon associated with a fluid flowing over an obstacle or with the movement of a natural or artificial body. Evident examples are the flows past an aeroplane, a submarine and an automobile, and wind blowing past a bridge and a high-rise building [40].

Flow over a bluff body has been the subject of considerable research interest because of their relevance to many engineering applications, such as heat exchangers, cables, chimneys, and bridges [41]. Such kind of flows has offered great opportunities to validate different approaches to turbulence modelling [42, 43] since the physics of these flows are very complex and they required special attention to their modelling and numerical solutions. Furthermore, the knowledge of the hydrodynamic forces

experienced by submerged objects such as offshore pipelines is essential for the design of such structure.

Flat plate, square and circular cylinder were investigated as bluff bodies to analyse the flow in the wake region area [44, 45]. The sphere has also received attention in this regard as a representative of the three-dimensional bluff body, and its wake structure is quite complex because of 3-D fluid structure in the wake region [46].

The flow past a cylinder is one of the basic flows that received a great deal of attention, with emphasis on studying the mechanics of the formation region of vortices that usually occurs behind the bluff bodies [47] and the vortex interaction in downstream flows. The flow structure in the wake region of the cylinder and the vortex shedding activity has motivated many studies to address these phenomena.

The flow over a cylinder usually experiences boundary layer separation and very strong flow oscillations in the wake region of the body. Separation occurs when the fluid, no longer able to follow the contour of the (curved) surface and breaks away from it. The breakaway of the boundary layer first occurs at the separation point where the velocity gradient within the boundary layer is equal to zero. Several aspects of this flow are interesting, most notably being the regular vortex-shedding pattern. The flow pattern in the wake of a circular cylinder depends mainly on Reynolds number of the upstream flow and the cylinder diameter. Reynolds number plays the key role in determining the state of such flows; Figure 2.3 shows different flow patterns at different Reynolds number behind a circular cylinder.

For very low values of Re (Re $<<1$), the inertia forces are negligible in comparison with the viscous forces, and the streamlines come together steadily and symmetrically behind the cylinder as shown in Figure 2.3 (a). As Re approaches the range 2-30, the upstream-downstream symmetry is lost, and the boundary layer separates and forms two steady vortices attached to the rear of the cylinder. Behind the vortices, the main flow streamlines come together again. When Re reaches a value around 40 an instability and a periodic oscillation of the wake is observed, and by the time we reach Re ~ 100 the vortices start to shed from the rear of the cylinder in a regular and periodic

manner, this famous phenomenon is known as Karman Vortex Street. The critical value of Re at which the vortex shedding starts is ~ 45.9 [43].

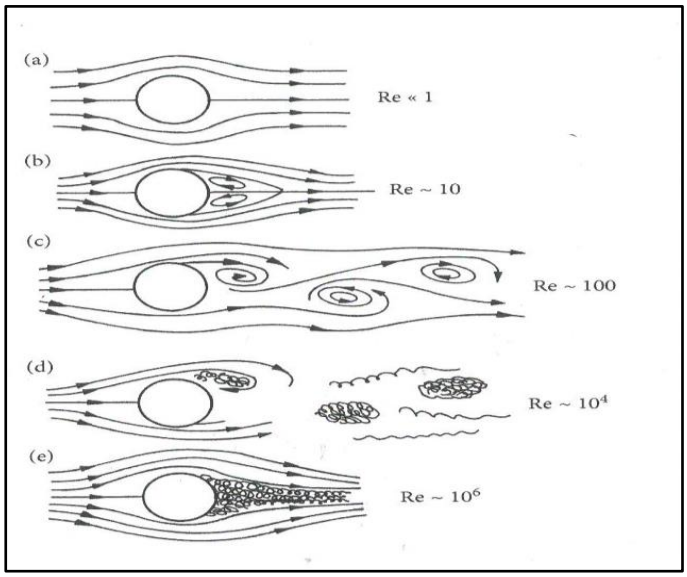

Figure 2.3: Flow pattern behind a cylinder at different Reynolds number [48]

The laminar Karman vortex street persists up to Re ~ 100 at which point three-dimensional instabilities develop. By Re ≥ 200 the flow becomes three-dimensional and turbulent, and vortex shedding also occurs but in more complicated patterns [49]. At high values of Re ~ 10^5, the turbulence spreads out of the vortices, and a fully turbulent wake is obtained, Figure 2.3,e. The point on the cylinder surface at where the free-stream flow hits the cylinder called the stagnation point.

The length of the wake vortices region was found to be a relevant length scale for the distribution of fluctuating velocity with distance close to the body [47], and it is varied linearly with Re of the free-stream flow, where Re is based on cylinder diameter [50]. Park et al. [51] defined the end of the vortex formation region as the point that has the maximum amount of streamwise velocity fluctuations. At the downstream flow, the formation region ends when viscous forces return to dominate again.

The periodic vortex shedding flow causes fluctuating forces on the cylinder, acoustic noise, thermoacoustic activity and fluid mixing among several other effects. The result of the fluctuating forces could be structural vibrations, which sometimes can lead to structural failure due to resonance [52]. However, in some applications, the vortex

shedding flow is induced deliberately to enhance heat transfer, as in researches by Wang et al. [53] and Ma et al. [54] since the heat and momentum transportation is associated with the disturbance of boundary layer. The thorough control of the flow allows destabilising the stable shear layer, disturbing the growth of the boundary layer, increasing the turbulence intensity by generating a secondary flow [55, 56]. The secondary flow is a relatively minor flow superimposed on the main flow and cannot be predicted when using the simple analytical techniques. It provides high values of the heat and transfer coefficients in addition to improving the mixing process.

Other most important characteristics of the flow around a cylinder are the drag forces. In the region of small Reynolds number, the drag forces varied with Re. The contributions of the viscous and pressure forces to the drag are very similar in this flow regime. Pressure drag depends on the form of a boundary layer on the body surface. Downstream of the separation, due to the highly turbulent motion in the wake, the energy is dissipated and the pressure there is reduced thus the pressure force tends to dominate the drag, while the viscous force decreases further [20]. Furthermore, the highly turbulent recirculation flow in the wake region increases the drag force fluctuations on the cylinder surface [57], which might cause destructive structural vibrations.

Controlling flows around objects has been extensively used in the aerodynamic community to reduce drag or to modify the global flow topology. There have been several attempts at controlling the wake structure behind a circular cylinder using both active and passive controls with emphasis on the suppression of vortex shedding [58]. Flow over a rotating cylinder has been extensively investigated for flow control technique and vortex shedding suppression.

Rotating circular cylinder are widely used for laboratory assessment of the effect of fluid velocity on corrosion rates. Application of rotating cylinders can also be found in viscosity determination devices, biological applications, rotating cylinder electrode electrochemical reactor (RCE) [59], reactors for seawater distillation [60], in laboratory evaluation of mineral scale formation in oil and gas production systems [61], and flame stabilisation [62, 63].

Rotation of a cylinder can promote or mitigate hydrodynamic instabilities. For instance, rotating circular cylinder in the fluid flow helps in considerably controlling wake structure [64, 65]. Because of cylinder rotation, there is a continuous layer of fluid attached to the cylinder surface that rotates with the cylinder, due to the effect of the viscous forces and the no-slip condition, and hence the stagnation points are lifted off the cylinder surface into the main-stream, Figure 2.4. Also, the symmetry of the generated vorticity on the top and bottom of the cylinder walls is destroyed; this is mainly because of the relatively different velocities, with respect to the free stream, on both sides of the cylinder, as one moving in the free-stream direction and the other against it. Therefore, rotation of the cylinder inhibits separation of the flow from the surface.

The flow past a rotating cylinder is a function of two non-dimensional parameters. These are the Reynolds number Re and the non-dimensional ratio α, which is represented in Equation 2.7 as the ratio of the rotational velocity of the cylinder wall to the oncoming flow velocity.

$$\propto = \frac{D\,\Omega}{2\,U_{\infty}} \qquad 2.7$$

Where, D is the cylinder diameter, Ω the constant angular velocity of the cylinder rotation, U_{∞} the incoming free stream velocity.

Several research groups have investigated the changes in flow topology of flows passing a rotating cylinder at low Reynolds numbers [52, 64, 66, 67]. Their findings revealed that, at low rotation rates ($\alpha \leq 2$), the classical Karman vortex street is observed, where vortices shed alternatively. At higher $\alpha > 2$, single-sided vortex shedding occurs, because of the vortex fade on the cylinder side where the peripheral velocity goes against the free stream velocity. Furthermore, at a highest rotational rate of the cylinder, the flow starts to develop three-dimensional and turbulent effects inside the fluid domain [68].

The effect of cylinder rotation and velocity gradients on its upper and lower sides implies a rise in the pressure on one side of the cylinder and lowering it on the other creating a lift force, also referred to as the Magnus effect [69].

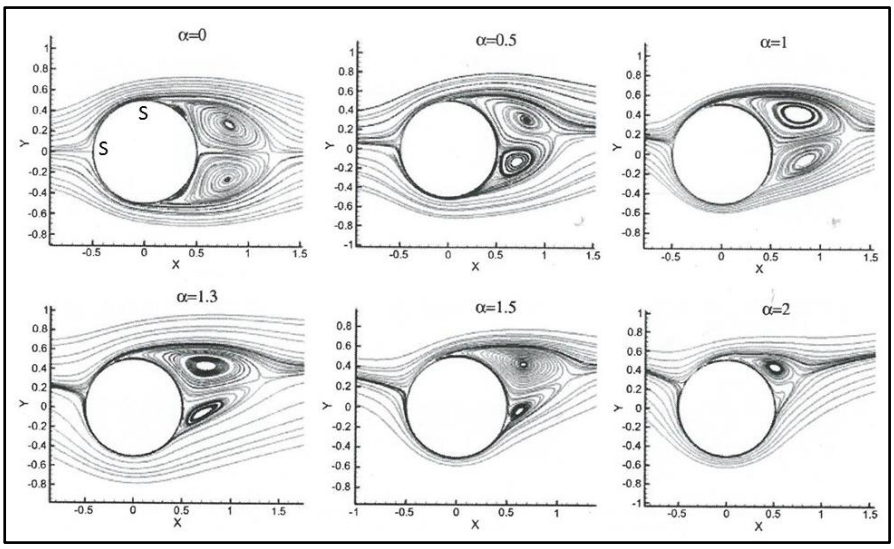

Figure 2.4: Upstream and downstream flow behaviour over a rotating cylinder [42]

It was found that the lift force is a linear function of rotation rate [67] and it is almost independent of Re. Research by Martin-Alcantara et al. [70] revealed that the main contribution to the lift is the generation of the upper vortex in its root close to the top front of the cylinder surface, where it generates at a low-pressure region. While in non-rotating cylinder case, this contribution is balanced by the opposite effect of the lower counter-rotating vortex, so the mean lift vanishes in the fully developed flow. Drag forces may decrease substantially to almost vanishing by increasing the rotation rate [71].

The phenomenon was exploited to provide a propulsive mechanism for ships and boats. As it happened in the 1920s when Anton Flettner proposed the use of rotating cylinders instead of sails to improve ships performance by inducing a propulsive force as a result of the interaction between the wind and the rotating cylinders. He built a ship with 18 m high rotor and 2.7 m diameter. After this modification, it was noticed that the ship become faster than before and able to sail much closer to the wind [18, 69].

In a quiescent fluid domain, the rotating cylinder was used to generate a flow that spans from laminar to turbulent regimes. Secondary flows induced by the cylinder rotation in a quiescent fluid depend on the rotational Reynolds number, Re_r [72]. Where Re_r is based on surface speed and cylinder diameter. At higher speeds a form of turbulent motion would be expected to occur in which particles of fluid are thrown off from the surface in an irregular manner, owing to centrifugal force and then be replaced by other particles drawn inwards.

An intensive investigation of fluid behaviour around a rotating cylinder was presented by Etemad et al. [73]. They reported that the flow around the cylinder develops a laminar Couette flow, then at $Re_r \sim 900$ first sign of unsteadiness in the laminar could be observed. Further increase in Re_r, a three-dimensional secondary flow began to develop. Above the critical value of $Re_r \sim 14500$, the secondary flow becomes turbulent. More recently, research by Ma et al. [74] demonstrated that the rotation effect on the flow structure near to the cylinder becomes more apparent at Re_r 11000 and the higher the rotational speed gets, the more obvious the disturbance becomes. The research extended to $Re_r = 42000$ at which the flow around the cylinder becomes entirely turbulent.

Recently, the rotating cylinder has been investigated by Escamilla-Ruiz et al. [23] to promote turbulence and secondary flows in stirred tanks, to enhance mixing quality. During cylinder rotation energy transfers to the fluid and produces a three-dimensional rotational flow in the direction of the rotating cylinder (primary flow), owing to the action of inertial forces produced by the cylinder movement. Secondary flows might be produced due to flow interaction with the walls of the geometry. The secondary flows can also be attributed to the effect of the centrifugal pressure gradient in the main flow.

2.7 Grain-Oriented Steel

Silicon steel has gained a wide spread application in transformers manufacturing since it was produced in the 1900s [4], due to its superior properties of low core loss and lower magnetostriction. Further improvement on silicon steel was the production of Grain-Oriented grades of silicon steel in the 1930s [7], which are usually used in

distribution and power transformers. The rise in social demands for low-loss steel in transformers cores begins with the first oil crisis in 1973 and the sharp rise in energy prices [75]. Since then, the reduction of electrical consumption has become an extremely crucial matter and the worldwide trend towards the preservation of the natural resources.

The grain-oriented is characterised by an exceptional high crystal grain size in the order of up to some ten millimetres and by the very sharp orientation of its grain in the so-called Goss texture [76]. In GO electrical steel, the metallurgical phenomenon called secondary recrystallisation is exploited to the alignment of the crystal orientation. Secondary recrystallisation is a phenomenon in which only grains with a near-Goss orientation among primary grains with a size of around 10 μm grow to 5 mm or larger. Some inhibitors, such as MnS; Se; Sb, are used to control the grain growth and align it with the <001> Goss orientation. The <001> axes are the directions of the easiest magnetisation in bcc-iron, which are oriented very close to the rolling direction. During secondary recrystallisation, the inhibitors tend to decompose and lost from the sheet surface layer during the purification process.

There are two main types of Grain-Oriented material, one is conventional Grain Oriented (CGO), and the other is High permeability Grain Oriented (HGO) or (Hi-B) as a trade name of Nippon Steel. Hi-B has been commercially produced since 1968 [77, 78], and it shows better performance when applied to a transformer core than the CGO material [79]. The Hi-B grades are characterised by an average misorientation of the <001> axis 3 degrees from the rolling direction instead of 7degrees for the CGO grades [5, 80].

At Cogent as of 2012 only Hi-B type material is manufactured as the cost benefits are much higher than CGO for a similar processing route and conditions. Figure 2.3, shows CGO and Hi-B production routes.

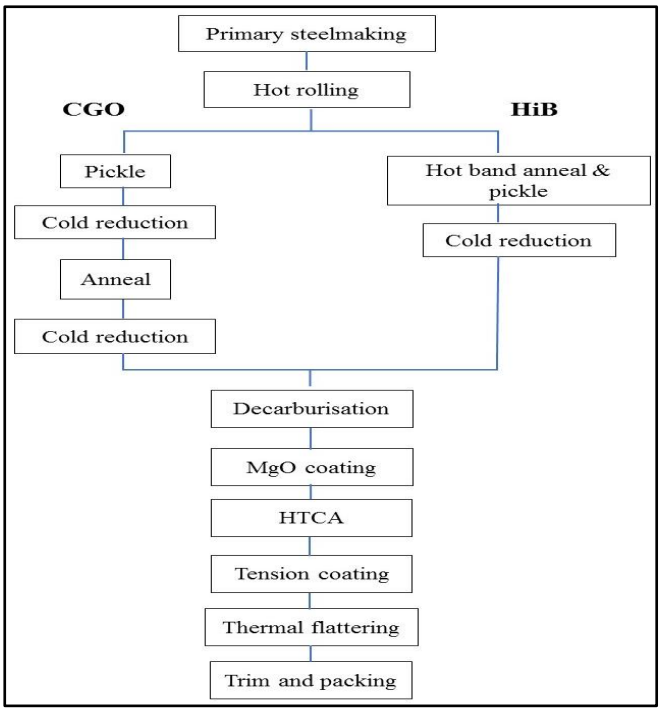

Figure 2.5: Diagram of the production routes for conventional and high permeability grain oriented material [81]

2.7.1 Hi-B process route

A brief description of the production cycle for high permeability material is illustrated below, Figure 2.6.

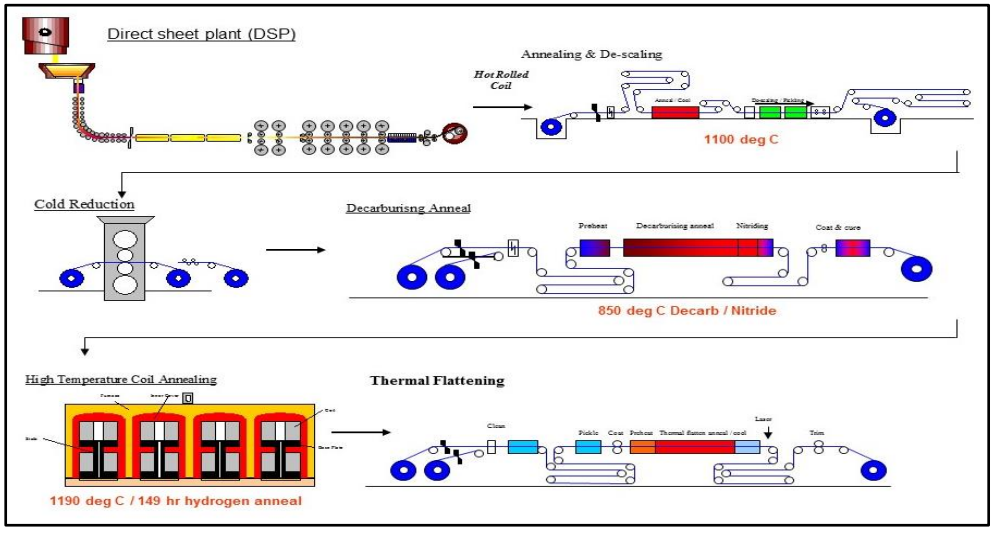

Figure 2.6: Production route for high permeability material [82]

2.7.1.1 Primary steel making, slab reheat and hot rolling

During primary steel making, ferrosilicon and the required inhibitor components are added to the melt. Steel slabs are then continuously cast, which results in the formation of large columnar grains extending from the centre to the surface of the slab due to cooling effects [83].

Those that are not broken up by a rolling stage will produce columnar grains and will give rise to fine streaky grains rather than coarse grains. The slab is typically heated to a temperature between 1350 and 1400, where the MnS particles can dissolve into the slab [5]. Directly afterwards, hot rolling at 950 ^{o}C occur which is needed to produce a good orientation of grains; substantially developed into Goss nuclei in the final product.

2.7.1.2 Side trimming, annealing and pickling

Before the trimming process, the edges of the steel strip are heated to become soft which facilitates the trimming. Steel sheet with silicon content 3% is very brittle and has the potential to cause rolling problems. The objective of the edges trimming process is to remove any cracked edge and prevents crack propagation resulting in the strip breaking on the line or the flaking of edges into other machines.

The strip is annealed to refine the metallurgical structure of the hot-rolled coil at around 900 ^{o}C; the temperature varies depending on final finishing thickness. The process removes precipitates and a particular oxide that was formed during hot-rolling.

The surface is then shot blasted using air with small iron pellets which loosen up the surface scale. An acid pickle is applied to the steel strip for removing the external oxide. Finally, the strip is covered with an oil layer to protect it against corrosion and help during cold rolling as a lubricant.

2.7.1.3 Cold rolling

The material is subjected to a heavy cold rolling reduction, aided by a water-based lubricant (5% oil), at approximately 85% in five passes to the final gauge 0.23-0.35mm [3].

2.7.1.4 Decarburisation and initial coating

Before the Magnesium Oxide (MgO) coating can be applied, the strip has to be cleaned by burners to remove any oil-based lubricant that remains from cold rolling and preheat the strip ready for the subsequent section. This is to ensure the MgO coating adheres to its best potential. Any staining on the steel substrate could also show through the coating if it is severe or if the coating that is eventually formed is too thin.

A decarburising anneal at 840 ºC in a wet hydrogen atmosphere reduces the level of carbon in the strip to a level <0.004-0.005% wt commercially, and initiates primary recrystallisation in the material [3]. The primary reaction to remove the carbon be seen below in Equation 2.8 but both may occur if the conditions favour Equation 2.9. The carbon presence in the following processes would be detrimental to the magnetic properties.

$$C_{(g)} + H_2O_{(g)} \rightarrow CO_{(g)} + H_{2(g)} \quad 2.8$$

$$C_{(s)} + 2H_{2(g)} \rightarrow CH_{4(g)} \quad 2.9$$

A silica-rich subsurface is created with an oxide in the form of fayalite at the surface. This will eventually react with the MgO coating to create a magnesium silicate ceramic layer commonly known as glass film during the HTCA.

2.7.1.5 High-temperature coil annealing (HTCA)

HTCA is an energy-intensive process that may last up to one week and reaches of 1200 ºC for 28 hours during the soaking cycle. During this process, large grains are produced via secondary recrystallisation from primary grains formed in the previous stage. Furthermore, impurities such as sulphur and nitrogen, are fully removed during this process. The process is performed in an atmosphere of inert gases NHx mixture to prevent oxidation.

Electrically insulating glass film is formed by reacting MgO slurry with the silica-rich surface layer which also helps to impart a tension to the strip [11]. The coating will also help to prevent the substrate oxidising as the coating is very un-reactive and creates a physical barrier.

2.7.1.6 Thermal flattening and insulation coating

These processes are at the end of the production cycle followed by slitting, packing and dispatch. The objectives of the process is a thermal flattening of the strip to remove or lessen the edge defects from the HTCA and the application of an insulating coating. During thermal flattening, the steel strip is heated and elongated in nitrogen-rich NHx mixtures. The amount of elongation depends on strip temperature, and the tension applied. Therefore, full monitoring of these conditions should be made.

The final coating complements the insulation properties of the glass film. It increases surface electrical resistance and imparts stress to the strip surface that reduces core loss.

2.8 High-Temperature Coil Annealing (HTCA) Process

The high-temperature batch annealing of electrical steel coils is a very crucial stage in the Hi-B production route. It is the process during which the magnetic properties of the steel are developed when the secondary recrystallisation, strip purification and glass film formation are achieved [84, 85]. The process is performed under careful control of heating rates and gas composition and annealing time that varies depending on the charge weight.

To achieve the desired mechanical and magnetic properties of electrical steel coil, an appropriate temperature profile should be delivered to the steel coil. High permeability material license holders prescribe precise heating rates, any deviation above or below this value can cause difficulty in creating the optimum Goss orientation [86].

The usual steel load/charge consists of eight strip coils; each coil is with an average diameter of ~1300 mm and weighs approximately 10 tonnes, thus requiring a long time to be heated. The coil bore heats slower than the outer surface during the heating process [87]. The heating process ceases when two indispensable conditions are satisfied: (1) the coil temperature reaches the one required by the annealing technology and (2) the temperature difference between the cold and hot points of the coils decreases to less than 30 ^{o}C [88].

The difference in coil temperatures is an important parameter in determining the performance of the annealing system as it can affect the required metallurgical changes and lead to non-uniform mechanical properties along the steel strip. During the heating phase (cycle) the glass film is formed, and secondary recrystallisation occurs, and therefore, it is important that the temperature difference is minimised to ensure uniform and correct microstructural changes throughout the coil. Furthermore, the presence of a temperature gradient results in the outer areas of the coil being exposed to annealing for longer than is ideally required, i.e., remain for longer periods at above-recrystallisation temperature and thus being over annealed, while the locations of slowest thermal response are susceptible to being under annealed.

To compensate any deficiency in the thermal cycle, extra hours might be added to the cycle by the process computer to provide additional time to allow the coil to soak satisfactory. Longer soaking time results in a reduction in the temperature difference between the outer and inner surfaces of the coil and, therefore, better uniformity of microstructure and mechanical properties [89]. However, longer cycle times limit productivity and increase the standard product cost through variable costs, such as energy. Furthermore, plant depreciation will also be higher since it is exposed to the annealing conditions for longer, which will influence service life.

2.8.1 A review of high-temperature coil annealing technology

To achieve the desired final properties in electrical steel strip, the annealing system must be capable of delivering appropriate heat to the charge without incurring excessive running costs. However, whether the system is incapable, or more than capable, the high cost and other restriction make their use less flexible in the low volume electrical steel sector. There are several versions of annealing electrical steel technologies that are used commercially.

The traditional process plant for annealing of the coil strip is a batch annealing furnace. Newer mills, especially in Japan, have been developed and installed at a significant capital cost, those are the continuous annealing lines [90].

Continuous annealing processing lines or CAPL was first introduced by the Nippon steel corporation in 1972 [91], and since then it has been adopted by the world's major steel grades producers. In the beginning, it was used as a process step in the production of hot dip galvanized steel; later several improvements have been made in the process, which allows several types of steels to be processed by this method [92].

This type of annealing involves uncoiled strips passing continuously through a fixed heating furnace, which comprises a heating zone, soaking zone and cooling zone, Figure 2.7. The cooling zone is divided into three sub-zones so that a specific thermal profile can be performed. The delivery equipment comprises a delivery looper where the strips are divided and recoiled.

The CAPL is preferred in the wide range of products in steel industry because of the short processing time leading to high productivity. Moreover, it allows better shape and surface properties as well as uniformity of the properties all along the coil. Although the CAPL advantages over the conventional batch annealing still it was not used for all applications, particularly in the final production process of the electrical steel [90]

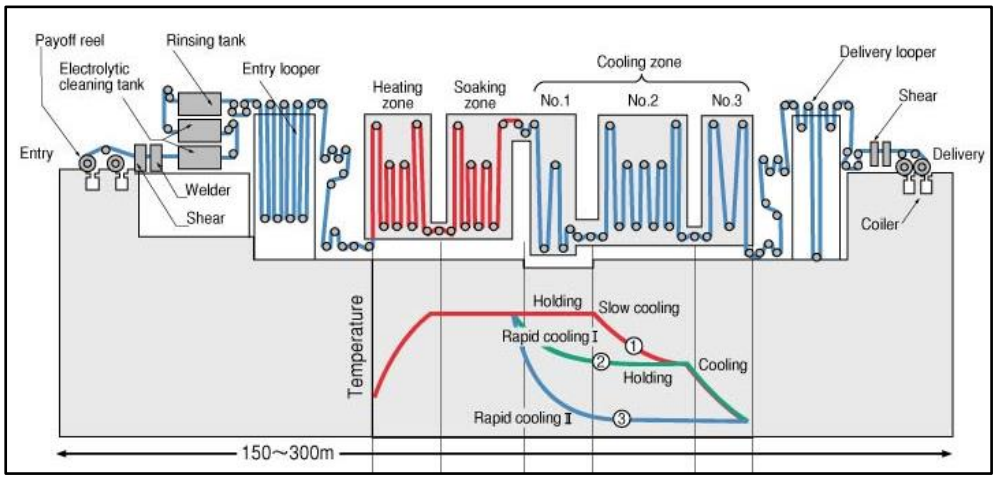

Figure 2.7: Schematic diagram of the sequence operations in a continuous tunnel furnace

This because it is uncertain whether sharp Goss texture can be achieved with short treatment time required for the secondary recrystallization, glass film formation and purification of the steel. Due to the higher cooling rate and the lack of time, the

removal carbon in the steel strip remained in supersaturation during the continuous annealing, resulting in poor ageing property of the continuous annealed steel. Furthermore, economic profitability is questionable regarding the extreme furnace length for realising short annealing times of ~ 15 min. Although the recent trend is towards the continuous process, the batch process still accounts for the majority of existing facilities, because of their versatility, economics and ease of operation [93].

Batch annealing, as its name suggests, involves the heating and cooling of steel coils in a portable furnace. The process is preferred where large ferrite grains are needed as in the case of electrical steel because it offers sufficient time to achieve the desired chemical changes in the steel coil. Improvements in batch annealing technology have focused on hardware performance enhancements and the determination of optimum cycle times to produce the desired metallurgical properties. One such hardware enhancement has been the adoption of high convection batch annealing using hydrogen [94, 95] due to the high thermal conductivity of the hydrogen. The application of 100% hydrogen gas has led to considerable progress in the annealing process; the most important of which is reduced process time [96].

Ordinary batch annealing furnace use NHx mixture, a combination of 10% hydrogen and 90% nitrogen as a protective gas and exhibit slow heating and cooling rates [96]. High convection batch annealing requires a high volume flow rate of recirculating gas to penetrate the steel coil layers.

The HTCA furnaces differ from conventional batch annealing facilities for several reasons that are a direct result of the very high temperature and processing conditions. In the conventional batch system, the charge is heated by a burner, and a fan placed at the furnace base, is used to circulate the atmospheric gas around the steel charge, typical furnace diagram is shown in Figure 2.8, whereas in HTCA furnace, the steel charge is heated by the electrical elements attached to the furnace wall. The high temperature and high content of hydrogen gas make the use of a fan to circulate the atmospheric gas of a great challenge for engineers.

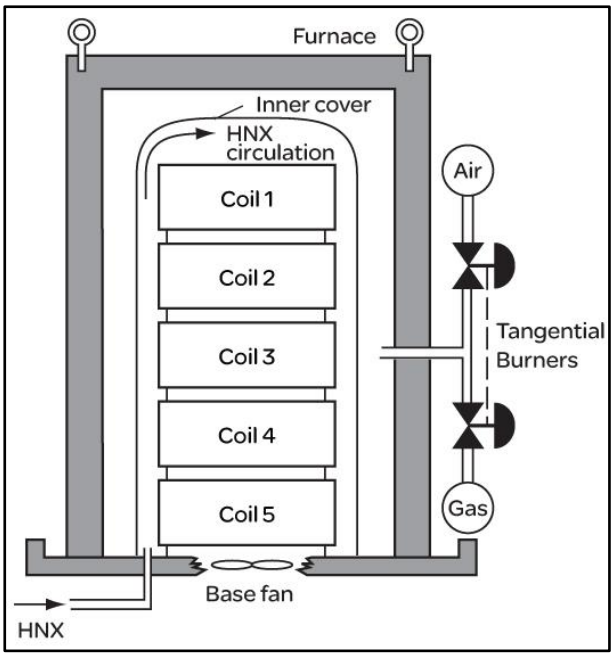

Figure 2.8: Cross-sectional schematic diagram of conventional batch annealing furnace [97]

2.9 High-Temperature Coil Annealing (HTCA) Furnace

In the HTCA furnace, the product develops the desired mechanical and magnetic properties where an appropriate thermal cycle is delivered. The furnace consists of two main sections: a base also called hearth, and a furnace and other stacking equipment: the inner covers and separator plates. The hearth is fixed, and the furnace is portable, which is lowered over the base once the charge of coils and the inner covers are correctly positioned. The annealing cycle is controlled by a process computer using temperature readings by thermocouples inserted at specific locations throughout the furnace and the base. Gas compositions and flow rates are monitored carefully during the cycle. The heating elements are distributed on the furnace walls and the base, as illustrated in Figure 2.9. The typical furnace capacity is eight coils per charge and a maximum weight of approximately 70 tonnes in total.

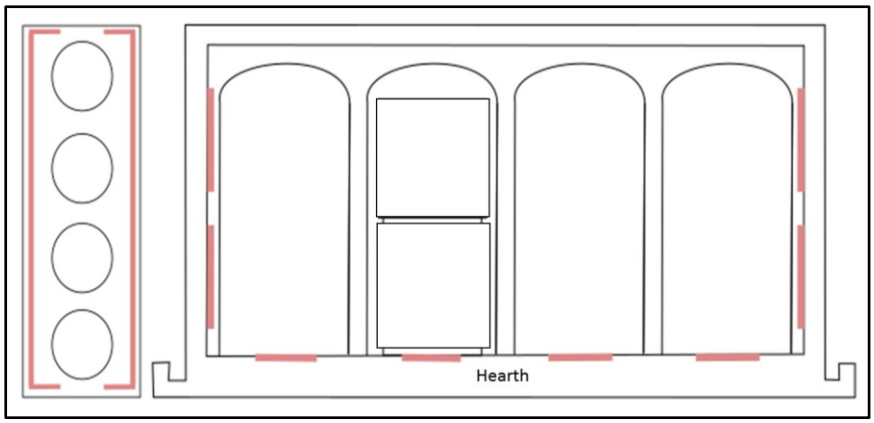

Figure 2.9: Plan and side view of furnaces under investigation. Red lines indicate the heating elements location

2.9.1 The hearth

The hearth is constructed around a steel frame and lined with firebricks. The rectangular hearth has two steel troughs around its periphery, which are longitudinally separated by a steel plate. The outer section is filled with water and the inner filled with sand to form an effective seal when two steel skirts, fitted to the furnace, are lowered into the two hearth troughs. The seal created here is the main furnace seal to prevent the entrance of air or the escape of furnace gas, which can create an explosion risk [98].

The hearth has four circular recesses, situated along its longitudinal axis, which contains electrical base heating elements. A steel base plate is positioned on the top of the recesses to facilitate coil loading. The hearth is supplied with four gas inlet pipes installed in the four recesses and an emergency nitrogen purge inlet, as shown in Figure 2.10.

Figure 2.10: Photograph of a hearth during reconditioning

2.9.2 The furnace

The section in Figure 2.11 shows the furnace placed upon the hearth in the absence of the charge and the separator plates. Electrical heating elements are arranged on the four vertical walls of the removable furnace, Figure 2.9; therefore, some coils receive a higher proportion of the total furnace energy than the other coils. The charge is heated by radiation from heating elements and some convection. Unfortunately, these variations cannot be controlled since the control system works on the average furnace temperature across several zones. During cooling, the gas filled the furnace cavity is drawn off and circulated through a heat exchanger attached to the furnace before re-entering to the furnace.

Figure 2.11 also shows the inner cover settles in the sand seal. The inner cover acts as a radiation shield and plays an important role in maintaining the atmospheric gas at a higher pressure than that in the furnace to avoid oxidation. The internal geometry of the furnace is tailored to minimise pressure losses and to ensure uniform heating and cooling of the charge.

HTCA furnaces and hearths require a great deal of maintenance due to the high temperature of the annealing treatment. The failure in the process equipment can be attributed to the electrical failure which occasionally occurs by means of a short circuit or worse when the current cannot flow, i.e. open circuit. It can occur because of

physical damages to the heating elements during the packing operation, or due to longer ramp up.

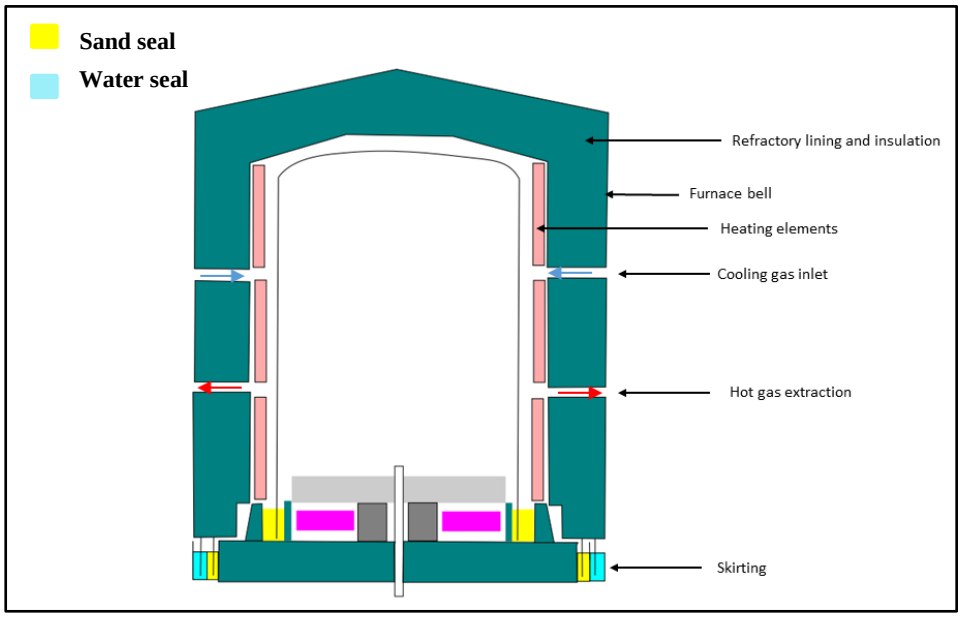

Figure 2.11: Furnace in position on the hearth

The effect of electrical failure is twofold; firstly, there is an extension in cycle time. Secondly, the failure of the process equipment, which results in the furnace being removed from service for maintenance.

2.9.3 Heat transfer in HTCA furnace

The protective cover is externally heated through radiative and convective modes of heat transfer, which heat the circulating hydrogen gas. The outer and inner surfaces of the coils get heated by convection from the circulating hydrogen gas inside the inner cover and by radiation between the cover and the coil. The coil's bore is heated by conduction. The latter process governs the full process time which is mainly affected by the low radial conductivity across the coils wrap [89]. The convective mode of heat transfer induced by the buoyancy forces that arise from density differences caused by the temperature variations inside the atmospheric gas. Radiation is the predominant heat transfer mode in the high-temperature annealing furnaces.

2.10 High-Temperature Coil Annealing (HTCA) Schedule

The HTCA, operates on a fixed base, upon which the steel charge is placed, in sequence; a steel charge, separated plates, inner covers and furnace. Each movement in the process is done with a travelling overhead crane. The process starts by stacking steel coils (2 coils per stack) and the separator plates, on the top of each other successively, onto an empty base. Steel covers are placed over the stacks of the loaded coils and settled in a sand seal at the base to enclose the protective atmosphere gas.

The flow of deoxidizing gas to purge the air from the space under the cover is then begun. The purpose of using the protective atmosphere gas is to fulfil the same main functions: decarburisation, prevention of oxidation and carbon pick up. Thus, the gas composition has a great effect on the development of the grain structures and the magnetic properties [99, 100]. Figure 2.12 shows the gas injection to the steel charge. The gas penetrates the sand seal and passes to space under furnace. A furnace is then lowered on the base. All the connections of the power supply, thermocouples and the cooling system pipework are made.

The thermal cycle begins by heating the coils slowly under gas conditions of a mixture of hydrogen and nitrogen. Then the charge is held in a dry hydrogen atmosphere at ~1200^{o}C with a carefully controlled heating rate. The holding time is proportional to the outer coil diameter, one hour per inch in section [6]. The heating process ceases once the annealing requirements, discussed in section 2.6, are fulfilled.

Cooling is carried out in an atmospheric gas of NHx mixture. In the cooling stage, the furnace is turned off, and the cooling fan is turned on. Once a sufficient low temperature is achieved, the furnace can then be removed and the charge left to be cooled naturally.

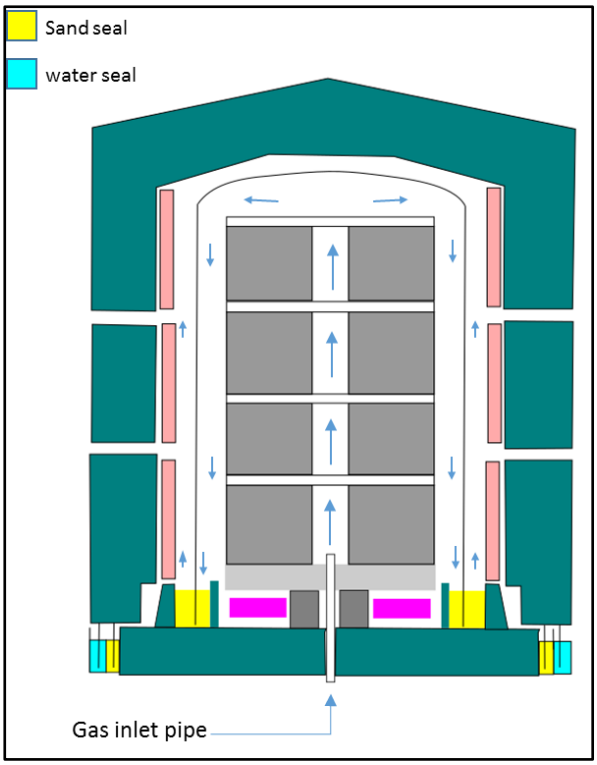

Figure 2.12: An axisymmetric section through a multi-stack convection furnace

In HTCA, hydrogen is used because of its thermos-physical properties, which make it an effective medium for promoting favourable heat transfer. The thermal conductivity of the hydrogen is approximately seven times greater than that of nitrogen at the same temperature [16]. Additionally, the hydrogen content affects the secondary recrystallisation development via influencing nitriding oxidising [101].

2.10.1 Process operating parameters

There are some parameters governing the annealing process which can be classified as controllable and fixed parameters. The controllable parameters tend to be restrictive to meet the requirements of the annealing process such as the gas composition and flow rates as well as the heating rates.

Controllable parameters

- Gas management
- Coil dimensions
- Heat input

The fixed is due to the properties of the material, furnace geometry and annealing technology.

Fixed parameters

- Furnace geometry
- Heating elements position

2.11 Challenges of Annealing Process of Hi-B Production

To remain competitive in the current economic climate, steel companies need to focus their attention on the cost of production. This challenge will be complex as the economy recovers with reshaped markets and as new and idled steel capacity is brought back on-line.

The industrial research activities are targeting on the one hand on superior GO products with lower losses, higher permeability or lower magnetostriction for the demands of more-efficient or less noisy transformers. On the other hand, industrial research is targeting with very high priority on reduction of manufacturing costs. This shall be obtained by enhancing processes, by saving energy and resources, to stay competitive in the market as well as to fit well with the ecological stipulations.

Great efforts and studies have been done to enhance the productivity of the Hi-B steel. The efforts have mainly focused on hardware performance enhancements and optimising the cycle times. For years, steel producers have tried to shorten cycle times and minimise the energy consumed by the annealing furnaces. Also, producers have examined modern furnace construction materials with the aim of extending furnace life, reducing maintenance and improve safety. However, the heating industry has been relatively slow to develop new technologies. This may be attributed to several reasons: the characteristics of the industry, the relatively small scale of the companies offering industrial heating systems and a strong dependence on the heating equipment with the operation of the entire plant.

At Cogent, there have been some efforts on enhancing the annealing process in the high-temperature coil annealing furnace (HTCA) in terms of enhancing convection

and thus optimising the annealing cycle time. Research by Buckley et al. [102], proposed a new furnace design in order to enhance convection at the HTCA furnace and reduce cycle time. Convection heat transfer is more appropriate than radiation for a material having a low surface emissivity as in the case with the electrical steel coils with an MgO coating. The proposed furnace redesign suggested using an impeller to increase the convection inside the furnace. The impeller circulates gas around the charge allowing heat to be scrubbed from locations experiencing excessive temperature and transported by the gas to cooler positions. However, in practice, using super-alloy fans/impellers to cope with the high annealing temperature has always been prohibitively expensive. Moreover, it requires engineering work to convert a base to be able to power and seal the fan perfectly, as the HTCA furnace operates in a hydrogen atmosphere.

Therefore, in this research, an alternative mechanical device was explored to generate gas circulation inside HTCA furnace during the annealing process in order to enhance convective heat transfer via fluid distribution method as explained in section 2.4.

The literature provides strong motivations for using the rotating cylinder for this purpose. Therefore, this research is exploring the technique of the rotating cylinder and the possibility of exploiting it in agitating the atmospheric gas inside HTCA furnaces to generate turbulent flow to enhance the convection heat transfer mechanism.

2.12 Summary

A literature review of the rotating cylinder technique and the high-temperature annealing technology has carried out in this chapter. It can be summarized as follow:

- The rotating cylinder technique has been utilised in a variety of applications either to generate or suppress turbulence due to its capability of promoting or mitigating hydrodynamic instabilities within the fluid domain.

- The inefficiencies of the thermal cycle of the HTCA process needs considerable attention. Efforts are required to improve the HTCA system performance to produce a product with the desired properties and to save energy consumption.

- The literature survey revealed that attempts to enhance thermal cycle in batch annealing, and specifically at Cogent, are scares. Furthermore, there is not certain information available about the use of rotating cylinders in industrial furnaces.

- The present research attempts to generate fluid recirculation, thus producing forced convection, within the furnace fluid domain using the rotating cylinders technique.

CHAPTER 3:

METHODOLOGY

Chapter 3

Methodology

3.1 Introduction

This work is aimed to examine, experimentally, the effect of the rotating cylinder technique on the flow field structure when using a range of rotational rates.

The work is also aimed at exploring numerically the technique's potential use in the high-temperature annealing furnaces to produce flow generation.

This chapter presents the techniques and the methodology that were used to accomplish the research objectives.

3.2 Experimental Methodology

The main physical properties of the flow are very much dependent, in the steady flow case, on the considered range of Reynolds number and on what conditions are assumed at large distances from the cylinder [64, 103]. Such conditions include the induced flow due to the cylinder rotation even at large distances away from the cylinder [49]. Therefore, the configuration of the fluid domain investigated in this study was with the size of 100D as shown in Figure 3.1.

This domain size was found numerically by Kang et al. [49], Mittal et al. [66] and Paramane et al. [104] to be sufficient enough for domain-independent results, and to be considered as unbounded flow for the range of Re, $40 \leq Re \leq 160$, and $0 \leq \alpha \leq 6$.

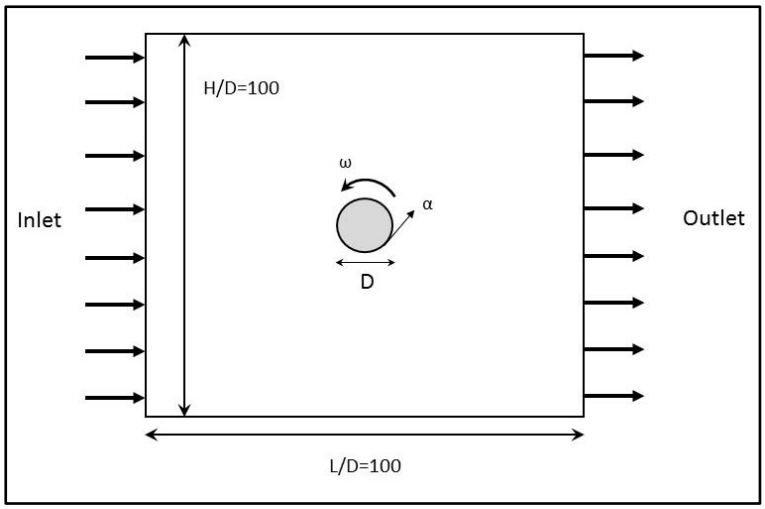

Figure 3.1: Schematic of the unbounded flow past a rotating circular cylinder

A wind tunnel with a configuration as shown in Figure 3.2 was used to investigate the flow passing a rotating and non-rotating cylinder. The rig consists of a circular cylinder of diameter D=12 mm located horizontally inside the wind tunnel with dimensions 1200 × 1200 mm. The flow was forced to pass over the cylinder using a suction fan installed at the exit of the tunnel. A valve was used to adjust the exit velocity and control the flow rate entering the wind tunnel, Figure 3.3. This procedure is governed by Bernoulli's principle, in which pressure and velocity are inversely proportional. The rig wall was made of a perspex material of clear Acrylic sheet of 10 mm thickness to gain optical access to the flow field.

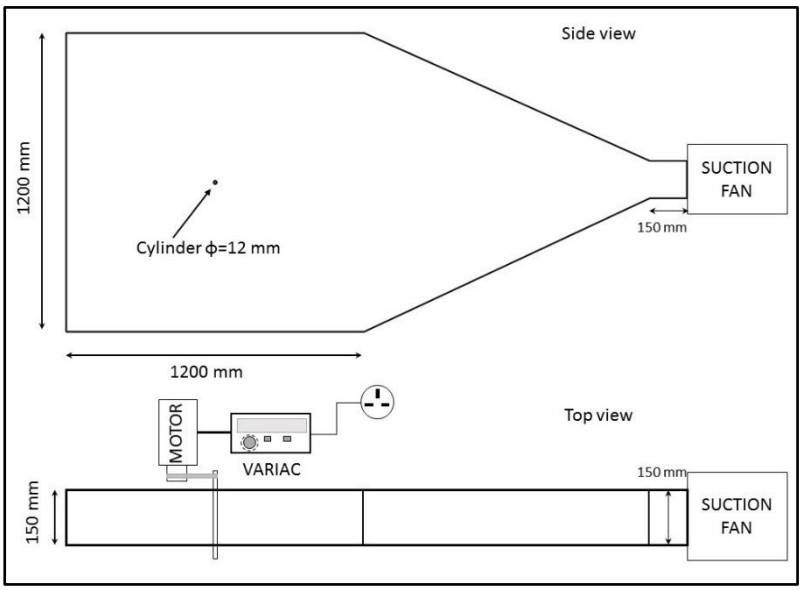

Figure 3.2: Wind tunnel test system

A variable speed DC motor model MT63B14-2 was used to drive the cylinder. An inverter (or a variac) that adjusts the supplied electric current and frequency was used to control the cylinder rotational speed. The system includes a tachometer, which used to monitor the rotational speed during the tests.

The cylinder rotational speed was set to be corresponding to the selected range of the non-dimensional ratio α, and it was calculated using Equation 3.1:

$$r.p.m = \frac{V_{in}\,\alpha}{D}\,\frac{60}{\pi}, \quad or\ \omega \times \frac{60}{\pi} \tag{3.1}$$

The velocity at the outlet of the rig was measured by using a hot wire anemometer. The continuity equation, expressed in Equation 3.2, was used to calculate the inlet flow velocity.

$$A_{in}V_{in} = A_{out}V_{out} \tag{3.2}$$

Reynolds number was calculated based on the cylinder diameter (D) and the inflow velocity calculated from Equation 3.3. Therefore, the formula of Re is:

$$Re = \frac{V_{in}D}{\upsilon} \tag{3.3}$$

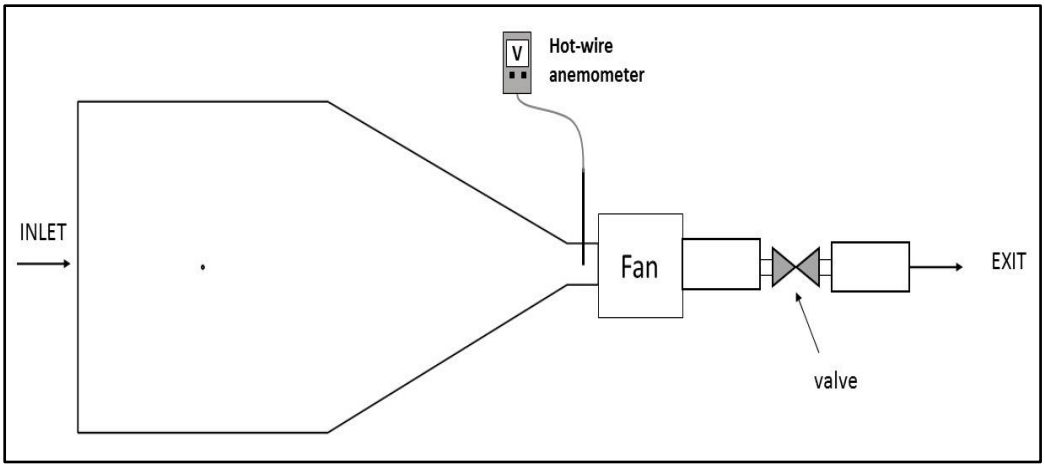

Figure 3.3: Test rig configuration

Laser Doppler velocimetry was used to measure the velocity and the flow turbulent around the cylinder.

3.2.1 Laser Doppler Velocimetry (LDV)

Laser Doppler velocimetry (LDV) is a laser-based technique for measurement of velocity and turbulence in gas, liquid, multiphase fluids, chemically reacting flows. It is widely used in applications such as combustion, flame, wave tanks, rotating machinery, wind or water tunnels, micro and macro channels, in biomedical applications and other scientific research, and industrial applications. It is preferable in applications where the conventional technique such as hot-wire or hot-film anemometers cannot be performed successfully [105, 106].

This optical method of local instantaneous velocity measurement is non-contact and non-intrusive and can be employed where the physical sensors are difficult or impossible to be used. It offers a very high accuracy without calibration because LDV measures the absolute velocity component. The most powerful feature of the LDV is that it can measure one, two or three instantaneous and time-averaged velocity components, simultaneously with velocities ranging from zero to supersonic.

The necessary conditions for the LDV operation are a transparent medium, a suitable concentration of tracer particles (or seeding) and optical access to the flow through windows, or via a submerged optical probe.

3.2.2 Principles of LDV

During the LDV operation, a laser beam splits, and the two branches are then crossed outside the sensor. This intersection region is called the probe volume or measurement volume, Figure 3.4. The main characteristic of this region is the generation of alternating light and dark bands; these bands are called fringes. The flow of interest must be seeded with small, neutrally buoyant particles that scatter light when passing through the fringe bands. The particles, eventually, follow the fluid path and their velocities are assumed to be equal to the velocity of the fluid flow [107].

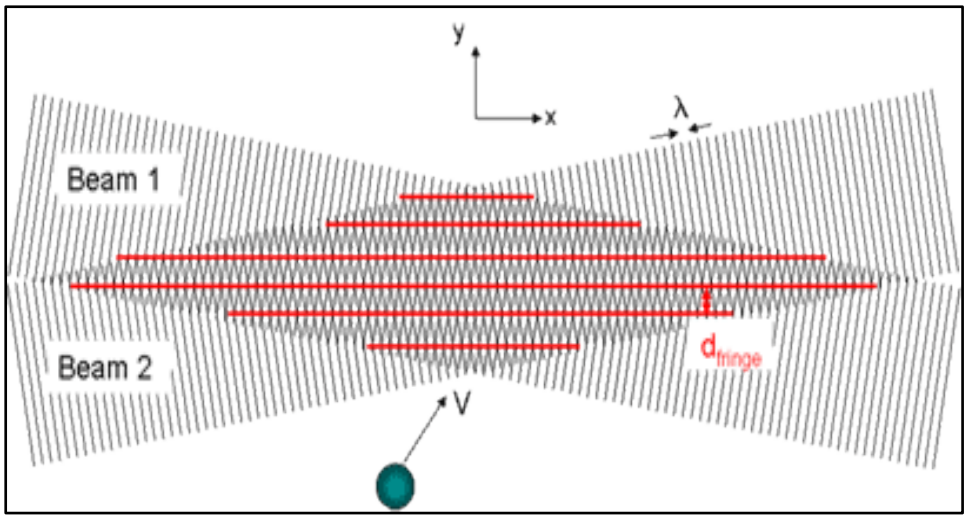

Figure 3.4: Probe volume [108]

The physical principle of the LDA is based on the well-known Doppler shift of frequency between transmitting and reflecting signals. A particle passing through the fringes scatters light, and the scattered intensity rises and falls as the particle passes through the bright and dark bands. The scattered light is then collected and focused on photomultiplier tubes (PMT) which generate a sinusoidal voltage signal representing the intensity of the scattered light from the particle, and hence it is proportional to the absorbed photon energy [109]. The frequency of the scattered light is shifted by an amount proportional to the speed of the particle. Therefore, the frequency of the signal generated by the PMT is also proportional to the velocity of the particle passing normal to the fringes. Variations in the voltage signal can be attributed to the particles passing the fringes light and dark strips.

The raw sinusoidal signal is processed by a signal processor to remove low-frequency components and obtain only the high-frequency component which contains the Doppler signal (f_D). The difference between the incident and scattered light frequencies is the Doppler shift as illustrated in Figure 3.5.

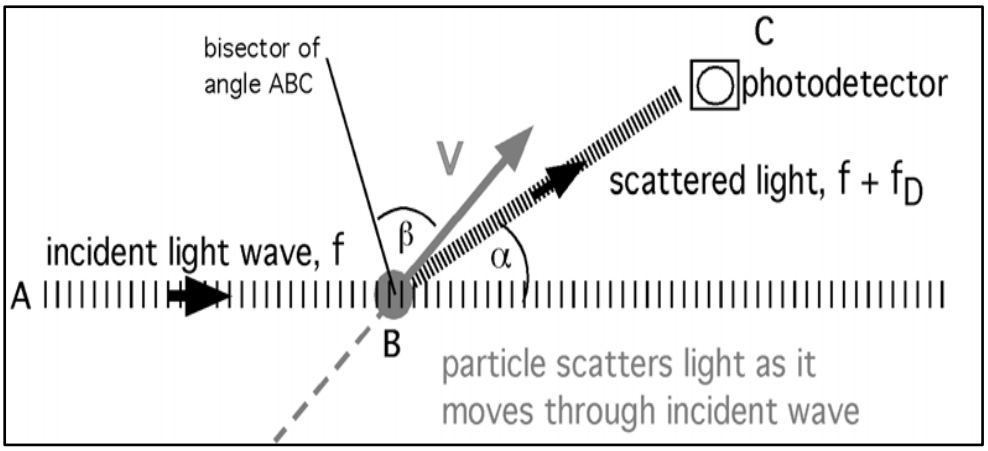

Figure 3.5: A particle moves through an incident light wave of frequency (*f*) and scatters light in all directions

The velocity of the flow can be calculated using Equation 3.4:

$$U = d_{fringe} \times f_{Doppler} \qquad 3.4$$

Where (f_{Doppler}) is the Doppler frequency of the sinusoidal signal, d_{fringe} is the distance between the fringes.

A single pair of incident beams measures a single velocity component; additional components can be measured by adding additional pairs of beams that cross at the same measurement point. Each pair must have a unique wavelength so that the scattered signals can be distinguished during the filtering process. Commonly, the blue, green, and violet lines are used for multi-component measurements.

3.2.3 LDV configurations

Some LDV systems have separate transmitter and receiving units, which allow both forward scatter and backscatter measurements. In the forward scatter, the particles scatter light in all directions, but the highest intensity of scattered light is on the forward side of the particle in a direction away from the incident light. In LDV measuring systems that work in the forward scatter mode, the transmitter and receiver are placed on opposite sides of the flow. However, one of the disadvantages of forward scatter is the difficulty of aligning the transmitter and the receiver. In the backscatter mode, the transmitter and the receiving unit are placed on the same side, and while

this method outputs lower signal levels, it allows for better optical access to the flow. Some LDV systems utilise a combined transmitter and receiver unit, operating in backscatter mode and with the advantage of being permanently aligned for precise measurements.

In this study, LDA of 543-TSI-A01 model was used, this model utilises an argon-ion laser for the light source. This laser output has multiple wavelengths. The two wavelengths used are 541.5 nm (green beam) to measure the (V_x) velocity component, and 488.0 nm (blue beam) to measure the (V_y) velocity component [109]. The two beams are transmitted and collected through one probe, 450500 model that represents both the transmitter and the receiving unit, Figure 3.6.

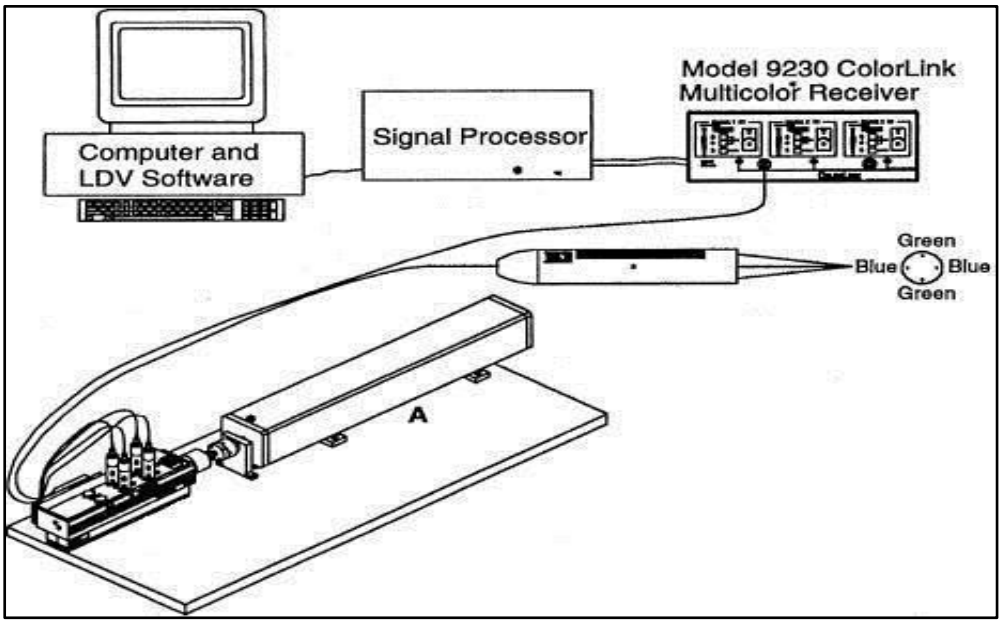

Figure 3.6: Schematic diagram of the TSI laser Doppler anemometry system

A photodetector module PDM 1000 model was used. The PDM receives optical signals from the fiberoptic probes and sends them as electrical signals to the FSA signal processor. The FSA signal processor receives these signals and extracts information such as frequency, phase, burst transit time and burst arrival time from these signals and sends it to the computer.

The data is analysed using the FlowSizer software running on the computer, which displays the detailed analysis. The FlowSizer software provides menu driven control

for data acquisition, analysis and storage. On-line histograms, distributions and correlations of size and velocity are also generated, as shown in Figure 3.7. A computerized 3D traverse system was used to mount the optical probe. FlowSizer software was used to control the traverse movement during the experiments.

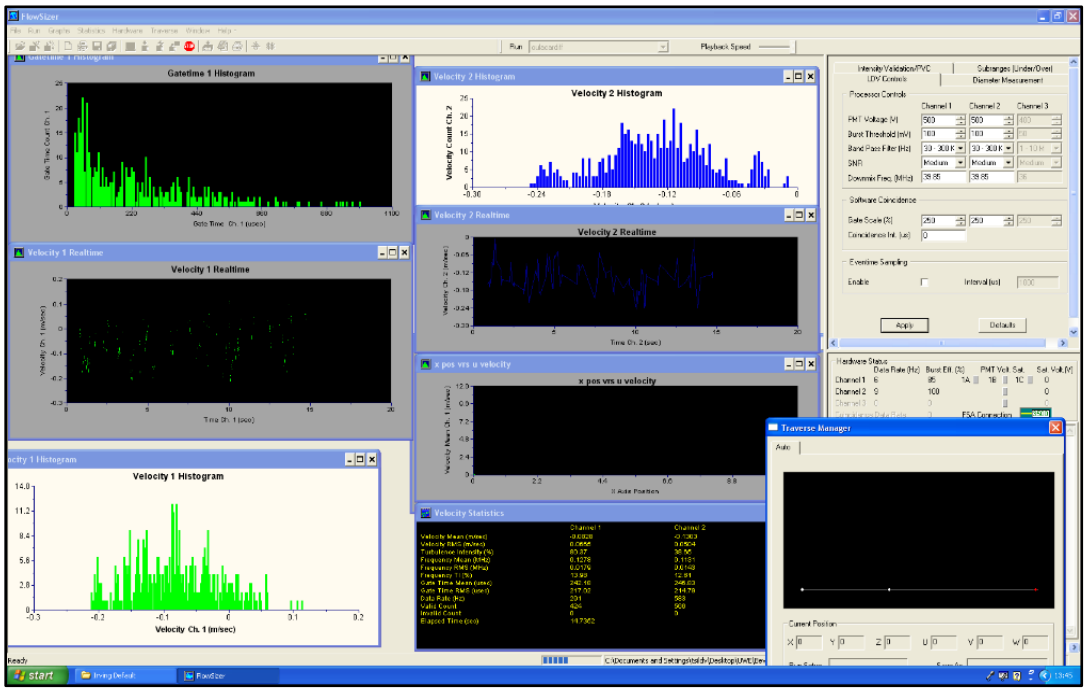

Figure 3.7: FlowSizer software

3.3 The Numerical Approach

The prediction of heat transfer and fluid flow processes can be obtained by two main methods: experimental investigation and theoretical calculation. The latter approach has two branches namely: analytical and computational fluid dynamics (CFD).

The analytical approach is structured about simplification of the governing equations and solving for the exact solution, and so it is restricted to simple geometries. An experimental investigation is considered more reliable; however, performing full-scale tests are, in most cases, prohibitively expensive and often impossible as in hazardous conditions.

The numerical or the computational approach focuses on discretising the governing equations and solving them by using Computer-Aided Engineering (CAE) softwares, the solution is approximate and not exact. The approach has been used widely in the fluid flow application as it is more cost-effective and more rapid than the experimental approach. The computational fluid dynamics has witnessed rapid growth since the advent of digital computers and following improvements in computer resources.

3.4 CFD Methodology

The computational fluid dynamics (CFD) is a tool for predicting fluid flow, heat and mass transfer, chemical reactions, and related phenomena by solving the set of governing mathematical equations numerically. The implementation of numerical simulations has led to several benefits for the scientific community including cost and time savings, improvement in product performance, and new product design and manufacturing.

The numerical simulation of fluid dynamics is closer to experimental than to theoretical fluid dynamics. The performance of each particular calculation on a computer closely resembles the performance of a physical experiment, in that the analyst turns on the equations and waits to see what happens, same as the physical experimenter does [110]. The CFD analysis complements testing and experimentation as it can provide information of all the relevant variables (such as velocity, pressure, temperature, turbulence intensity, etc.) throughout the domain where the probes in the

physical model cannot be used conveniently. Furthermore, the CFD analysis offers the opportunity to validate the experimental work.

The development of high powered, super-fast computers as well as the more efficient CFD software has significantly increased the use of the numerical methods in various branches of science and engineering such as aerodynamics of aircraft, hydrodynamics of ships, power plant combustion, internal combustion engines and gas turbines [111]. Many complicated problems can now be solved at very little cost and in a very short time by the computer. The approach is helping industry in testing new applications prior to the experimental investigation, which results in the development of new products and performance improvements.

3.4.1 CFD mechanism

The core of the CFD is based on the solving Navier-Stokes equations, which describe how the velocity, pressure, temperature and density of a moving fluid are related. The CFD approach is structured around solving the N-S equations numerically using a computer system. This approach allows easy access to the solvers and provides a deep examination of the outputs. Broadly, the CFD approach contains three successive elements: (a) pre-processing, (b) solver, and (c) post-processing.

3.4.1.1 Pre-processing

In the pre-processing stage, the problem of interest is being introduced to the solver, through identifying the geometry or the boundaries of the region of interest, i.e. the computational domain, the boundary conditions that are associated with the phenomena under investigation and the properties of the computational domain.

During this stage, a grid of the fluid domain is generated. The reason behind discretizing the fluid domain into small subdomains or elements is to transform the governing equations from partial differential form to the algebraic form, which can be solved computationally in iterative processes. Much as the accuracy of experimental data depends on the quality of the tools utilised, the accuracy of numerical solutions is dependent on the quality of discretizations used [112]. In general the larger the number of cells the better the solution accuracy. As the number of grid points becomes

very large, the solution of the algebraic equations is expected to approach the exact solution of the corresponding differential equation. However, large mesh numbers has always been computationally expensive and has led to the need for mesh independency analysis.

3.4.1.2 Solver

Presently there are three distinct approaches for solving the N-S partial differential equations. These are the finite difference, the finite volume and spectral method. Each method has its own advantages depending on the nature of the physical problem to be solved. The main differences between the three methods are associated with the way in which the flow variables are approximated and with the discretisation processes.

The spectral methods approximate the unknown by means of a truncated Fourier series or a series of Chebyshv polynomials. Unlike the finite element methods, the spectral use bases functions that are nonzero over the whole domain, in other word the approximations are not local but are valid through the entire computational domain. Such approach is known as a global-approach, where the computation at any given point depends not only on information at neighbouring points, but also on information from the entire domain [113].

The finite difference method is the easiest method to use for simple geometries. The special requirement of this method is the structured grids, as the grid lines serve as local coordinate lines, where the unknown of the flow problem is described by means of point samples at the nodal points of the grid coordinate lines. Truncation Taylor series is used to generate finite difference approximation of derivatives of the variable at each grid point and its immediate neighbours [111]. The results is one algebraic equation per grid node where the variable value appears as unknown. However, the restriction to simple geometries is a significant disadvantage in complex flows [114].

The finite volume method is one of the most frequently used methods for solving the partial differential equations that govern the fluid motion. It is an integral scheme integrating the governing equations over a control volume. The integral of the governing equations yield discretised equations, which are the key step of the finite

volume method. The concept of the finite volume algorithm is based on dividing the fluid domain into a finite number of contiguous control volumes (CVs), where the variable of interest is located at the centroid of the control element. The method consists of using a simple approximation of unknown variables to transform partial differential equations into algebraic equations. The resulting linear algebraic equations are then solved in an iterative fashion to obtain the distribution of the variable (φ) at nodal points [111].

This method requires intensive use of a computer and can be applied to solve almost all problems encountered in practice: steady or transient problems in linear and nonlinear regions for one-, two- and three-dimensional domains [115]. Nowadays most of the commercial codes such as STAR-CD, ABAQUS, ANSYS, etc. are finite volume based because it can accommodate any shape of grid and so it is suitable for complex geometries.

3.4.1.3 Post-processing

Post-processing CFD data is a vital step in order to accurately derive the right conclusions from the models. It is a useful tool to obtain a complete insight into fluid dynamics simulation results. Therefore, this element of the computational fluid dynamics has received a great attention and tremendous efforts have been made to develop it.

The modern CFD packages are now equipped with versatile data visualisation tools that offer different formats for visualising the simulation outputs such as; vector plots, line and shaded contour plots, domain geometry and a grid display, etc. The post-processing graphics outputs facilitate the communication of ideas to the non-specialists.

3.4.2 Conservation laws of fluid motion

The cornerstone of computational fluid dynamics is the fundamental governing equations of fluid dynamics—the continuity, momentum and energy equations. They are the mathematical statements of three fundamental conservation laws of physics upon which all of fluid dynamics is based:

- The mass of fluid is conserved.
- The rate of changes of momentum equals the sum of the forces on a fluid particle (Newton's second law)
- The rate of change of energy is equal to the sum of the rate of heat addition to and the rate of work done on a fluid particle (first law of thermodynamics).

3.4.2.1 Mass conservation equation

In fluid dynamics, the mass conservation equation or (continuity equation) states that the rate at which mass enters a system is equal to the rate at which mass leaves the system plus the accumulation of mass within the system. This can be expressed mathematically in Cartesian coordinates by [18]:

$$\frac{\partial \rho}{\partial t} + \frac{\partial \rho u}{\partial x} + \frac{\partial \rho v}{\partial y} + \frac{\partial \rho w}{\partial z} = 0 \qquad 3.5$$

Or by using the vector notation:

$$\frac{\partial \rho}{\partial t} + \rho \nabla . U = 0 \qquad 3.6$$

Both equations are unsteady, three-dimensional mass conservation or continuity equation for compressible fluid. Equation 3.6 consists of two terms; the first term on the left-hand side is the rate of change of density (mass per unit volume), if the fluid is incompressible, ρ = constant, independent of space and time, so that $\frac{\partial \rho}{\partial t} = 0$. The second term describes the net flow of mass out of the element across its boundaries and is called the convective term [116].

3.4.2.2 Momentum equation

The momentum equation is a statement of Newton's Second Law and relates the sum of the forces acting on an element of fluid to its acceleration or rate of change of momentum. Applying this to a fluid passing through infinitesimally, fixed control volume, yields the following equations:

The x-component of the momentum equation

$$\rho \frac{Du}{Dt} = -\frac{\partial p}{\partial x} + \frac{\partial \tau_{xx}}{\partial x} + \frac{\partial \tau_{yx}}{\partial y} + \frac{\partial \tau_{zx}}{\partial z} + \rho f_x \qquad 3.7a$$

The y-component of the momentum equation

$$\rho \frac{Dv}{Dt} = -\frac{\partial p}{\partial y} + \frac{\partial \tau_{xy}}{\partial x} + \frac{\partial \tau_{yy}}{\partial y} + \frac{\partial \tau_{zy}}{\partial z} + \rho f_y \quad 3.7b$$

The z-component of the momentum equation

$$\rho \frac{Dw}{Dt} = -\frac{\partial p}{\partial z} + \frac{\partial \tau_{xz}}{\partial x} + \frac{\partial \tau_{yz}}{\partial y} + \frac{\partial \tau_{zz}}{\partial z} + \rho f_z \quad 3.7c$$

Equations (3.7a-c) are x-, y-, and z-momentum equations, and the term (ρf) represents the body forces, which are characterized by buoyancy, and gravitational forces. The three scalar equations are known as Navier-Stokes equations. In Newtonian fluid, the shear stress (τ) is proportional to the time-rate-of-strain, i.e. velocity gradients [17].

$$\tau_{xx} = \lambda \nabla . \vec{V} + 2\mu \frac{\partial u}{\partial x} \quad 3.8$$

$$\tau_{xy} = \tau_{yx} = \mu \left(\frac{\partial v}{\partial x} + \frac{\partial u}{\partial y} \right) \quad 3.9$$

Other components of the stress tensor (τ) are available in the most of textbooks that concern fluid motion, for instance [117]. The three-dimensional form of Newton's law of viscosity for compressible flow involves two constants of proportionality: the dynamic viscosity, $\boldsymbol{\mu}$ and the bulk viscosity, $\boldsymbol{\lambda}$ that related to volumetric deformation $(\lambda = -\frac{2}{3}\mu)$ [116]. Replacing the values of viscous stress in the momentum equations yields the so-called Navier-Stokes equations:

$$\rho \frac{Du}{Dt} = -\nabla p + \mu \nabla^2 u + \rho f_x \quad 3.10a$$

$$\rho \frac{Dv}{Dt} = -\nabla p + \mu \nabla^2 v + \rho f_y \quad 3.10b$$

$$\rho \frac{Dw}{Dt} = -\nabla p + \mu \nabla^2 w + \rho f_z \quad 3.10c$$

3.4.2.3 Energy Equation

The energy equation derived from the first law of thermodynamics, which states that the rate of change in energy of a fluid particle is equal to the rate of heat addition to the fluid particle plus the rate of work done on the particle.

$$\left\{\begin{matrix} Rate\ of\ change \\ of\ enrgy \\ inside\ the\ fluid\ element \end{matrix}\right\} = \left\{\begin{matrix} Net\ flux\ of\ heat \\ into\ the\ element \end{matrix}\right\} + \left\{\begin{matrix} Rate\ of\ work \\ done\ on \\ the\ element\ due \\ to\ body\ and \\ surface\ forces \end{matrix}\right\}$$

The rate of change of energy of a fluid particle per unit volume is given by $\rho\frac{DE}{Dt}$. The total rate of work done on a fluid particle by a surface stresses can be expressed as per Equation 3.11 [111].

$$Work = -\nabla.(pu) + \frac{\partial(u\,\tau_{xx})}{\partial x} + \frac{\partial(u\,\tau_{yx})}{\partial y} + \frac{\partial(u\,\tau_{zx})}{\partial z} + \frac{\partial(v\,\tau_{xy})}{\partial x} + \frac{\partial(v\,\tau_{yy})}{\partial y} + \frac{\partial(v\,\tau_{zy})}{\partial z} + \frac{\partial(w\,\tau_{xz})}{\partial x} + \frac{\partial(w\,\tau_{yz})}{\partial y} + \frac{\partial(w\,\tau_{zz})}{\partial z} \quad 3.11$$

The net rate of heat transfer to the fluid particle due to heat conduction across element boundaries can be written as:

$$-\nabla.q = K\nabla^2 T \quad 3.12$$

Any other sources of energy (S_h) to the system should be taken in the consideration and added to the energy equation. The final form of the energy equation become:

$$\rho\frac{DE}{Dt} = -\nabla.(\rho u) + \left[\frac{\partial(u\,\tau_{xx})}{\partial x} + \frac{\partial(u\,\tau_{yx})}{\partial y} + \frac{\partial(u\,\tau_{zx})}{\partial z} + \frac{\partial(v\,\tau_{xy})}{\partial x} + \frac{\partial(v\,\tau_{yy})}{\partial y} + \frac{\partial(v\,\tau_{zy})}{\partial z} + \frac{\partial(w\,\tau_{xz})}{\partial x} + \frac{\partial(w\,\tau_{yz})}{\partial y} + \frac{\partial(w\,\tau_{zz})}{\partial z}\right] + K\nabla^2 T + S_h \quad 3.13$$

3.4.3 Grid topology

The first step of CFD simulation is to prepare the model for analysis. Therefore, to analyse fluid flow, the fluid domains are split into smaller subdomains in a process known as meshing. The governing equations are then solved inside each of these subdomains numerically.

The mesh applied to the model is extremely important as it dictates solution accuracy and model run time. Some mesh generators enable the user to create unstructured and/or structured meshes, to suit a particular application. The unstructured mesh is represented by the triangular elements (2D)/tetrahedral (3D) whereas the structured grid is represented by the quadrilateral (2D)/ hexahedral (3D). However, it is possible to have wedges and pyramids elements in (3D) to match specific boundaries through the model, Figure 3.8 shows structured and unstructured grid for a 2D model.

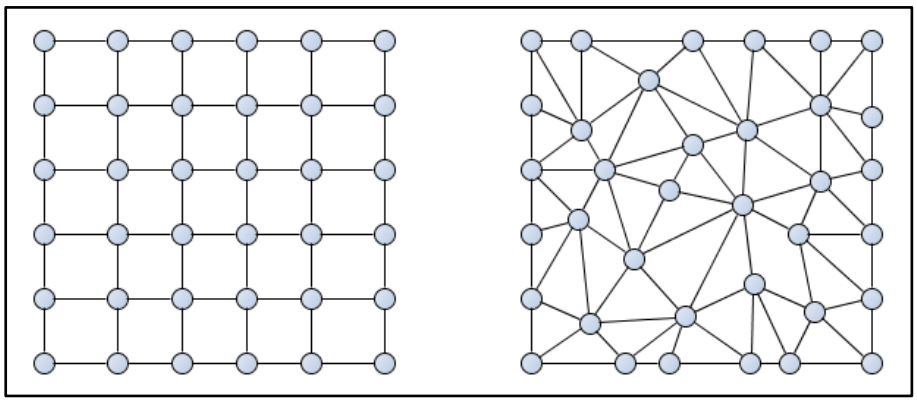

Figure 3.8: Structured (left) and unstructured (right) meshes [118]

The structured mesh follows a uniform or repeated pattern where every node is uniquely defined and indexed according to a specified algorithm; whereas the unstructured mesh is distributed randomly and no regular pattern is followed. Moreover, the nodes in the unstructured grid might cluster heavily at some areas through the geometry and that would create a non-uniformly discretised mathematical model, which would require more work to improve mesh quality.

Each cell in the discretised model is used to define nodes where fluid properties are calculated. The solution is iterated at each node based on the values obtained from the

neighbouring nodes. Thus, a high number of elements results in a higher number of nodes and ultimately more calculations required, i.e. higher computational time.

In a structured grid, unlike the unstructured, a node is surrounded by an equal number of neighbouring nodes, which are defined according to a specified pattern. This facilitates the loop through the orderly indexed neighbours during the numerical solution, and no large computational memory would be required for storing elements, nodes and connectivity table of these nodes [118, 119].

In order to, adequately, resolve the boundary layer near the boundaries, the mesh inflation concept was used in this study. This concept concerns accommodating higher number of cells in the direction normal to the boundaries, which are subjective to the boundary layer formation [120].

3.4.4 Solution convergence

For any iterative numerical technique, each successive iteration results in a solution that moves progressively closer to the true solution. This is known as convergence. A numerical method is not always guaranteed to produce converging results. Convergence is subject to satisfying certain conditions. If these conditions are not met, the solution would experience some errors

In numerical computations, the term error refers to the difference between an approximate solution and the exact solution of the partial differential equations. The degree to which the approximate solution approaches the exact solution as space and time increments become smaller and smaller is called convergence of the finite difference representation.

There are some factors that can hinder the solution to achieve convergence, such as size and number of computational cells, inappropriate model selection. Convergence is often measured by the level of residual and monitoring relevant integrated quantities such as drag/lift coefficients.

3.5 CFD Fluent Solver

Fluent is a CFD solver based on finite volume method and it is integrated into ANSYS Workbench. It can simulate a wide range of phenomena: aerodynamics, combustion, hydrodynamics, mixtures of liquids/solids/gas, particle dispersions, reacting flows, heat transfer, etc. Steady-state and transient flow phenomena are easily and quickly solved.

The finite volume method is based on dividing the computational fluid domain into small subdomains or control-volumes where the governing partial differential equations for the conservation of mass, momentum, and scalars such as energy, turbulence, and chemical species are integrated over each control-volume resulting in discretised equations for temperature, pressure velocity etc. The discretised equations are non-linear which is then need to be linearized to produce a system of equations for the dependant variable in every computational cell, in which the resultant linear system is then solved to yield an updated flow-field solution [121]. The variable of interest within the cell is then computed using the known and unknown values from the neighbouring cells. The most popular solution procedures are the TDMA (tri-diagonal matrix algorithm) line-by-line solver of the algebraic equations.

Fluent CFD solver employs two numerical methods namely; segregated solver and coupled solver, both have similar discretization process of finite-volume, but the approach used to linearize and solve the discretized equations is different. The segregated approach solves the non-linear governing equations sequentially by performing several iterations of the solution loop before a converged solution is obtained, steps of iteration illustrated in Figure 3.9A.

The coupled solver solves the governing equations instantaneously all together. Because the governing equations are non-linear (and coupled), several iterations of the solution loop must be performed before a converged solution is obtained, Figure 3.9B shows steps of iteration in this approach.

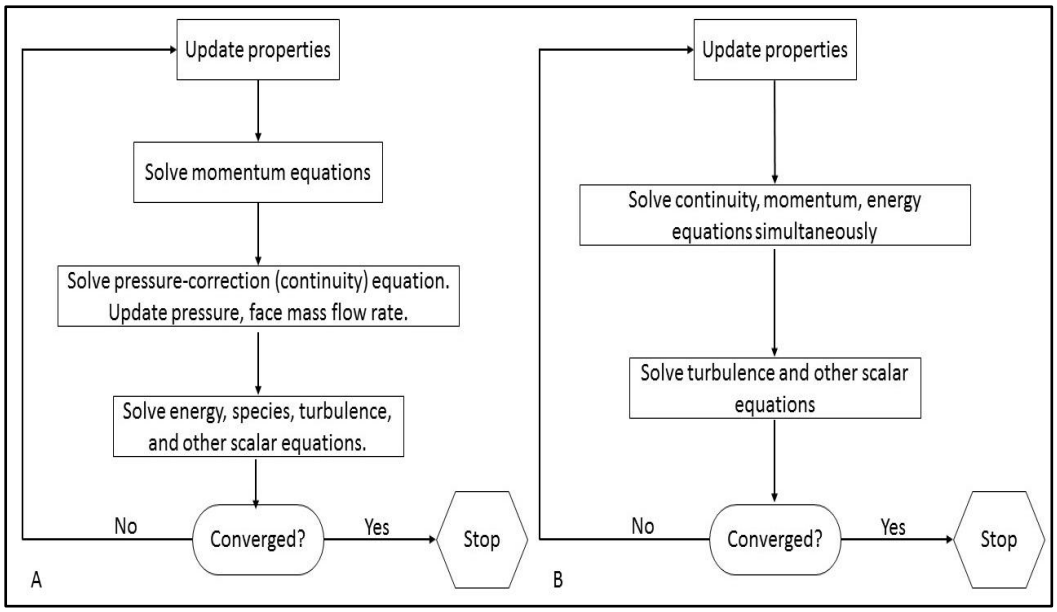

Figure 3.9: Overview of the segregate (A) and Coupled (B) solution methods [121]

ANSYS Fluent allows the user to choose one of the two numerical methods; pressure-based solver and density-based solver. In both methods, the velocity field is obtained from the momentum equations. In the density-based approach, the continuity equation is used to obtain the density field while the pressure field is determined from the equation of state [122]. On the other hand, in the pressure-based approach, the pressure field is extracted by solving a pressure or pressure correction equation, which is obtained by manipulating continuity and momentum equations.

Four segregated types of algorithms are provided in Fluent; PISO, SIMPLE and SIMPLEC. These schemes are indicated as the pressure based segregated algorithm.

3.5.1 Fluent mechanism

There are three main steps to the ANSYS/Fluent software. The first is CAD package, following by a grid generator and finally, the boundary conditions and physical models are assigned in the solver software.

The geometry file is imported into the grid generator package where the grid is produced, and boundary conditions are identified to the surfaces dictated by the geometry. The grid is then imported into the solver software, which embodies the physical models and facilitates adjustments to the grid and the boundary conditions.

The stages of producing a complete simulation are:

1. Create the model geometry and grid
2. Start the solver, import the grid, check the grid
3. Chose the equations to be solved
4. Specify the material properties
5. Specify the boundary conditions
6. Adjust solution control parameters
7. Initialise the flow field
8. Calculate a solution
9. Examine the results and consider revision

The main limitation of these analyses is the model run time. A large number of nodes, a long cycle time and small time steps will ultimately result in long solution run times. This may be minimised by grid improvements, nodes reduction and, use of larger time steps, all of which can be manipulated from within the main solver software.

3.5.2 Turbulence modelling in CFD

Turbulence modelling is one of three key elements in computational fluid dynamics alongside with grid generation and algorithm development. Virtually all engineering applications that contain fluid motions are turbulent and hence required a turbulence model to predict or examine the effect of turbulence. Because of the tremendous increase in the capability of digital computers, it has become possible to model the turbulent process using transport equations derived by the Navier-Stokes equation. There are four main categories of turbulence models:

1. Algebraic (zero-equation) Models
2. One-Equation Models
3. Two-Equation Models
4. Second-Order Closure Models

By definition, an **n**-equation model signifies a model that requires solution of (**n**) additional differential transport equations in addition to those expressing conservation

of mass, momentum and energy. Such additional equations are related to the kinetic energy of the turbulent fluctuation (k), the rate of dissipation of energy in unit volume and time (ω) and Reynolds-stress tensor [123].

3.5.2.1 Modelling turbulent flow in Fluent

Fluent provides a variety of mathematical models to suit the demands of individual types of problems. The optimal choice of turbulence model will depend on several considerations such as the physics encompassed in the flow, the level of accuracy required, the available computational resources, and the amount of time available for the simulation as well as the capabilities and limitations of the various options.

Turbulence models available in Fluent are [124]:

- Spalart-Allmaras Model
- k-$\boldsymbol{\varepsilon}$ Models
  - Realisable k-ε Model
  - Standard k-ε Model
  - RNG k-ε Model
- k-$\boldsymbol{\omega}$ Models
  - Standard k-$\boldsymbol{\omega}$ Model
  - Sear stress transport (SST) k- $\boldsymbol{\omega}$ Model
- v^2-f Model
- Reynolds stress Model (RSM)
- Detached eddy simulation (DES) Model
- Large eddy simulation (LES) Model

Table 3.1 shows the RANS Models with a brief description of their most important features and applications. The RSM model was used in the numerical simulation of the present research.

Table 3.1: RANS turbulence models in Fluent

Model	Feature	Description
Spalart-Allmaras model	One equation model	Designed especially for aerospace applications, involving wall-bounded high speed flow
Standard k- ε model	Two equation models	Robust. Valid for fully turbulent flows only
(RNG) k- ε models	Variant of standard k- $\boldsymbol{\varepsilon}$ Has an additional term in equation	Capability in modelling highly strained and swirling flows.
Realisable k- ε model	Variant of Standard k- $\boldsymbol{\varepsilon}$ model New formulation for turbulent viscosity New transport equation for $\boldsymbol{\varepsilon}$	Suggested for flows with boundary layers under strong adverse Δp, separation and recirculation.
Standard k-ω model	Solves for k-$\boldsymbol{\omega}$ $\boldsymbol{\omega}$ = Specific dissipation rate ($\boldsymbol{\varepsilon}$/k)	Recommended for low-Re Flows, for wall boundary layer, and for transitional flows
(SST) k-ω model	Variant of Standard k- $\boldsymbol{\omega}$ model Behaves like k- $\boldsymbol{\omega}$ in near wall region Behaves like standard k – $\boldsymbol{\varepsilon}$ in the free stream	More accurate and reliable for a wider class of flows, like adverse Δp in aerofoils, transonic shock waves, etc.
Reynolds stress model	Five equation model	Suitable for complex 3D flows with strong swirl / rotation. Run time and memory intensive

3.5.2.2 RSM model

The RSM accounts for the effects of streamline curvature, swirl, rotation, and rapid changes in strain rate in a more rigorous manner than one-equation and two-equation models, it has greater potential to give accurate predictions for complex flows. It is able to capture complex strains like swirling flows and secondary flows. For swirling flows, such as cyclones, RSM is the only accurate closure.

The RSM closes the Reynolds-averaged Navier-Stokes equations by solving transport equations for the Reynolds stresses, together with an equation for the dissipation rate. This means that five additional transport equations are required in 2D flows and seven additional transport equations must be solved in 3D.

The exact transport equations for the transport of the Reynolds stresses $\rho\,\overline{u_i' u_j'}$ may be written as follows:

$$\frac{\partial}{\partial t}\left(\rho\,\overline{u_i' u_j'}\right) + \frac{\partial}{\partial xk}\left(\rho uk\,\overline{u_i' u_j'}\right) = -\frac{\partial}{\partial xk}\left[\rho\,\overline{u_i' u_j' u_k'} + \overline{p\left(\delta_{kj}\,u_i' + \delta_{ik}\,u_j'\right)}\right] + \frac{\partial}{\partial xk}\left(\mu\,\frac{\partial}{\partial xk}\,\overline{u_i' u_j'}\right) - \rho\left(\overline{u_i' u_k'}\,\frac{\partial u_j}{\partial x_k} + \overline{u_j' u_k'}\,\frac{\partial u_i}{\partial x_k}\right) - \rho\beta\left(g_i\,\overline{u_j'\,\theta} + g_j\,\overline{u_i'\,\theta}\right) + \overline{p\left(\frac{\partial u_i'}{\partial x_j} + \frac{\partial u_j'}{\partial x_i}\right)} - 2\mu\,\overline{\frac{\partial u_i'}{\partial x_k} + \frac{\partial u_j'}{\partial x_k}} - 2\rho\Omega_k\left(\overline{u_j' u_m'}\,\epsilon_{ikm} + \overline{u_i' u_m'}\,\epsilon_{jkm}\right) + S_{user} \qquad 3.14$$

The model was developed from work by P. Chou [125]. In Reynolds Stress Models, the eddy viscosity approach is avoided and the individual components of the Reynolds stress tensor are directly computed. These models rely on the exact Reynolds stress transport equation.

Limitations of RSM include:

- Computational expense
- Sensitivity to initial conditions
- Amount of modelling required
- Requirement of high-quality mesh

3.6 Summary

This chapter describes both the experimental and CFD approaches, along with the methodology to operate them.

Firstly, the experimental techniques were described including the equipment used and their specifications. A wind tunnel with dimensions of 1200*1200 mm equipped with a rotating cylinder with a diameter of 12 mm was used as the test rig. LDV technique for velocity measurements was described.

Secondly, descriptions of the Computational Fluid Dynamics (CFD) techniques and turbulence models used in this work were presented. CFD is presented as an important tool in simulating a variety of industrial process. The main function of CFD is to analyse fluid flows and heat transfer. Fluent ANSYS was used to analyse the flow in the batch annealing furnace.

CHAPTER 4:

ENERGY ANALYSIS OF THE HTCA FURNACES

Chapter 4

Energy Analysis of the HTCA Furnaces

4.1 Introduction

The increase in the energy prices and the global warming problem have resulted in an increased emphasis on energy efficiency measures. Large energy-consuming industries are interested in energy efficiency to control costs and ensure competitiveness. Government policies are trying to encourage industries to set targets for energy efficiency and establish energy benchmarking [126].

The term of *energy efficiency* refers to using less energy to produce the same amount of services or useful output. Energy efficiency assists industrial companies or facilities in understanding how they use energy and help to identify the areas where waste occurs and where opportunities for improvement exist [127]. It is also considered as one of the key instruments to restrain growing global energy demands and therefore to abate greenhouse-gas emission. The energy benchmarking process involves estimation of the best possible performance for a given process by analysing and comparing the outcomes of the energy efficiency measures. It is a powerful tool to assess a company's performance relative to that of its competitors.

Cogent Power, one of the largest steelmaking specialised facilities across the UK, is renowned for its high-quality products, although the company appreciates that there is considerable scope for energy efficiency improvements. Cogent pays roughly ~£1M a month on energy consumption, indicating the scope for efficiency improvement. Therefore, this chapter aims to establish the potential for improvement through the analysis of energy consumption in the high-temperature annealing unit, one of the most energy-intensive units in the production route of the grain-oriented electrical steel. The analysis will identify the most prominent contributors to the high energy consumption, as well as establish an energy performance benchmark for the present study.

4.2 HTCA Unit Topology and Monitoring

The HTCA unit at Cogent consists of eight batteries indexed from A to H, Figure 4.1. Each battery contains of four bases (hearths) except battery C, which has only two bases.

The annealing cycle at each base is monitored carefully, by the HTCA monitoring system. The system helps the operators of the HTCA furnaces to be updated of the process status. Figure 4.1 shows, in detail, the status of each charge, though some details have been hidden to protect confidentiality. Some of these details such as cycle no., soaking time and cycle duration are of relevance to energy consumption and productivity statistics. Therefore, these are always recorded and saved in charge history records for every single charge.

Figure 4.1: Annealing furnaces battery status

Each battery is provided with two power supplies that are indexed (supply A & supply B). The four bases of each battery are competing for only two supplies, except battery C for which the number of supplies is equal to the number of hearths, making it more productive than other batteries. Figure 4.2 shows the number of steel charges that are

processed in the HTCA unit at the different batteries. Battery C had the greatest number of processed steel charges over the time period considered. However, the scheduling of the processes is tailored in accordance with the batteries' capacity to ensure attaining maximum productivity for all batteries in the HTCA unit.

There are 25 furnaces in use at the HTCA unit, and different furnaces can be applied to different bases. The single furnace can be applied to the following base immediately after being lifted from a completed cycle, unless some maintenance work is required. The continuous use of the furnace before it cools down, could save time and energy required to heat the structure of the furnace including refractory, internal supports, etc. up to the operating temperature [128].

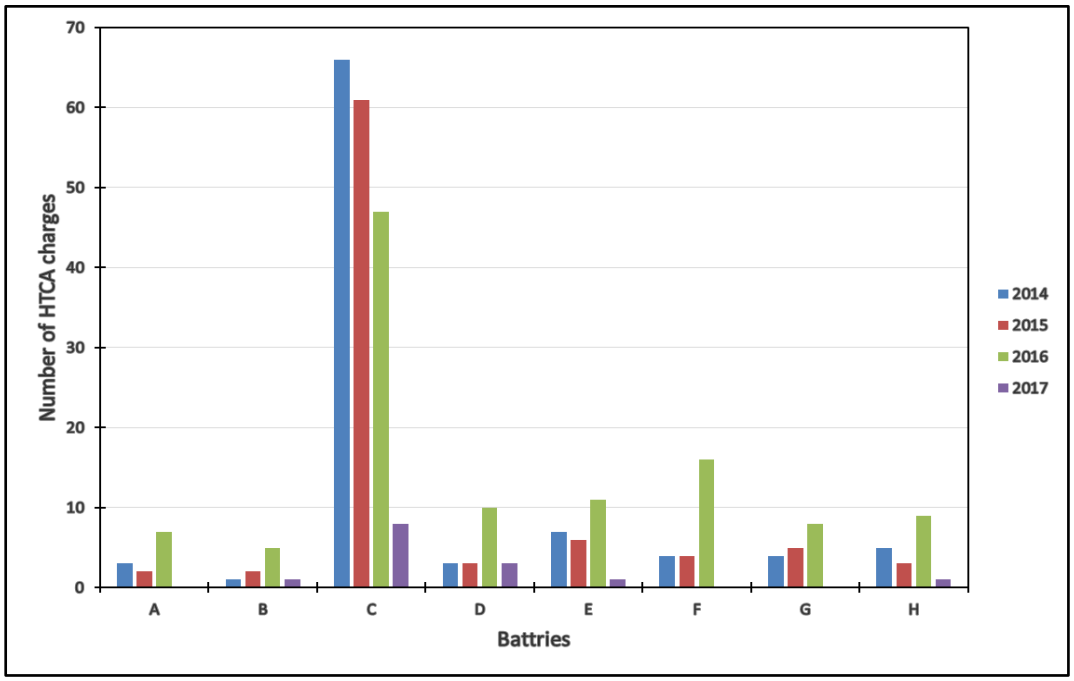

Figure 4.2: HTCA batteries productivity statistics for the years 2014 to 2016

Figure 4.3 shows the monitoring screen of the four bases in one of the HTCA's batteries. The four bases are working in a harmony that is when two bases are running the other two bases are either being discharged of the steel coils or being prepared for a new cycle. Once the process ends at one of the occupied bases, the supply can then be reconnected immediately to another base, and a new cycle commences.

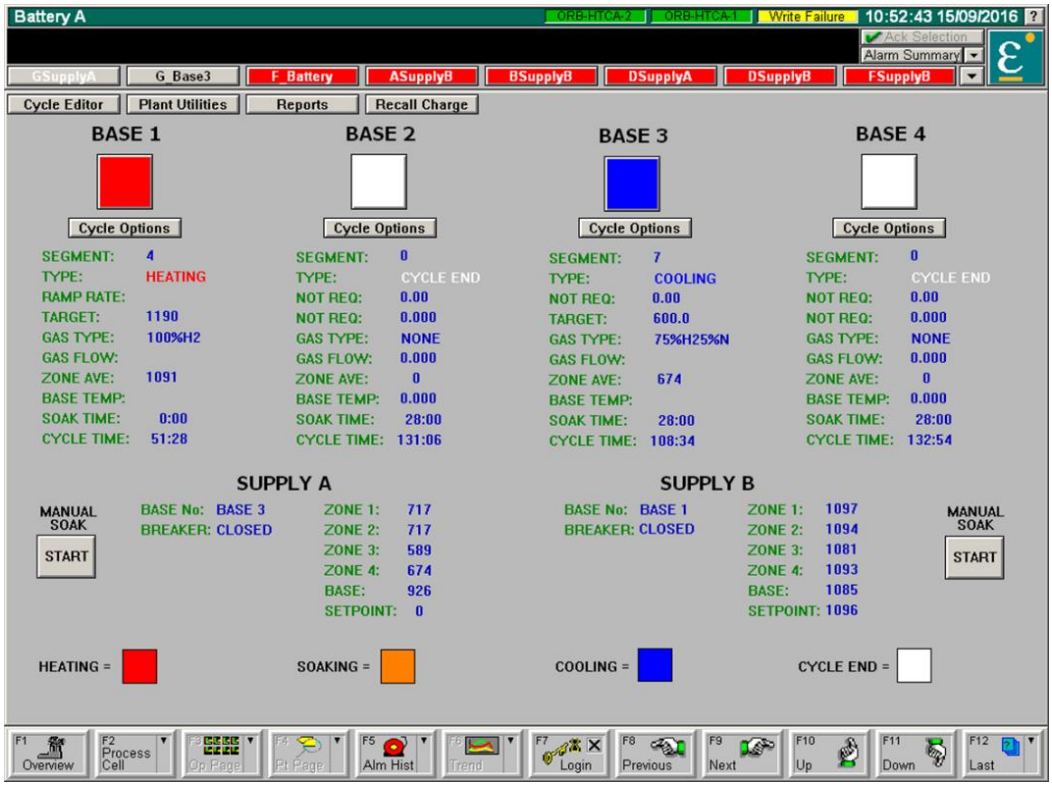

Figure 4.3: Battery and base monitoring

4.3 Grain-Oriented Electrical Steel Cycles

Cycles of steel charges are indexed according to the coil material and the strip thickness. The data collected from Cogent Info Hub shows that the cycles which are processed during the period from 2014 to 2016 were DMR01, DMR05, DMR35, NB01, NB02, NB03 and NB06 as shown in the Figure 4.4. Each one of these codes represents a Cogent HTCA cycle that has special annealing requirements for number of heating, soaking and cooling segments, heating rates and gas compositions.

The statistical Figures show that, broadly, the most processed cycles were DMR01, DMR05 and NB02. The steel strip gauge in those cycles are varied; 0.23 mm, 0.27 mm and can reach up to 0.30 mm and 0.35 mm in the DMR05 cycle. Each cycle has specific annealing requirements of number of heating and soaking segments. The main difference between DMR01/DMR05 and NB02 is that the latter is soaked at 1190 C for 28 hours, whereas the other two cycles are soaked twice, one at 710 C for 15 hours and another soaking stage at 1190 ^{o}C for 28 hours. Figure 4.5 shows the heating cycle of NB02 (top) and DMR05 (bottom).

Hence, some cycles required slightly longer/shorter time than the other HTCA cycles. Any extra hours added to the cycle time by the process system is to compensate any deficiency in the thermal profile.

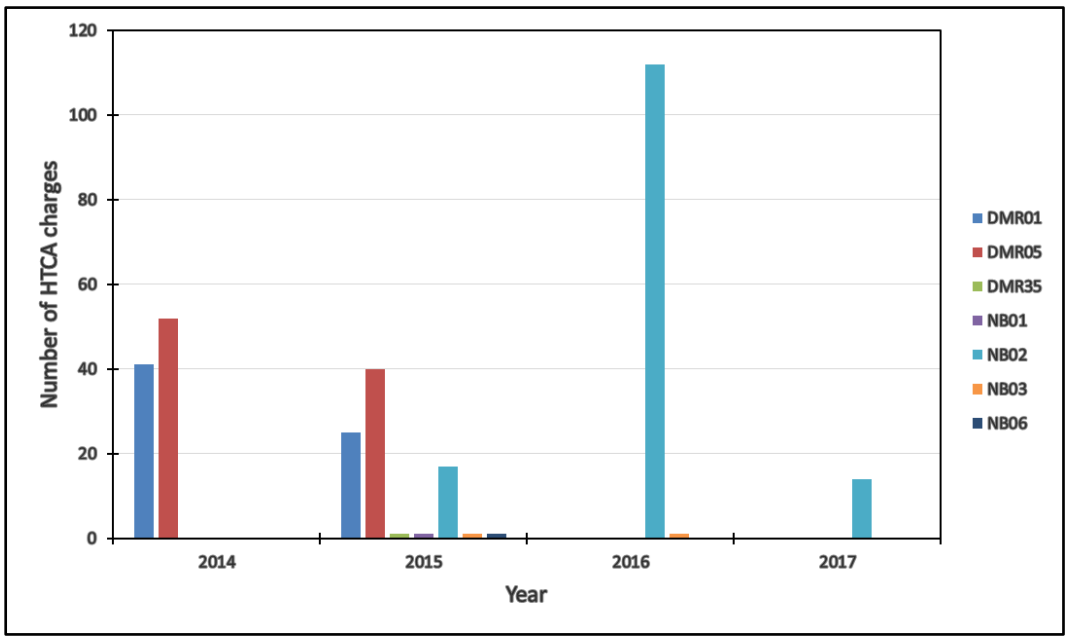

Figure 4.4: Cycle production productivity statistics

For a typical annealing cycle, the total heating time is 67-72 hours, total soaking time 28 hours and total cooling time is 33 hours. However, the annealing process sometimes experiences the occurance of some events that distrub the process, such as failure of the heating element which affects the heating time, and fan failure which affects the cooling time. To examine the effect of various parameters on the energy consumption at the HTCA furnaces, some data was collected and analysed, as shown in the following section.

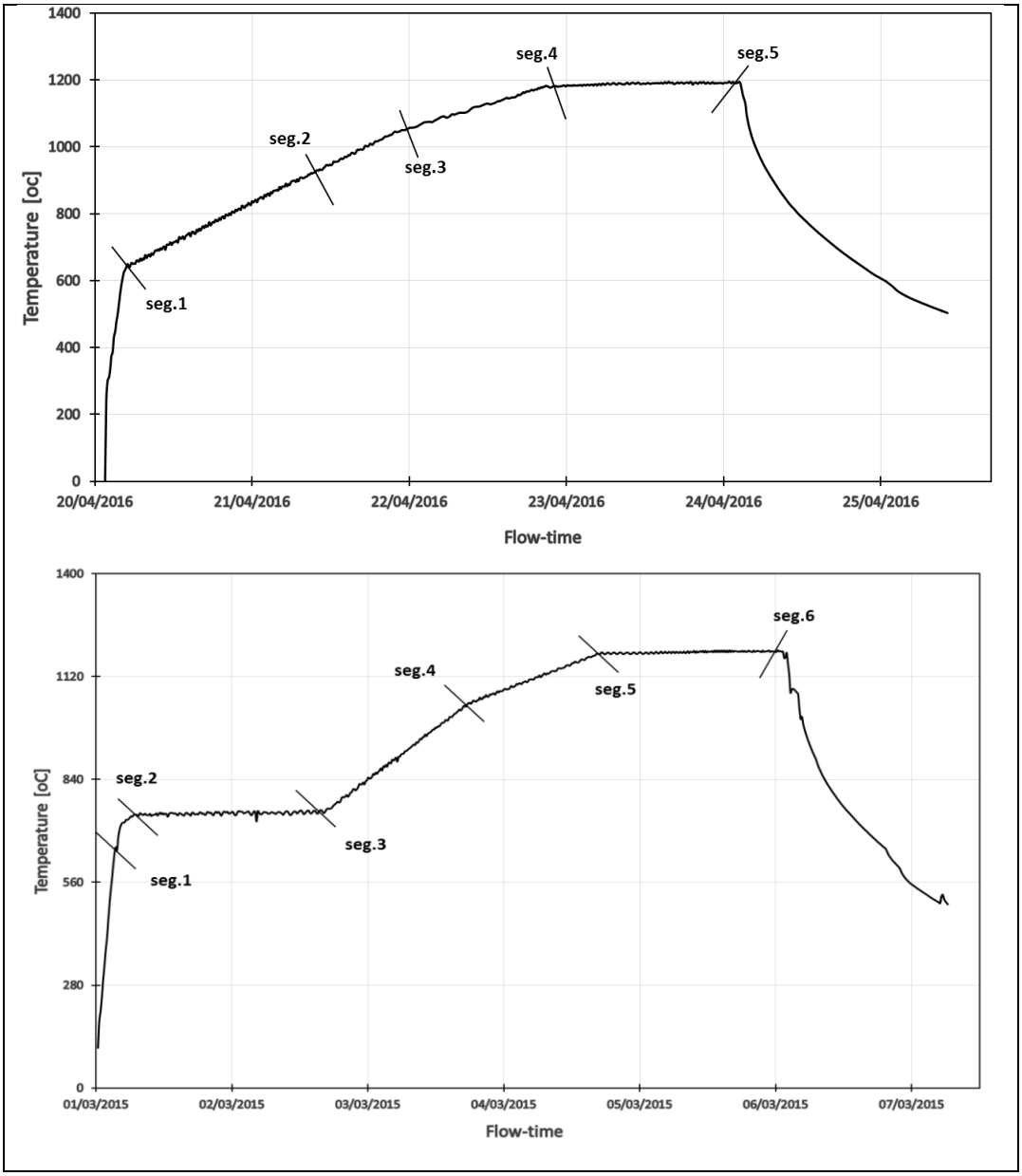

Figure 4.5: Full annealing thermal cycle of NB02 (top) and DMR05 (bottom)

4.4 Data Collection

The raw data that was collected from Cogent Info Hub represents the daily records of the energy consumption of the eight batteries of the HTCA unit. The data was collected for years; 2014, 2015, 2016 and up to week 22 of 2017.

The daily energy consumption records were first processed to identify a time interval when there is only one charge of steel coils in process at the appointed battery. This task required careful attention, as the data contains some energy overlapping which

causes difficulties in identifying the time interval for a single steel charge, Figure 4.6. The energy overlapping is mainly caused by the short time between two cycles at the same battery, as well as the direct usage of the same supply on another base during the same day, as discussed in section 4.2.

The criteria that were followed to check the samples was the standard duration of the annealing cycle that is 4 to 6 days, thus records for more or less than that period were considered as energy overlapping, Figure 4.6.

After identifying the sample of steel charges from the raw data, another set of data was used to collect the necessary information about every single charge such as charge number, cycle number, furnace number, charge weight and heating and soaking time.

About 300 sample of charges were collected for years 2014, 2015, 2016 and 2017, Figure 4.7, and examined to evaluate the effect of some energy consumption contributors.

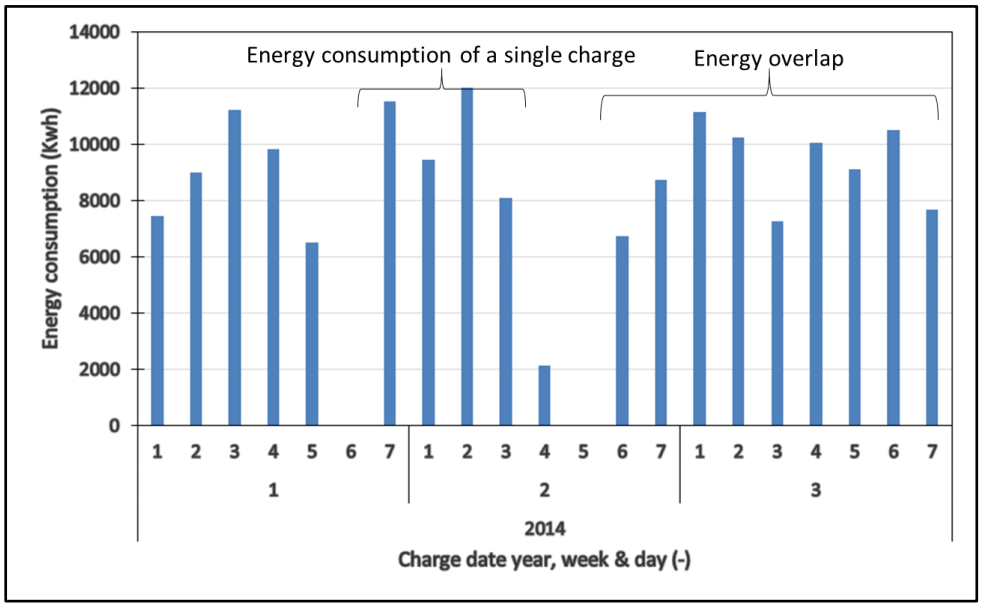

Figure 4.6: The daily records of the energy consumption of the steel charges

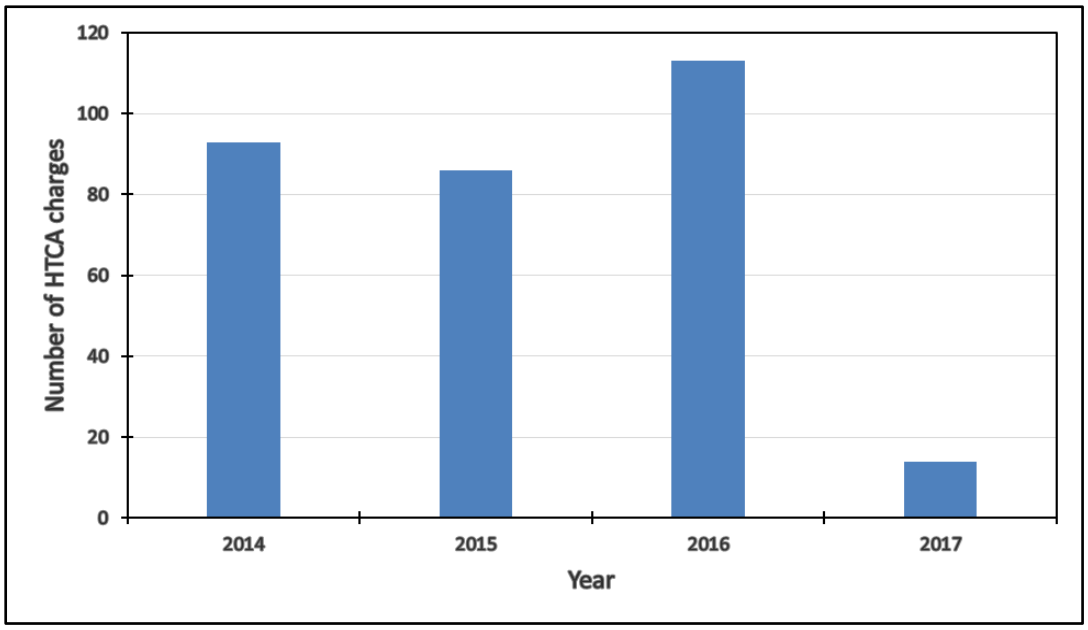

Figure 4.7: Collected charge samples

4.5 Energy Consumption Contributors

Investigating the different process parameters and identifying the parameters that influence energy consumption most, is the first step towards energy saving. This section was devoted to exploring two potential energy consumers namely (i) the charge weight and (ii) the process on-time using the data collected from Cogent Info Hub.

Figure 4.8 shows the distribution of consumed energy (kWh) of HTCA charges during the years 2014 to 2017. Charges of energy consumption 24,000 to 28,000 kWh were considered as outliers and were omitted from further energy analysis. They represent only 1% of the collected charges as well as showing significant differences to values in a range of samples. Furthermore, the omission of the outliers was based on their frequencies over the time interval investigated, where similar values did not appear. The rogue observations were only noted in 2014 and disappeared in the following years of the period covered.

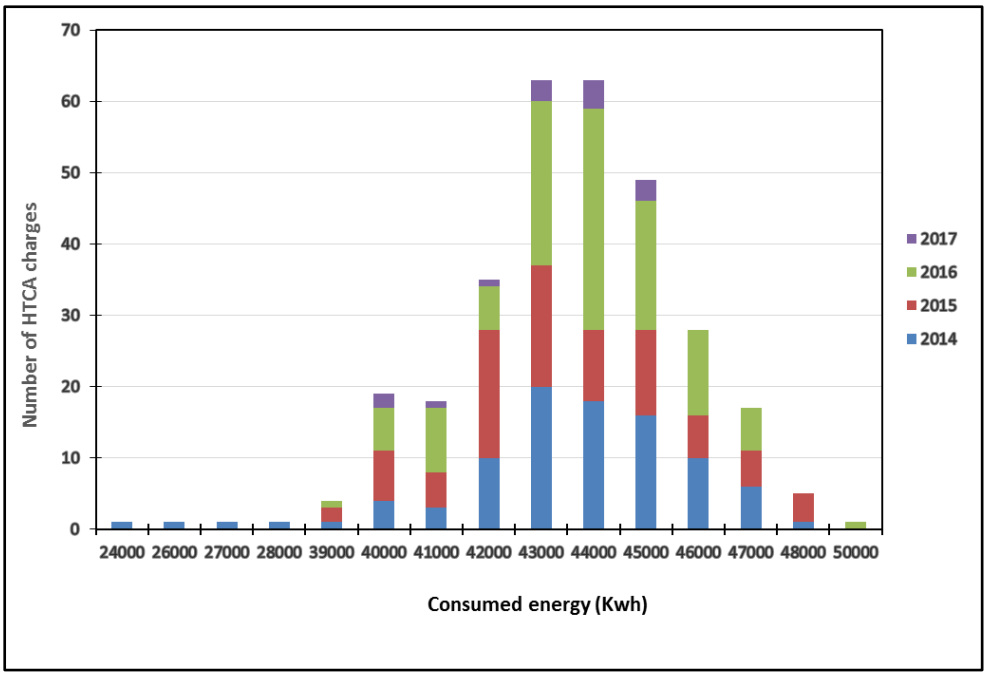

Figure 4.8: Distribution of energy consumed in HTCA charges

In the following sections, two different energy consumption contributors will be investigated; the charge weight and cycle's on-time. The coefficient of determination was used to gain insight into the degree of dependency of the energy consumption on the variation of those contributors.

The correlation coefficient (R^2) is a key output of regression analysis. It is interpreted as the proportion of the variance in the dependent variable (consumed energy) that is predictable from the independent variable (contributors).

For a linear regression model with one independent variable, R^2 can be calculated as:

$$R^2 = \{(1/N) * \sum[(X_i - \bar{X}) * (y_i - \bar{y})]/(\sigma_X * \sigma_y)\} \quad 4.1$$

where N is the number of observations/data, X_i is the X value for observation i, $\bar{X}$ is the mean X value, y_i is the y value for observation i, $\bar{y}$ is the mean y value, σ_X and σ_y is the standard deviation of X and y respectively [129].

The value of the coefficient ranges from 0 to 1, when R^2 =0 means that the energy consumptions cannot be predicted from the contributor and vice versa for R^2 =1. A

value between 0 and 1 indicates the extent of which the dependent variable is predictable.

4.5.1 Charge weight

The fuel economy of furnaces is commonly expressed in units of fuel or electrical energy expended to heat a unit weight of load [130]. A significant amount of heating energy is absorbed by the steel coils to achieve the required chemical changes during the heat treatment process. This heating energy is proportional to the charge weight. Therefore, it is considered as a useful energy and is quantified as:

$$Q = \dot{m} \int_{T_{initial}}^{T_{final}} c_p(T)\, dT \qquad 4.2$$

where C_p represents the specific heat capacity of the steel and it is a temperature dependent material properties. For electrical steel with a silicon concentration of 3.15%, the variation of the C_p value variations with temperature was reported by Buckley [131].

The theoretical energy which is required to heat 70 tonnes of steel to the annealing temperature of 1190 C was calculated using Equation 4.2 and it is roughly equal to 91.84 GJ. During the process, specific flow rates of gases, (H_2, N_2, and 3HN), are regularly added to the furnace at the ambient temperature, therefore heat is required to heat the injected gases. The theoretical energy was calculated based on the change in the gas enthalpies of the entrance state and the final state, which is varied throughout the segments. The total energy to heat the injected gases throughout the annealing process was found to be approximately 1.9 GJ.

A group of steel charges was chosen carefully to investigate the actual dependency of the energy consumption on the charge weight. A potential contributor such as abnormal long cycle time was omitted when selecting the group in order to obtain results as reliable as possible. The cycle time was set to be of a typical annealing process via setting up the soaking time to strictly 28 hrs.

Figures 4.9 and 4.10 show the consumed energy versus charges weight for NB02 and DMR05 cycles respectively. The figures show that it seems hard to predict the amount of energy required out of the charge weight during actual annealing process. For instance there are some charges of high weight consumed less energy than low weight charges. This mainly depends on the conditions of the process and the efficiency of the furnace used during the process.

The values of the R^2 coefficient 0.25 and 0.12, suggests that only 25% and 12% of the consumed energy is predictable from the charge weigh for the cycles NB02 and DMR05, respectively.

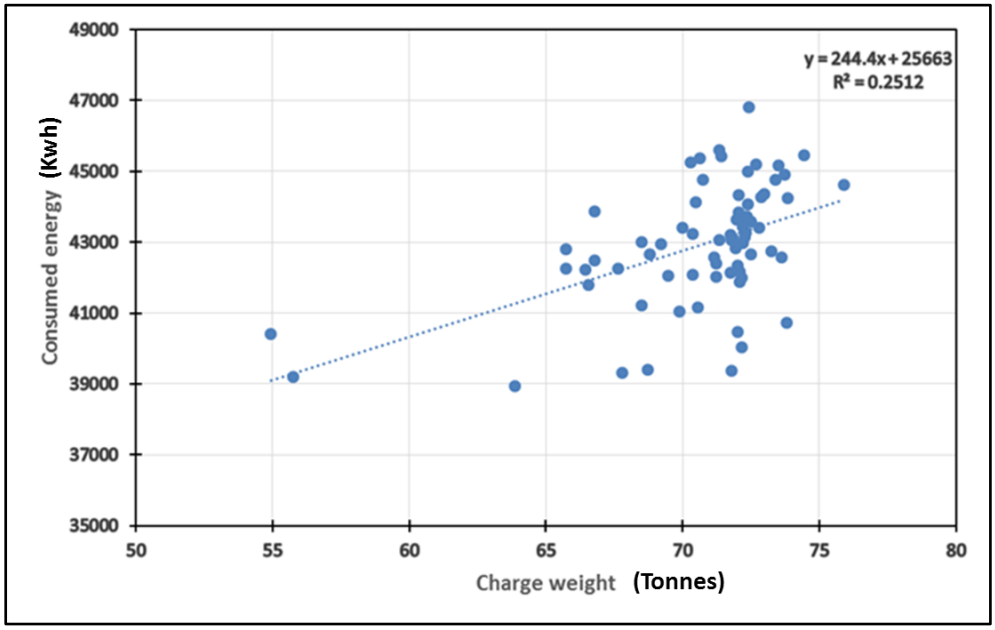

Figure 4.9: NB02 charges vs consumed energy

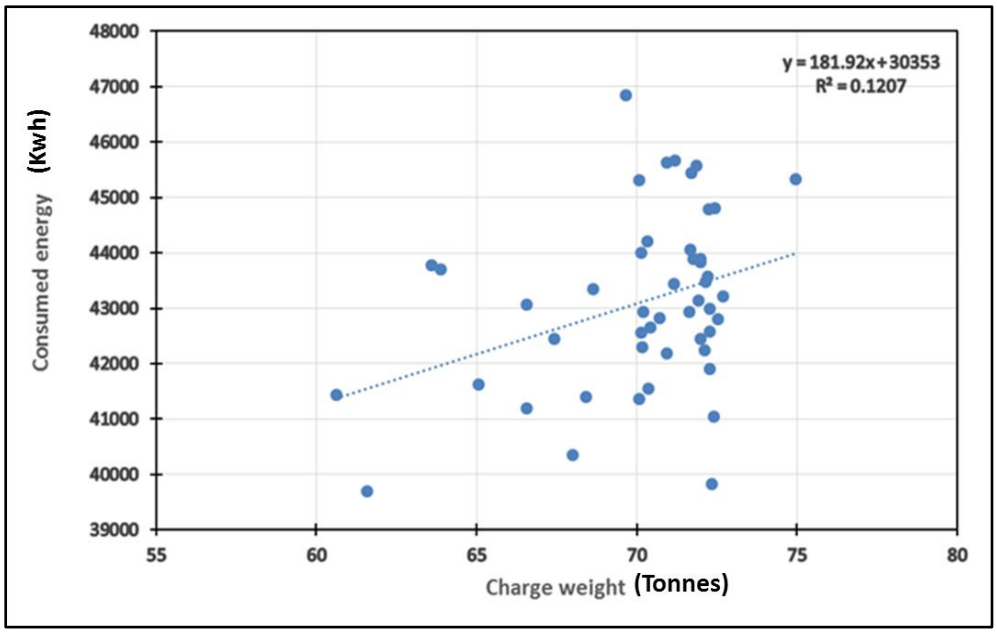

Figure 4.10: DMR05 charges vs consumed energy

4.5.2 Furnace on-time

The on-time represents the time interval when the furnace is in operation and this includes both heating and soaking segments together. It varies depending on the process conditions, such as cycle's specific requirements, furnace thermal condition, and any disruptive events occurring during the process. A group of charges of a weight range 70-72 tonnes was selected to examine how far the consumed energy can be predicted from the process on-time. Any disruptive events, which cause long cycle time, were omitted.

The electrical energy (E) consumed is proportional to the running time, and can be calculated from Equation 4.3, where t_{total} is the on-time and P is the active power load.

$$E = P\, t_{total} \qquad 4.3$$

It can be seen from Figures 4.11 and 4.12 that generally, the DMR05 cycle takes longer time than the NB02, which is due to the specific requirements dictated by the annealing process for the two cycles as explained in section 4.3.

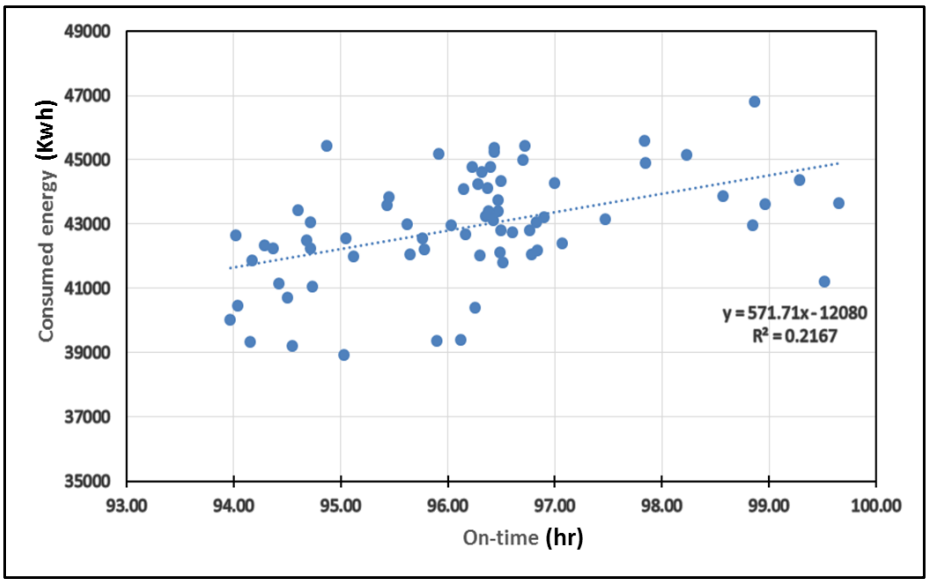

Figure 4.11: Consumed energy vs on-time for NB02

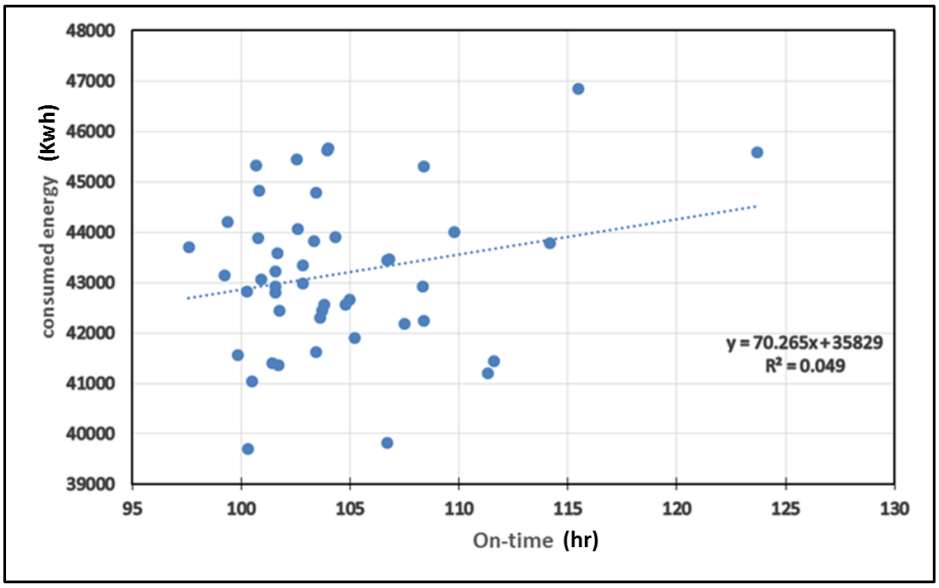

Figure 4.12: Consumed energy vs on-time for DMR05

It is observed that some charges are showing illogical discrepancies and disagreement with Equation 4.3. Some charges with high on-time consumed less energy than those cycle with low on-time. The coefficient of determination is also showing low degrees of predictions (21% & 4%) of the consumed energy over the cycle on-time 21% & 4%.

The following section will examine one of the most important factors that affect the annealing cycle time significantly. This is the electrical failure of the heating elements.

4.5.2.1 Heating elements of the HTCA furnace

The furnace is equipped with electrical heating elements situated underneath each base plate in the hearth and other elements are attached to the furnace's internal walls. Figure 4.13 shows the four heating zones of the furnace and their configuration and distribution.

According to the HTCA manufacturer (Almor Group) the existing HTCA furnaces at Cogent have a total connected thermal input of 770 kW gross. Based on a typical efficiency of 97% for the electric resistance heating elements, this gives a total available nett capacity of 747 kW. However, 87 kW nett input is in the hearth of the furnace underneath each coil stack. The heating elements that are located in the base only serve to maintain the refractory material in the base at temperature and applies very little heating to the product coil itself.

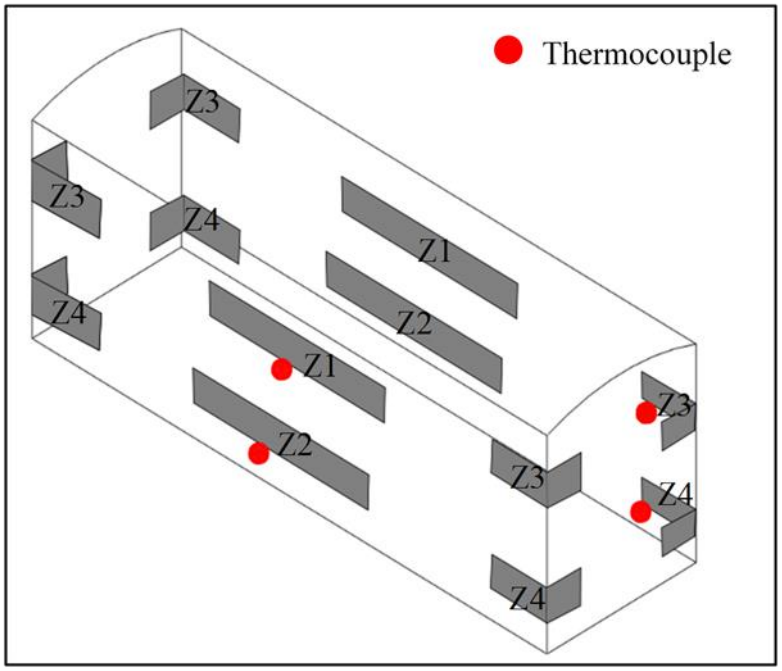

Figure 4.13: Schematic diagram of the furnace's heating elements and thermocouples distribution

The thermal profile of the process is monitored by thermocouples that are permanently installed at the base and the furnace internal walls, Figure 4.13. They are used to measure the temperature of the base plate and the furnace atmospheric temperature at the four different zones.

The elements work at their upper limit of performance and consequently need close monitoring to ensure they are fit for service. The state of each heating zone and the base is monitored by the HTCA monitoring system to detect any sag or failure in the heating elements during the annealing process. In the example shown in Figure 4.14, zone 4 is experiencing a sag condition during the process and is marked as a "fault". Any failure happening during the charge is reported in the charge history records.

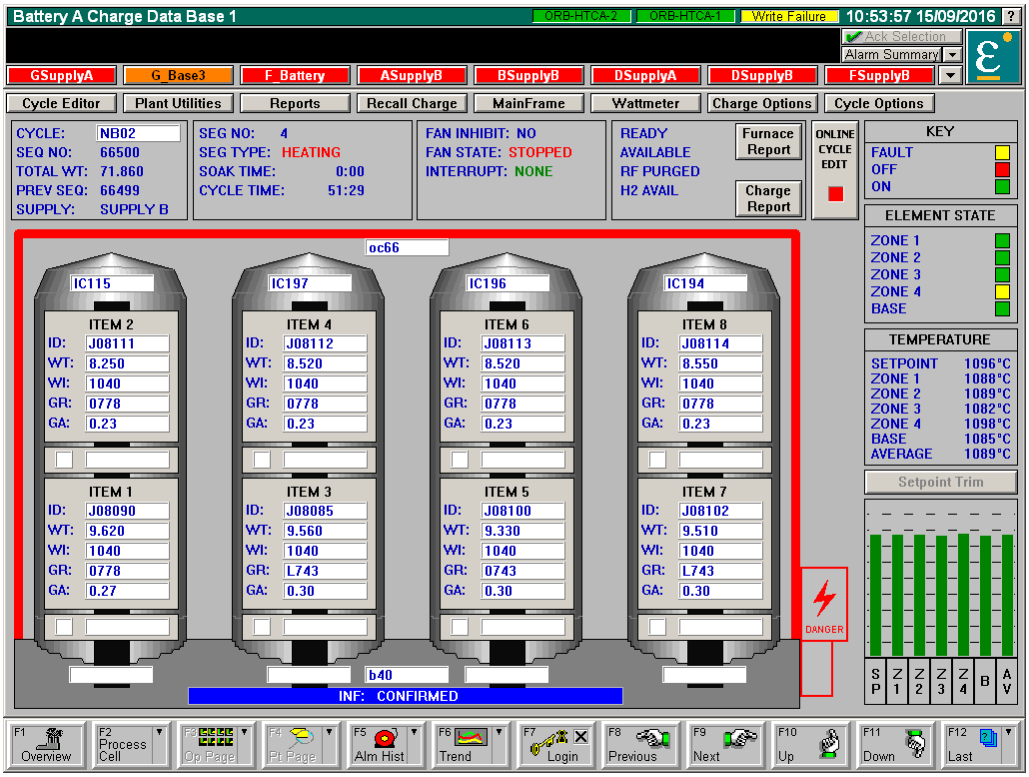

Figure 4.14: HTCA Charge details as displayed in the furnace monitoring system

Occasionally the elements sag or experience short circuit when the current cannot flow. An electrical failure in the hearth elements is considered more problematic than a wall element failure because a heat loss through the base material refractory will occur. This results in a zone with a deficit of heat which can subsequently mean that the coils in that area are not receiving the correct heat treatment, which affects the final product properties and the process duration, as well as the total energy consumed.

Figure 4.15 shows the energy consumption of steel charges that are annealed in typical annealing conditions in terms of soaking time 28 hr, heating time 67-72 hr and no failure events occurred. The HTCA charge weight was set at 70-72 tonnes.

Although the charges were processed in different furnaces with different efficiencies, the average consumed energy was ~ 42,000 kWh a value that is considered a standard consumption for processing a typical annealing cycle.

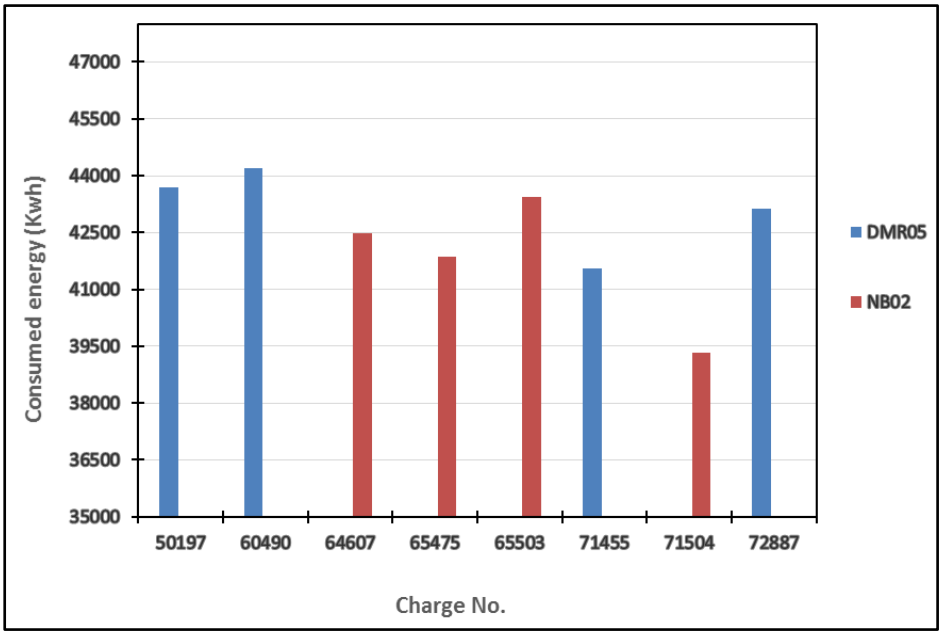

Figure 4.15: Energy consumption benchmarking NB02 and DMR05 during a typical annealing process

Figure 4.16 shows an energy benchmarking of the two most produced cycles, NB02 and DMR05. The samples of charges were selected carefully to emphasise the effect of a long process duration on the energy consumptions and how it relates to the events of electrical failure. All the selected chargers were within the weight range of 70-72 tonnes, and had experienced electrical failures in some of the wall and base heating elements and took exactly 36 hours for soaking at 1190 ^{o}C. During soaking time, energy is still being consumed both to maintain the soak temperature of 1190 ^{o}C and to allow some of the lagging parts of the coils (close to the inactive heating elements) to get to the temperature to the same value as for the high-temperature soak period.

Although the failure in the heating elements, some charges consumed less energy than other charges which had roughly same circumstances. The strong possibility is that the charges were processed in a furnace with a very high performance and low shell losses.

Therefore, the major energy consumer is the long cycle time, which is dramatically affected by the electrical failure in the heating elements. The failure may be due to erosion, hotspots or bad welds. A regular inspection enables the operators to detect any erosion, bad welds or physical damages in the elements in order to prevent any failure during the process. The elements operate at their operating limit and can create local hotspots which due to the lack of convection to take the excess heat away, can lead to element failure. Producing fluid circulation inside the furnace chamber can help in reducing hotspot thus eliminating the occurring of electrical failure.

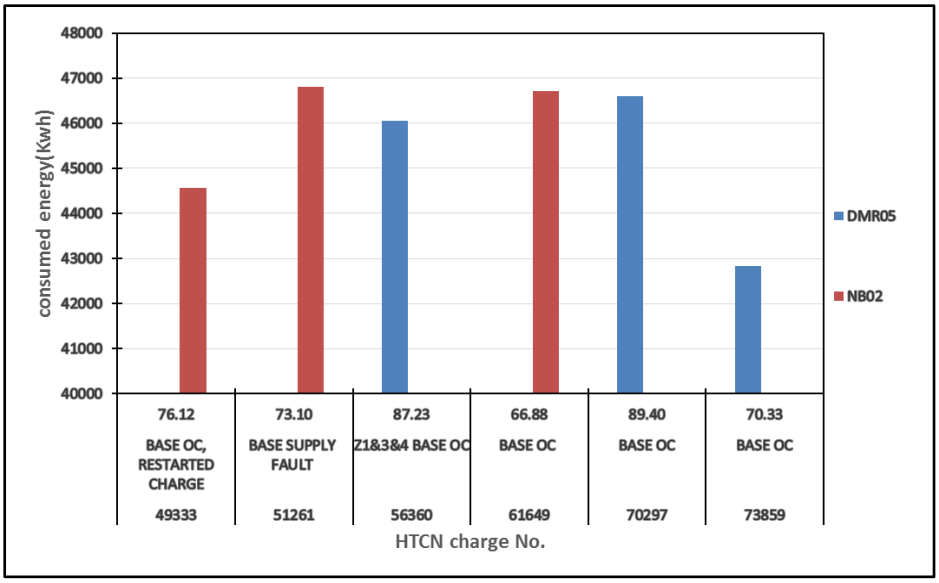

Figure 4.16: Energy consumption benchmarking for NB02 and DMR05 during electrical failure

4.6 Thermal Effeciency of HTCA Furnaces

An evaluation of the HTCA furnaces performance presented in this section is based on energy efficiency reports that were carried out in 2013 at Cogent [132]. The reports identified three main factors for the high energy consumption of the HTCA unit:

1. Losses through the furnace outer shell (shell losses)
2. Losses due to maintenance
3. Losses due to long thermal cycling

The design of the furnaces is over 50 years old, and the materials used for the lining allow significant heat loss from the casing. According to the reports, the losses from radiation and convection from the outside surface of the furnace through the completed heating and soaking stages of the annealing cycle was estimated of over 7 GWh per annum for all 25 furnaces. In monetary terms this equates to over £400,000, a figure which may increase with increases in energy prices.

The heat in the furnace at the time it is removed is lost, as it has to be cooled down to make any necessary maintenance or inspection. This has been reported as over 80 MWh per year across all 25 furnaces.

The losses due to long thermal cycling are based on the extra time and therefore energy that is lost when the heating cycle is extended due to open circuits occurring. These direct losses amount to over £50k per annum. This is due to typically an eight-hour extension to the cycle for a base open circuit and a two-hour extension for a zone open circuit.

The following section will focus on the performance of an ideal and actual HTCA furnace, in order to set a clear benchmark of the energy consumption in the HTCA system.

4.6.1 Ideal and actual furnace performance

The ideal furnace was assumed to be a brand new furnace. Unfortunately, the HTCA furnaces supplier Almor Group has never performed an energy analysis on newly fabricated furnaces. Thus, any data/information concerning energy consumption in a new HTCA furnace is not available. Therefore, the performance of an actual HTCA furnace will establish the energy benchmarking in the present study.

Figure 4.17 illustrates an energy flow diagram of a standard HTCA furnace. The energy provided to the furnace is mainly derived from electrical power inputs of about (~95%) and some residual heat (~5%) in the furnace refractory and internal components. During the annealing process, an amount of the heat supplied is lost from the furnace to the surroundings, which is characterised by the shell loss (~10%).

Another energy loss occurs through the heating of the inert gases (~20%), however, these losses have never alerted the total energy consumed during the cycle as the injected gases rapidly become hot when it is inside the sealed charge with the steel coils, inner covers and furnace elements. The remaining energy portion is absorbed by the steel mass and exchanged to achieve the chemical changes for secondary recrystallization within the steel coils, [133].

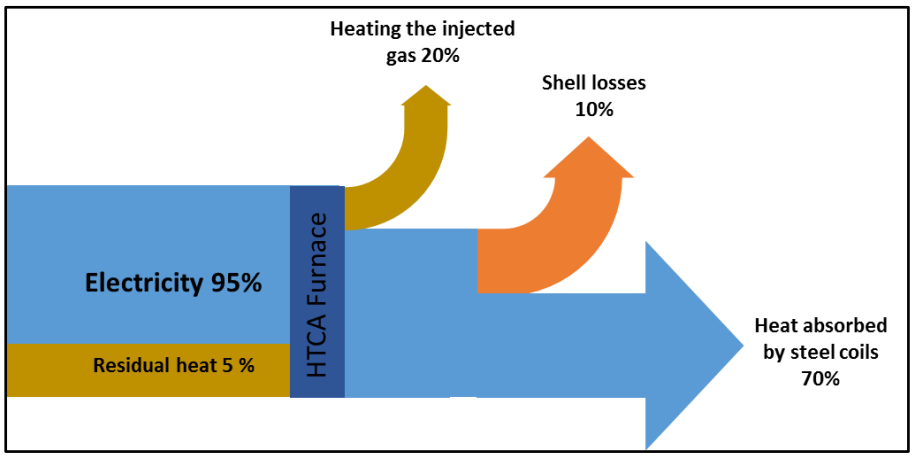

Figure 4.17: Energy flow diagram for HTCA furnace

Data of actual current records for steel charges were collected to calculate the actual energy consumption using MATLAB R2017a. Unlike the other calculations presented in the previous sections, these calculations focused on a specific HTCA furnace which its performance was classified to be a standard in terms of low shell losses, to establish the energy benchmark for this study. The steel charges were classified as red or green charges. This classification was based on the condition of the process. The charge was described to be a green charge when all the following conditions were fulfilled.

- No open circuits (furnace, base or supply)
- Hydrogen control normal
- Atmosphere pressure normal, 4mBar
- Charge weights similar with 8 positions occupied and top coil weights >7 tonnes
- Soak time 28 hours
- No interruption to charge
- Fan operational during cooling

The calculations showed that the average energy consumption in green charges was roughly 40,000 kWh, whereas, in red charges, that had exclusively experienced open circuit events (i.e. electrical failure) in the furnace heating elements, the average energy consumption was approximately 48,000 kWh. This means that about 8,000 kWh extra was consumed to compensate the thermal deficiency.

The energy consumption can be reduced by eliminating cycle duration. Shorter cycle time can be achieved by eliminating the occurrence of hotspots which are suspected to be the main reason for electrical failure. To achieve this, fluid recirculation needs to be introduced during the annealing cycle. Such fluid recirculation can help in redistributing heat inside the furnace chamber thus preventing the formation of the hotspots.

4.7 Summary

This chapter presents an energy analysis of the HTCA furnace for only the heating segments of the annealing process. Therefore, the energy consumed by the cooling system, including the centrifugal fan and the water pump of the heat exchanger, was not considered.

The data of about 300 charges was collected, processed and analysed to examine the energy consumption in the HTCA furnaces. Two potential contributors to the energy consumption were investigated, namely the charge mass and the furnace on-time.

The largest steel mass, the highest energy required to process it. However, reducing the steel mass to reduce the energy consumption eliminates the unit productivity.

The statistics show that the high on-time contributes more to energy consumption and it was found that the long process duration is mainly caused by the electrical failure of the heating elements during the process. Due to the failure, extra hours are added to the cycle to allow the steel charge to reach the annealing temperature. The failure occurs due to the formation of hotspots because of the lack of fluid recirculation.

A furnace of standard performance consumed approximately 8,000 kWh extra to overcome the thermal inefficiencies in a defective charge due to the electrical failure during the annealing process. Therefore, it is necessary investigating the opportunities of improving the thermal cycle in the HTCA furnace to eliminate the energy consumption via reducing the hotspots and the cycle time.

CHAPTER 5:

EFFECT OF A ROTATING CYLINDER ON THE FLOW STRUCTURE

Chapter 5

Effect of a Rotating Cylinder on the Flow Structure

5.1 Introduction

Cylinders are considered an excellent example of bluff bodies that facilitates understanding of vortex shedding phenomenon and vortex interaction in downstream flow. Good understanding of the phenomena related to these flows could have a considerable impact on the practical applications.

This research is proposing the using of the rotating cylinders to generate fluid instabilities in the HTCA furnace to introduce forced convection in order to overcome the thermal inefficiencies explained in Chapter 4.

This chapter is exploring, experimentally, the technique and its effect on the flow structure. Experimental results for a flow passing a rotating and non-rotating cylinder will be presented. A laser Doppler velocimetry (LDV) technique was used to examine the flow. Velocity profiles of different Reynolds number will be presented; the LDV data was analysed using MATLAB R2017a software to calculate turbulence related parameters such as turbulence intensity.

5.2 Experimental Setup

A laser Doppler anemometer explained in section 3.3, and the test rig described in section 3.2 were used to measure the instantaneous velocity components for a flow passing a rotating and non-rotating circular cylinder. The flow of interest was set at Reynolds numbers of 80, 120, and 160. The non-dimensional rotational rate α was set at 0 to 6 in step of 2, i.e. with an angular velocity range of $0 \leq \omega \leq 1800$ rpm.

The experiments aimed at examining the effect of rotation on the flow parameters, such as velocity and turbulence intensity, experimentally using the laser Doppler velocimetry technique.

The flow velocity was measured along the centreline of the cylinder wake, Figure 5.1. Ten measuring points were obtained, the distance between every two points is 10 mm.

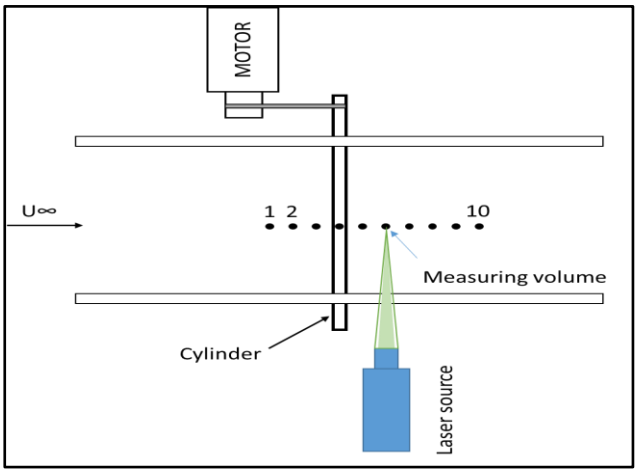

Figure 5.1: Top view showing the LDV measuring points

Smoke was utilized as a seeding since the densities of the smoke and air are close enough; this allows a good particle suspension. A smoke generator tool was used to generate the smoke, and it was located at the entrance of the wind tunnel so that the smoke particles can accurately follow the flow. The probe was set up at 45° from the horizontal to reduce the dispersion of the laser beams. The range of Reynolds number was chosen for the reason stated in section 3.2. Table 5.1 shows inlet and outlet velocities that are corresponding to the range of Reynolds numbers involved.

Table 5.1: Test parameters, inlet Re is based on cylinder diameter

V_{out} (m/s)	A_{out} (m^2)	V_{in} (m/s)	A_{in} (m^2)	Re_{in}
0.78	0.0225	0.0975	0.18	80
1.17		0.14625		120
1.56		0.195		160

All the test was repeated twice, and the average was reported in this chapter.

5.3 Results and Discussion

5.3.1 Velocity components

The LDV technique measures the velocity of each particle passing the probe volume at a specific point in the flow field over a specific time interval. Therefore the velocity at that point can be obtained by calculating the mean value of the recorded velocities. In the present study, the stream-wise (u) and cross-stream (v) velocity components were both measured using the LDV technique. Then the resultant velocity was measured using Equation 5.1, [134].

$$V = \sqrt{u^2 + v^2} \qquad 5.1$$

Figures 5.2 to 5.5, show (u) and (v) velocity components as well as their resultant velocity at the ten measuring points over the rotating cylinder shown in Figure 5.1.

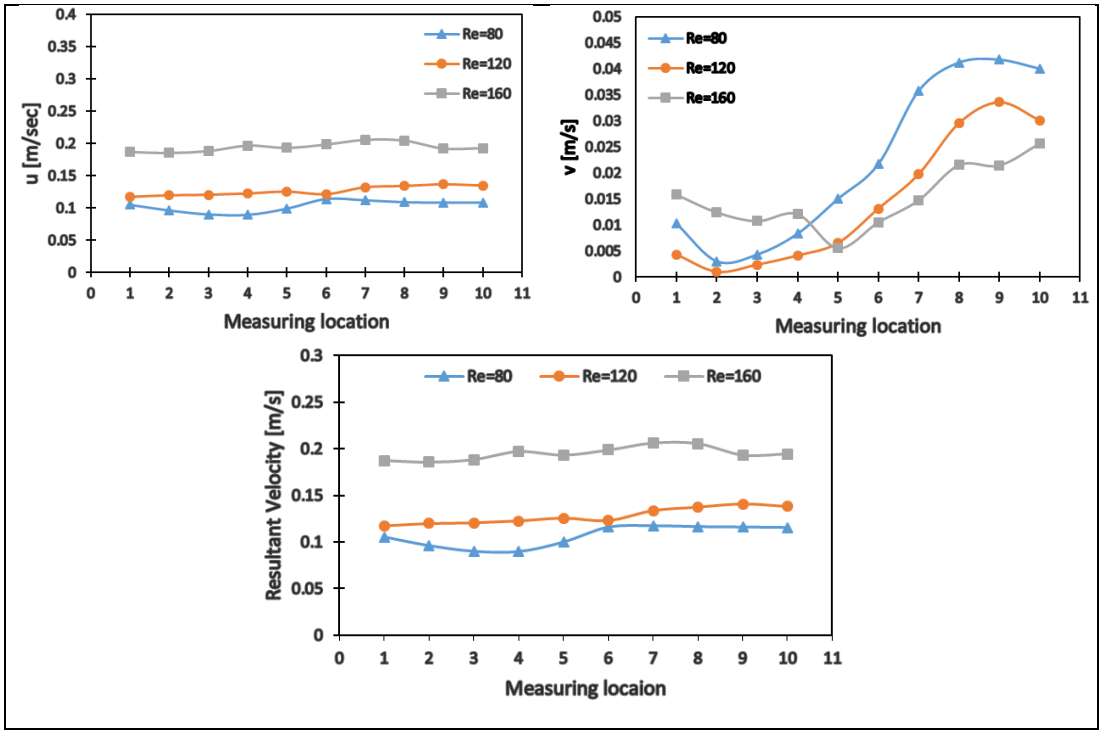

Figure 5.2: Velocity profiles (u, v and resultant velocity) at alpha=0, Re=80,120 and 160

In the different cases, the effect of the cylinder can be examined by tracking the behaviour of (u) component patterns particularly at the locations near the cylinder. The stream-wise velocity component seems to decrease at locations 3, 4, and 5, due to the development of the boundary layer and the occurrence of the reverse flow caused by the cylinder's rotation [42].

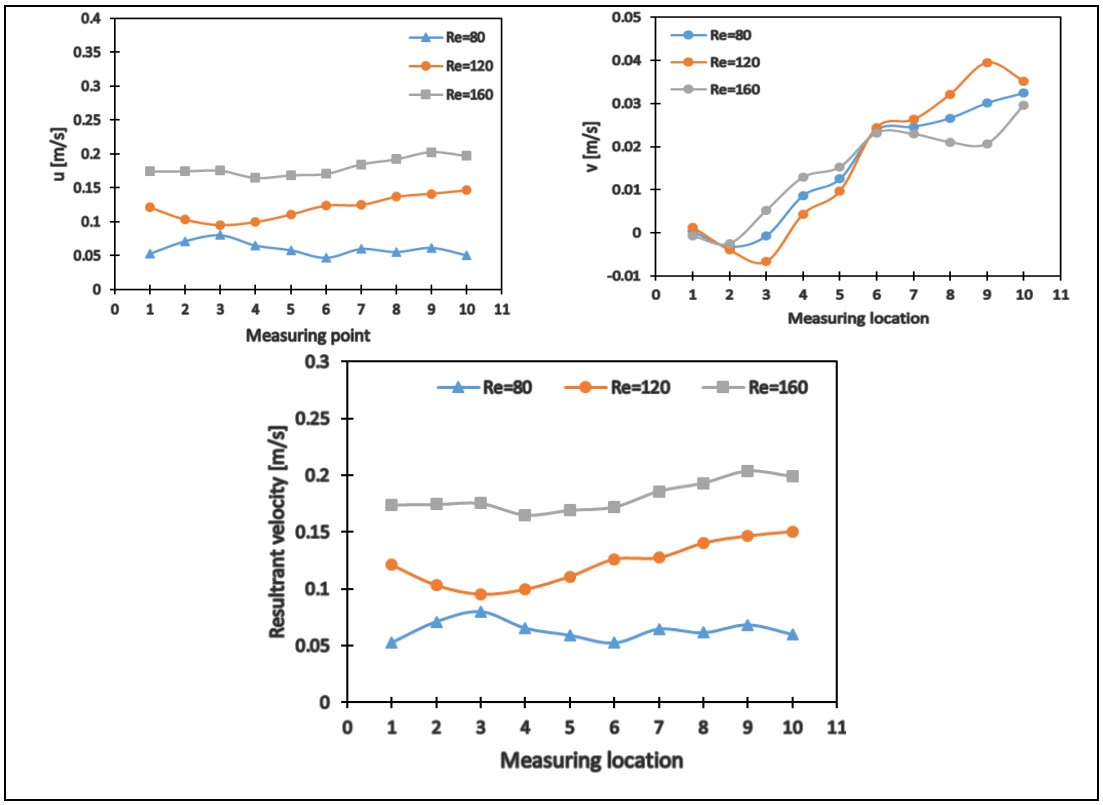

Figure 5.3: Velocity profiles (u, v and resultant velocity) at alpha=2, Re=80,120 and 160

The distinct behaviour of the cross-stream velocity (v) component in all cases is almost the same; some sharpness in the velocity profile can be noticed at location 3 in those cases of rotating cylinder. This is due to the location of point 3 in the zone where the flow and the cylinder surface meet, stagnation point. Additionally, as they become close enough, fluid elements approaching the cylinder straight on begin to slow.

The decrease in velocity at location 3, can be attributed to the increase of the boundary layer thickness due to the rotation and the shifting of the stagnation and separation points as shown in Figure 2.4, [42]

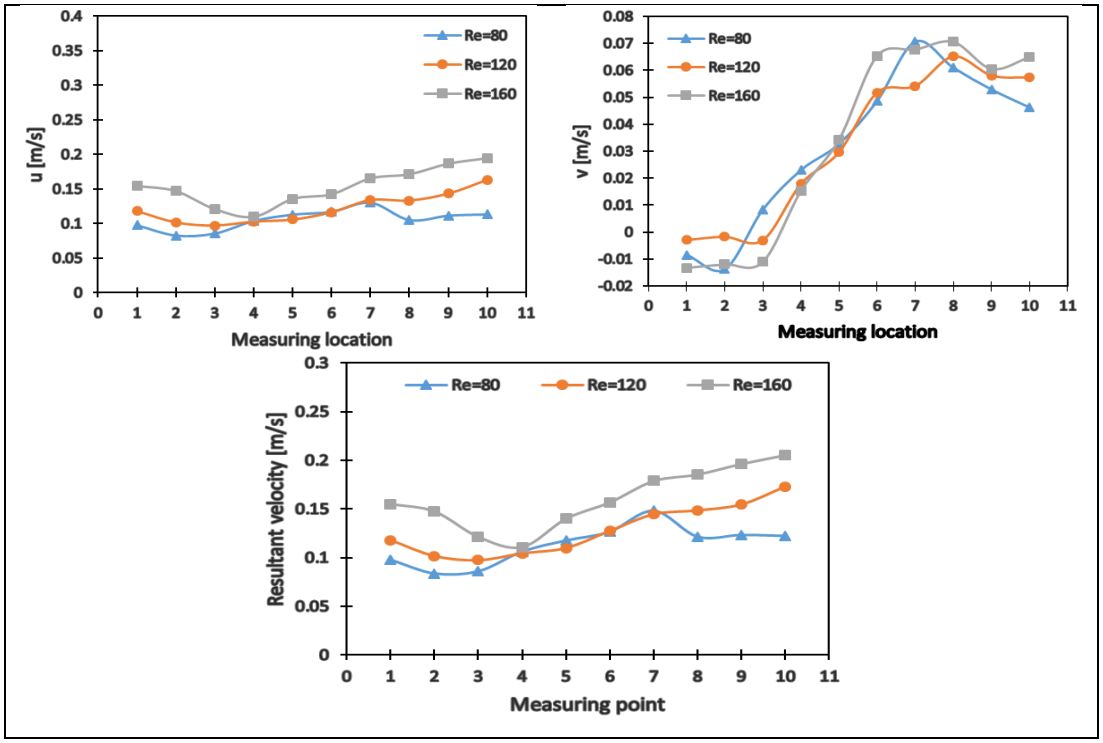

Figure 5.4: Velocity profiles (u, v and resultant velocity) at alpha=4, Re=80,120 and 160

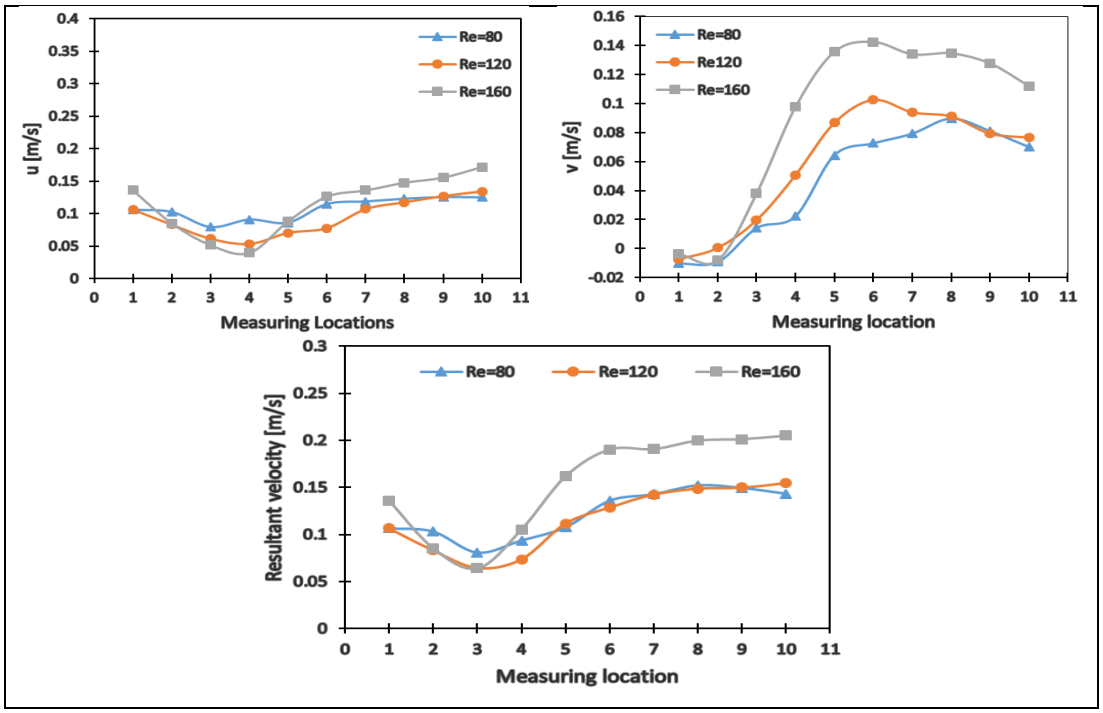

Figure 5.5: Velocity profiles (u, v and resultant velocity) at alpha=6, Re=80,120 and 160

The negative values of the (v) component observed in Figure 5.3 are due to the motion of the flow mass in the opposite direction relative to the main flow. During cylinder rotation, the top attached fluid layer travelled against the main flow direction due to the centrifugal force while the lower layer is moving with the main flow.

5.3.2 Turbulence intensity

The most remarkable characteristic of the turbulent flow is the existence of eddies in various scales where energy is stored. They produce unsteadiness to the majority of the flow features. Since all turbulent flows consist of fluctuations of velocity superimposed on the main velocity, the root mean square value of the fluctuations gives a quantitative measure of the turbulence strength.

The turbulence intensity is a scale characterising the strength of the turbulence, and it is expressed as a percentage (%). Turbulent eddies create fluctuations in the flow velocity, and both are varying in time due to the eddies continuous development. The turbulence intensity, in general, increases as Reynolds number increases, i.e. when the turbulent flow exists. Because the turbulent motion is associated with the random nature of the eddies, the turbulent flow can therefore be characterised by the mean values of flow properties (u, v, w, p etc.) and some statistical properties of their fluctuations ($\acute{u}, \acute{v}, \acute{w}, \acute{p}$ etc.), this phenomena is known as Reynolds decomposition [17, 111]. Figure 5.6 shows velocity components of turbulent fluctuations.

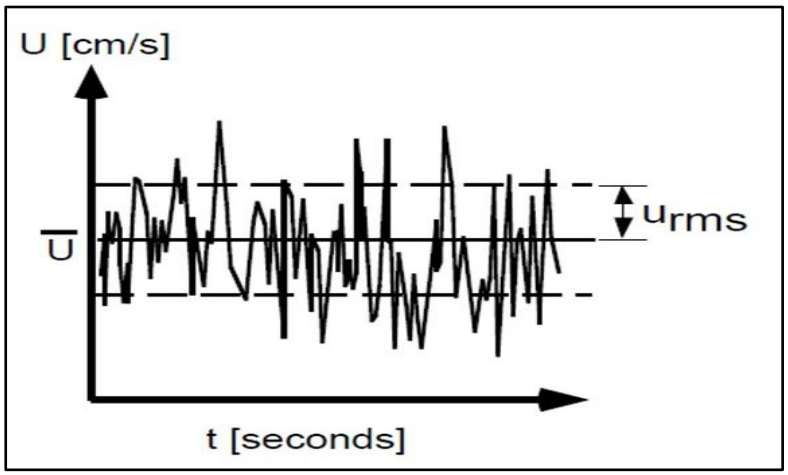

Figure 5.6: Recorded velocity fluctuations of a turbulent flow

The frequency with which the fluctuations at a particular point change sign is an indication of the size of the eddies and therefore of the scale of the turbulence.

In practice, the measured velocity records are a series of discrete points, u_i, Equation 5.2.

$$u_i = \bar{u} + u_i' \quad 5.2$$

And $$u_i' = u_i - \bar{u} \quad 5.3$$

Where u' is the turbulent velocity fluctuations at a particular location over a specified time period. The root- mean- square (RMS) of the perturbation component can be calculated as shown in Equation 5.4.

$$u_{RMS} = \sqrt{\frac{I}{N} \sum_{i=1}^{N} (u_i')^2} \quad 5.4$$

and $\bar{u}$ in Equation 5.3 represents the avearge velocity at the same location over a same time period, Equation 5.5.

$$\bar{u} = \frac{1}{N} \sum_{i=1}^{N} u_i \quad 5.5$$

Where N is the number of samples recorded by the LDV measuring volume (velocity tracers), i = 1, .., N. The turbulence intensity can then be calculated at each measuring point as:

$$\text{Turbulence intensity (T.I.) \%} = \frac{1}{\bar{u}} \sqrt{\frac{I}{N} \sum_{i=1}^{N} u_i'^2} \quad 5.6$$

The raw velocity time-series data obtained from LDV measurements were digitally analysed and transformed using Fourier Fast Transform (FFT) into the frequency domain signal. Then the frequency spectrum of the noisy velocity signal was filtered out through low-pass filter (LPF) approach to obtain a “chopped” spectrum, which was then transformed back into the time domain to give the turbulent signal from which the turbulent intensity is calculated [135]. The calculation process is shown

schematically in Figure 5.7, the processes were performed using MATLAB R2017a software, Figure 5.8.

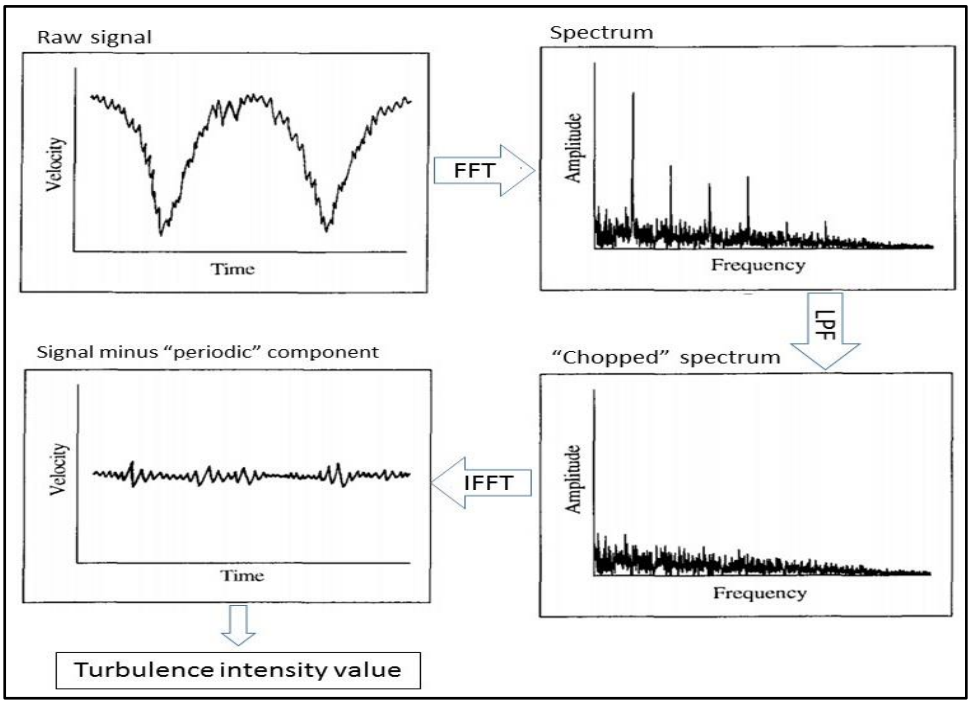

Figure 5.7: Fourier transforms calculation procedure

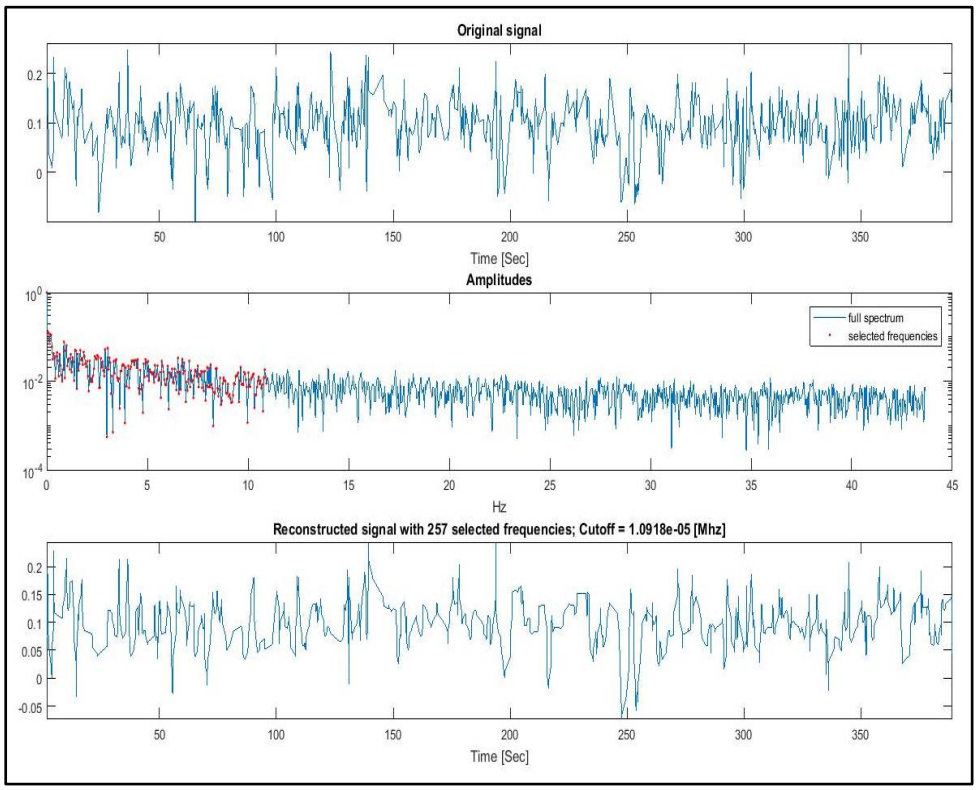

Figure 5.8: MATLAB Fourier transforms outputs

Figure 5.9 shows the turbulence intensity distributions calculated upstream and downstream of the rotating and non-rotating cylinder. A non-rotational rate of $\alpha = 4$ was chosen because it is the rate at which the classical Karman vortex street is expected tp dissipate [52].

In non-rotating cylinder condition (A), the turbulence intensity increases as the flow moving downstream, due to the vortex shedding activity in the wake of the cylinder. Whereas in rotating cylinder with a rotational rate of α=4, Figure 5.9, B, the effect of the cylinder's rotation can be observed clearly. The vortex shedding is suppressed in the downstream flow under the effect of the cylinder rotation results in less turbulence in the downstream flow [65].

The turbulence intensity values were higher at the upstream flow than the downstream, Figure 5.9, B. That is because of the velocity differences, with respect to the free stream flow, on both cylinder's sides, as the bottom flow mass is moving with the main flow direction and the top fluid mass against it owing to the cylinder counter-clockwise rotation.

Due to the differences in velocity, it is expected more turbulence would be generated in the upstream flow because of the clash of the main flow mass with the reversed fluid mass induced by the cylinder inertial forces.

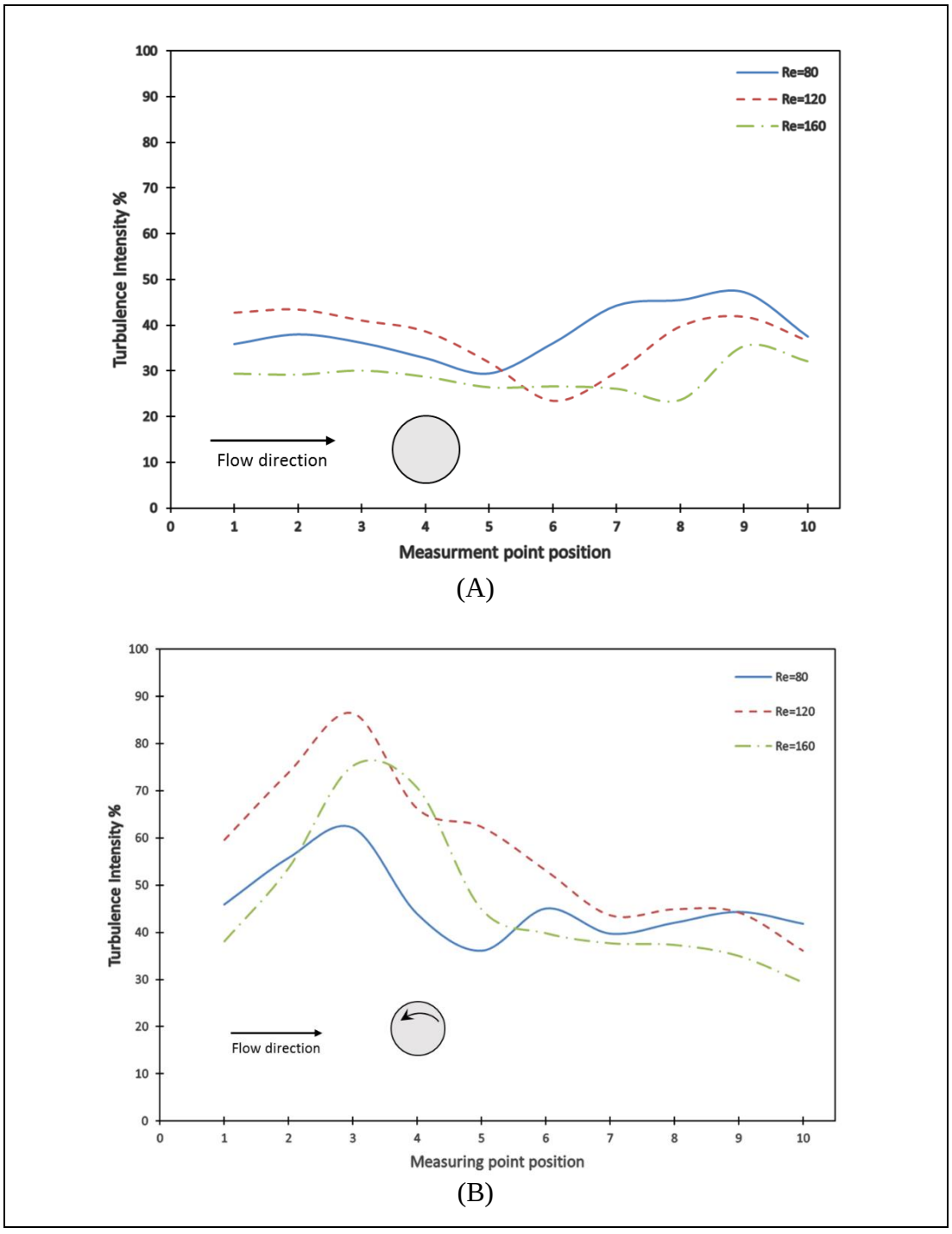

Figure 5.9: Turbulence intensity values at Re=80,120and 160. At alpha =0 (A) and 4 (B)

5.3.3 Strouhal Number

Further FFT analysis was performed to determine the peak frequencies of the recorded signal, Figure 5.10, at point 4 for rotating and non-rotating cylinder's conditions [23]. The frequency signal is an indication to the generation of the vortices. The results contributed to the calculations of the Strouhal number, St [136].

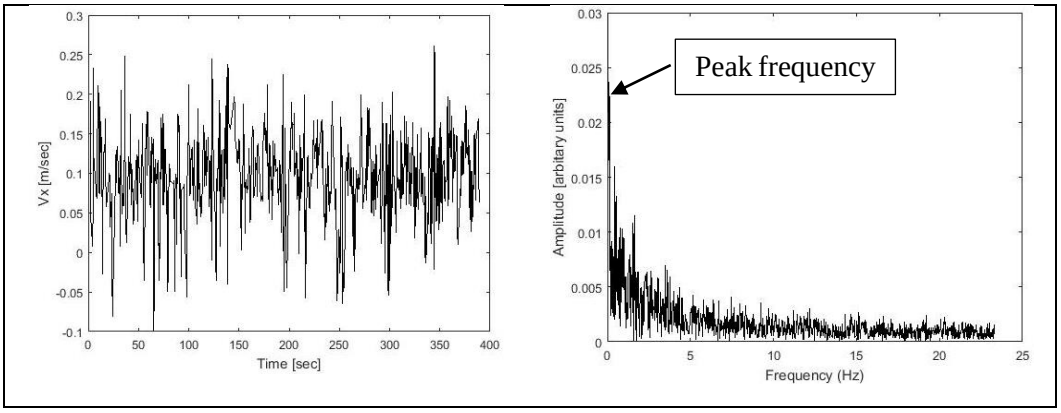

Figure 5.10: Data collected at point 4 and alpha=4. Left: the time evolution of the x velocity component. Right: frequency spectrum of the velocity signal.

In fluid dynamics, the dimensionless number, Strouhal number (St), represents a measure of the ratio of the inertial forces due to the unsteadiness of the flow or local acceleration to the inertial forces due to changes in velocity from one point to another in the flow field. It describes the oscillating flow mechanisms. It is often given as:

$$St = \frac{f\,D}{V_{in}} \qquad 5.7$$

Where (f) is the vortex frequency, D is the cylinder diameter and V_{in} is the flow velocity. The variation in Strouhal number is associated with the changes in the flow structure. From Equation 5.7, it can be concluded that Strouhal number decreases with increasing the flow velocity (i.e. Reynolds number).

Figure 5.11, shows Strouhal number plot against different Reynolds numbers, Table (5.1), for a rotating and non-rotating cylinder of a diameter =12 mm. At alpha=0, St decreases with increasing Re, which agrees with the predictions based on Equation 5.7. At alpha=4, Strouhal number increases with increasing Reynolds number, which agrees with the findings by Bard et al. [137]. The increase could be attributed to the

effect of the cylinder rotation on the flow topology near the cylinder; this is showing a discrepancy with Kumar et al. [52] who found a decreasing trend of St with respect to the cylinder rotation at Reynolds number of 200, 300 and 400. The decreasing trend of St at α =2 and 6, seems to support the assumptions by Bader et al. [137], that St is nearly independent of α at flow of a range of $60 \leq Re \leq 200$.

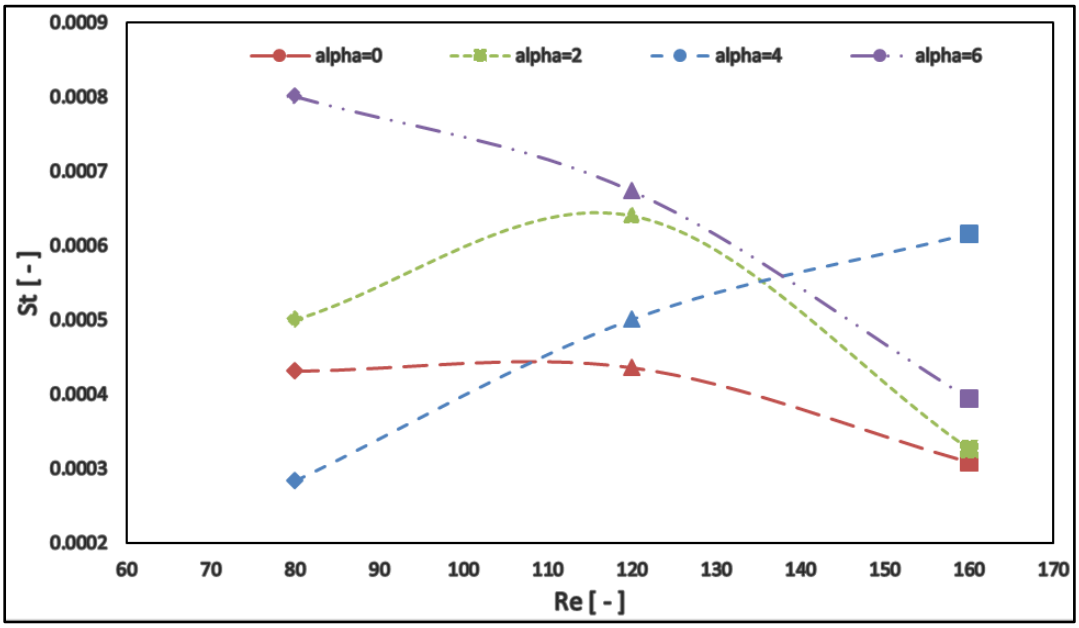

Figure 5.11: Strouhal number as a function of Reynolds number, at alpha=0, 2, 4 and 6

5.4 Summary

A flow passing a rotating and non-rotating cylinder was investigated experimentally. Three Reynolds numbers were investigated which are 80, 120 and 160. The cylinder's non-dimensional rotational rate was 2, 4 and 6. The new experimental data of the velocities, turbulence intensities and Strouhal number, could offer opportunities for validations of the numerical investigations on such type of flows.

The experiments were performed using a wind tunnel test rig. The technique of Laser Doppler Velocimetry (LDV), was utilised to measure the instantaneous velocity components in cylinder's wake region and the upstream flow region.

The velocity charts show that the velocity profile is slowing down as the flow approaching the cylinder. Due to the rotation, the fluid velocity in the upstream region is decreasing as it is exposed to pressure gradients due to the formation of the boundary layer.

The results of the turbulence intensity provide quantitative insight into the effect of rotation on the flow. The turbulence intensity results show that the turbulence strength decrease in the wake region of the rotating cylinder at rotational rate α =4 and Reynolds number 80, 120 and 160. This is due to the vortex suppression and the change in the flow structure near the cylinder represented by the velocity gradients on the top and bottom side of the cylinder.

The results of Strouhal number show independence to the cylinders rotational rates within the range of Reynolds number chosen for these experiments, and St value decreases with increasing the Reynolds number of the flow.

The technique of rotating cylinders is proposed in this study to generate fluid mixing inside the HTCA furnaces, this is because of its capability of generating turbulence within the fluid domain due to the effect of rotation and the continuous growth of the fluid viscous layers on the surface. The following Chapter investigates, numerically, the use of the technique in the HTCA furnaces.

CHAPTER 6:

ROTATING CYLINDER TECHNIQUE FOR FLOW GENERATION

Chapter 6

Rotating Cylinders Technique for Flow Generation

6.1 Introduction

The annealing process in the HTCA furnaces experiences some thermal inefficiencies represented by the formation of hotspots as stated earlier in chapter 4. The heating elements operate at their operating limit and can create local hotspots which sometimes lead to element failure.

When one of the heating elements fails, the remaining zones will need to work harder to try to deliver the requested thermal cycle. Because of the lack of fluid recirculation, to transport the excess heat away, the areas close to the active heating elements receive a great amount of energy by radiation and become hotter than the areas near to the inactive heating zone, which are relying only on some convection induced by the buoyancy forces from areas nearby. The situation gives rise to formation of the hotspots and further issues such as non-uniform properties of the steel coil.

Therefore, in this chapter, the rotating cylinder technique was explored as an option to generate beneficial flow inside the annealing furnaces. This proposed technique was investigated numerically using the CFD approach outlined in Chapter 3 to appraise its effectiveness in producing fluid flow inside high-temperature furnaces.

6.2 The Proposed Technique- Rotating Cylinders

To overcome the stagnate nature of the HTCA furnace, which is caused by the long operation conditions and space limitation, fluid recirculation needs to be introduced inside the furnace chamber to enhance the gas mixing and thus promote forced convection during the annealing process.

The rotating cylinder technique has been investigated widely as a flow controller and turbulence generator in a variety of engineering and scientific applications such as viscosity determination devices, biological applications, reactors for sea water

distillation and flame stabilisation (see section 2.5). Therefore, the present study proposes the use of this technique to produce fluid recirculation inside the HTCA furnaces.

The technique was investigated numerically a CFD approach, with the commercial software ANSYS/Fluent. The furnace with internal dimensions as shown in Figure 6.1 was simulated.

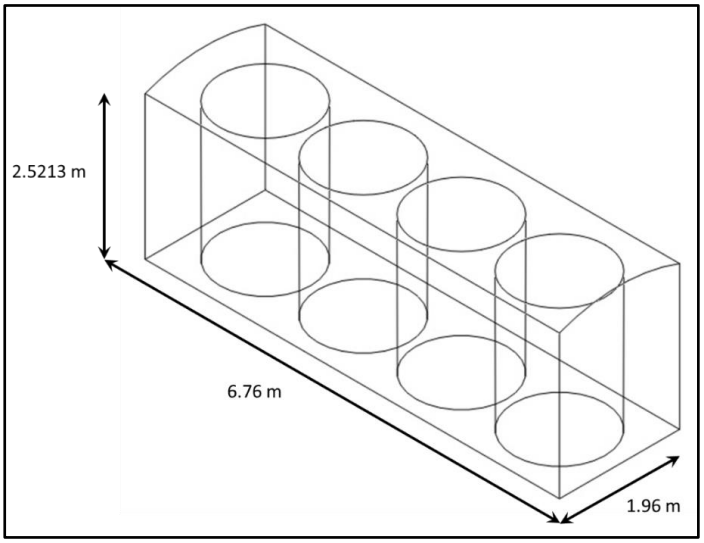

Figure 6.1: The furnace fluid domain

The rotating cylinders are installed inside the furnace chamber. Six different cases of cylinder arrangements inside the furnace were investigated, from which the optimal layout which offers the best gas recirculation can be selected. Due to the relatively large scale of the furnace, more than one cylinder is used to ensure sufficient flow recirculation throughout the furnace. The internal size of the furnace and the process equipment layout, as well as the limited space available, were all considered when selecting the cylinders dimensions and locations.

In the Layout 1 (Figure 6.2), six cylinders were installed vertically in the base of the furnace close to the heating elements where hotspots usually form. Installing the cylinders in such a way inside the furnace can circulate the atmospheric gas that is injected through the pipes located in the base. The number of cylinders in Layout 2 was reduced and the cylinders at the corners were removed. From a practical

standpoint, the cylinders at the corners are more exposed to damage when placing the furnace on the base.

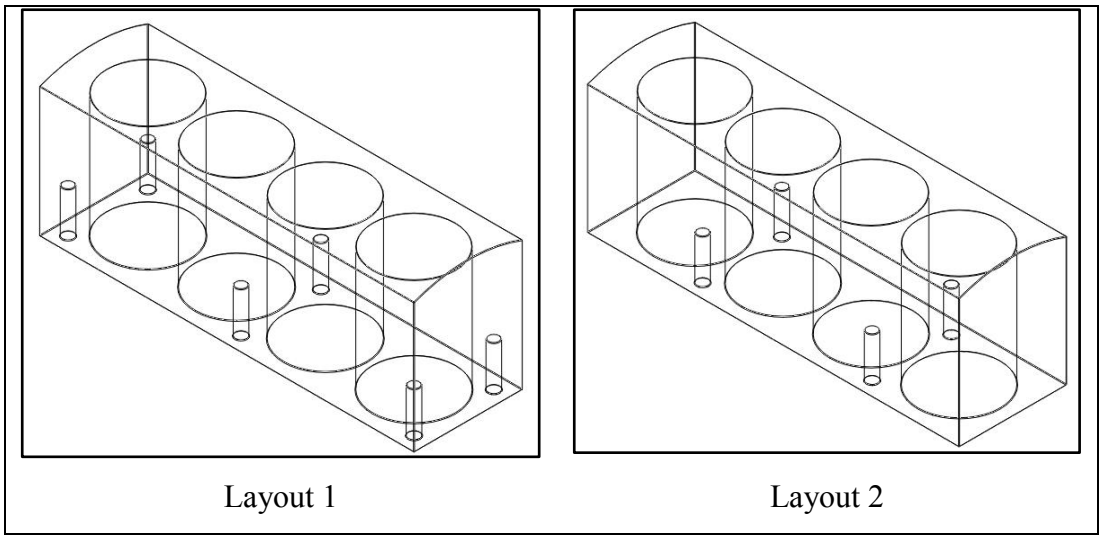

Layout 1 Layout 2

Figure 6.2: Schematic diagrams of Layouts 1&2

In Layouts 3 and 4 (Figure 6.3), the cylinders were installed horizontally at the top of the furnace container. During the heating process, the atmospheric gas becomes hot and rises to the top of the furnace due to the buoyancy forces and the differences in densities. Therefore, locating the cylinders horizontally at the top can convert some of the energy of the raised gas to a turbulent motion due to the cylinders' rotation, thus creating a fluid circulation.

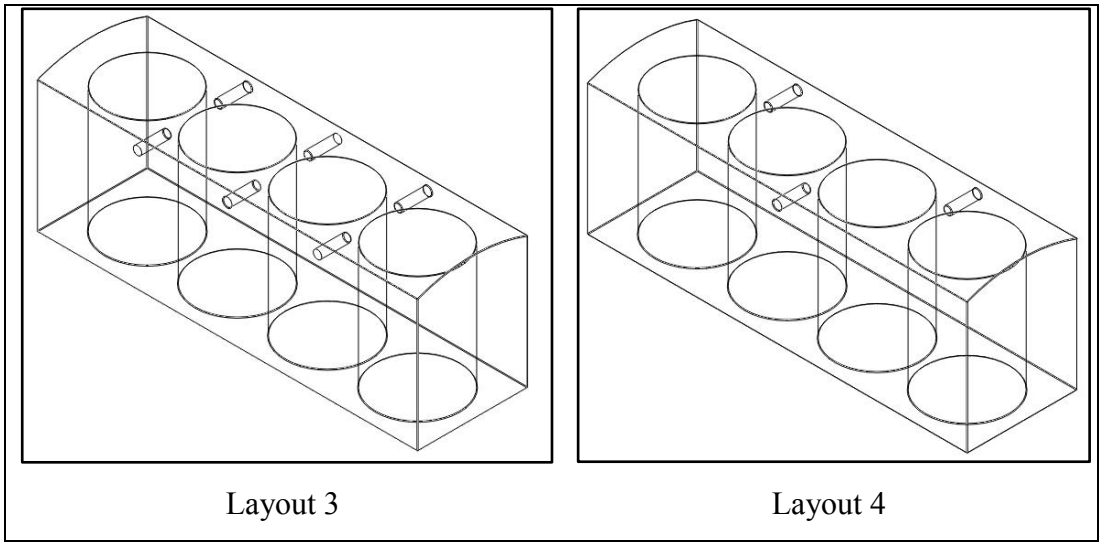

Layout 3 Layout 4

Figure 6.3: Schematic diagrams of Layouts 3&4

Some modifications on the furnace geometry were suggested as presented in Layout 5 & 6. The modifications were some enlargement on the furnace chamber so that the cylinder can be installed above the inner covers, represented in Layout 6 (Figure 6.4). The extra enlargement in Layout 5 was based on performing some variation to the containers without having to change the base. This way, if the cylinders posed a problem, the enlargement could be removed and sealed without major complications. Also, the volumetric region currently allocated for gas recirculation would not be reduced (as with all the previous cases) but increased. Therefore, this configuration was recommended by the industrial sponsors for analyses.

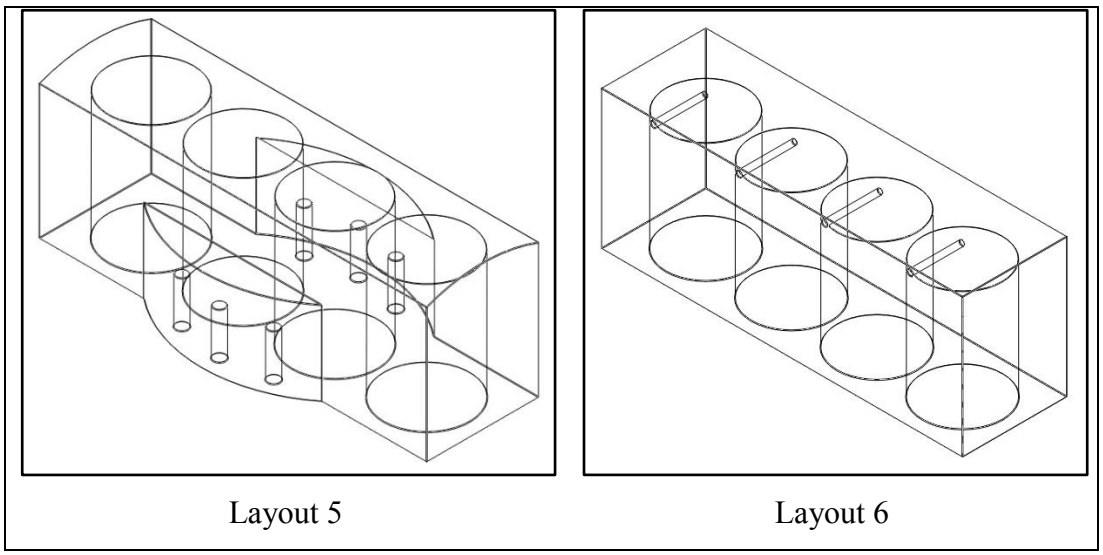

Figure 6.4: Schematic diagrams of Layouts 5&6

As the heating elements are distributed on the furnace wall symmetrically, the temperature provided to the furnace was assume to be uniform across all surface boundaries, hence the direction of rotation is arbitrary. However, the majority of previous studies e.g. [23, 138] have chosen a counter-clockwise rotation and for consistency and comparison counter-clockwise has been chosen in this thesis.

6.3 CFD Simulation of HTCA Furnace

In the present chapter a primary model was created to test the validity of the proposed technique in the HTCA furnaces. The model has focused on simulating the rotating cylinders inside HTCA furnace at high temperatures and for one specific atmospheric.

Modelling a rotating cylinder in quiescent fluid domain as in HTCA furnace is a hard task. This is mainly because the volume of the fluid continues to grow within the fluid domain. Therefore, some assumptions were made to make this task less complicated, as will be shown in the following subsections.

The model passed through several stages of modifications and development to reach the final model employed for this study. Starting by understanding the physical phenomena associated with the problem and identifying the relevant system boundaries were the initial tasks performed through this work. Then, changes in mesh size (as previously presented), combining not only fluid mechanics but also heat transfer mode (i.e. starting with simple thermal boundary conditions, moving on to complex systems that comprised radiation and eventually convection (both natural and forced) and finally the addition of moving boundaries to simulate the rotation were all progressive steps that needed to be performed to create a close representation of the intended technique. Finally, the development of bespoke User Defined Functions relevant only to this process at Cogent was also attempted through complex data analysis, heat transfer studies, and numerical simulation proficiency. To the knowledge of the author of this work, this User Defined Function (UDF) has never been attempted or documented anywhere else. The reason for this uniqueness is the complexity of this function combined with a bespoke algorithm that can only be employed for Cogent's particular process. Briefly speaking, this process from fundamental understanding to complex development was carried out over the entire duration of the present project. The main challenge was the solution divergence when the solution experiences some errors due to the successive iterations produce a result that progressively moves away from the true solution. This was resolved throughout intensive examination to the turbulence model utilised to model the process and the boundary conditions as well as the mesh quality.

6.3.1 The computational model

The fluid domain of interest was identified to be the atmospheric gas that occupies the space between the internal walls of the furnace and the inner covers when the furnace is applied during the annealing process (Figure 6.1). Therefore, the inner covers, the furnace internal walls, and the rotating cylinders were introduced as boundaries of the fluid domain. This assumption saves a considerable amount of computational time and effort.

6.3.2 The physical model

The ANSYS/Fluent solver can model both the cylinder's rotation and the parameters of the HTCA furnace, such as radiative and convective heat transfer and laminar and turbulent flow. ANSYS physical models allow the user to simulate many aspects of the problem under scrutiny by specifying several models, in this instance heat transfer and fluid flow.

The present model focused on the rotating cylinder in the fluid domain of the furnace, thus particular attention was given to choose the physical model that can capture the effect of rotation on the fluid domain and the formation of the vortices within the fluid domain. In this study, the Reynolds Stress Model was considered. It is the most elaborate turbulence model that Fluent provides. Furthermore, the model enables applying body forces in the form of buoyancy and gravity on the atmospheric gas used during the process. Constants associated with the RSM was assumed to have the default values suggested in Fluent V18.2.

6.3.3 Mesh generation

A three-dimensional model of the furnace fluid domain obtained from SolidWorks was used for the simulation. A hexahedral structured mesh was created using ANSYS mesh generator, Figure 6.5, as it gives fast and stable solutions, and offers more accurate results and a better convergence.

Since the aim of the study was to examine the effect of the cylinders rotation on the fluid domain inside the furnace chamber, the mesh was generated as fine as possible throughout the fluid domain, within the constraints posed by computer resources

available for the numerical calculations. The fine mesh aims to capture the small changes in the flow variables.

Moreover, there are few zones that received particular attention where the mesh was finer than other regions, such as the cylinders and the furnace wall where the heat sources are located as shown in Figure 6.5, i.e. the z-y plane.

A grid independency analysis was performed in this study by examining the numerical outputs of four meshes with different densities. Table 6.1 shows element number identifier and the cell maximum volume.

The four different meshes were performed on Layout 2. The mesh of 3,905,080 elements was found to be satisfactory in terms of accuracy and calculating time. The same element size was applied to the rest of the configurations. The comparison criteria used for the selection of the best mesh was based on the mean velocity of the flow at location (P3), as shown in Figure 6.7.

Table 6.1: Grid independency test data

Grid no	**No of elements**	**Maximum volume**	**u (m/s)**	**Δ u (m/s)**
1	407,790	7.525131e-5	0.0874	-
2	692,484	3.504943e-5	0.093	0.0056
3	1,237,720	2.506045e-5	0.0978	0.0048
4	3,905,080	1.064479e-5	0.1181	0.002

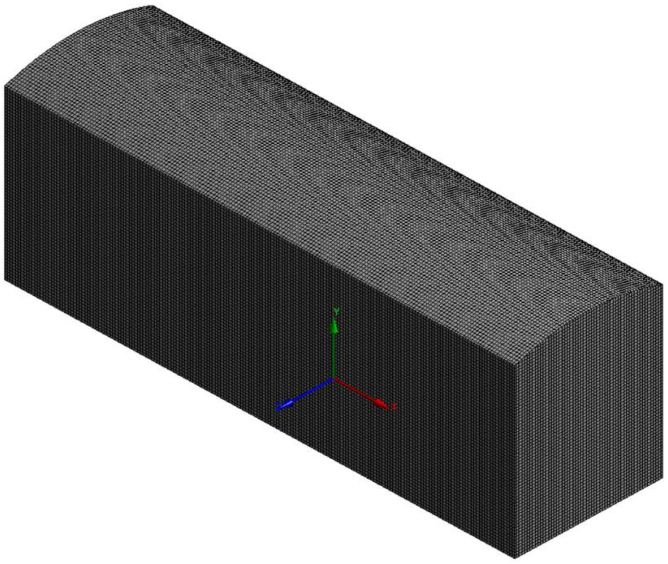

Isometric view

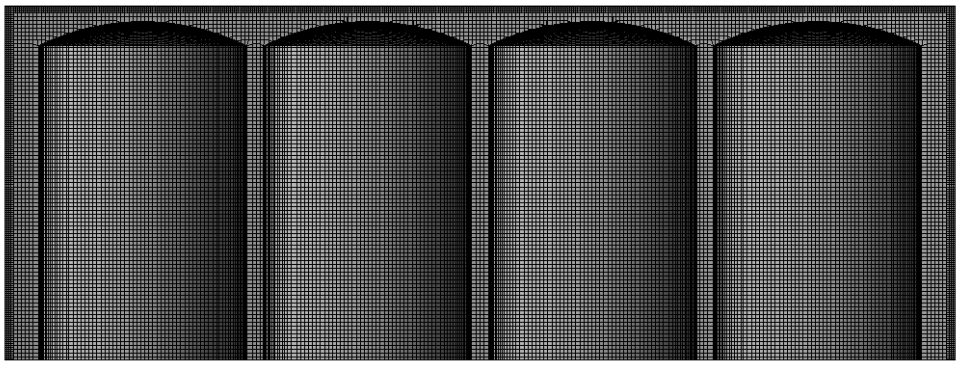

Section on x-y plane

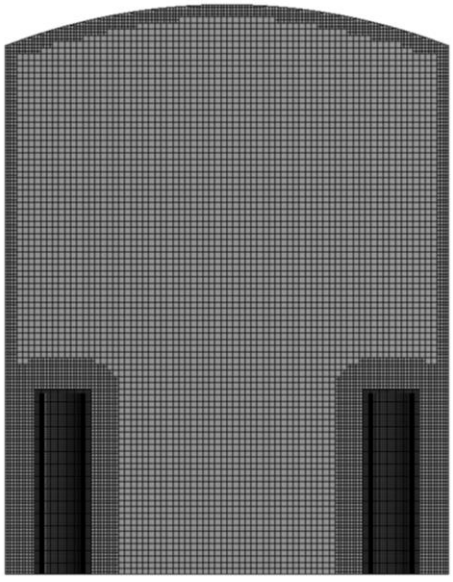

Section on z-y plane

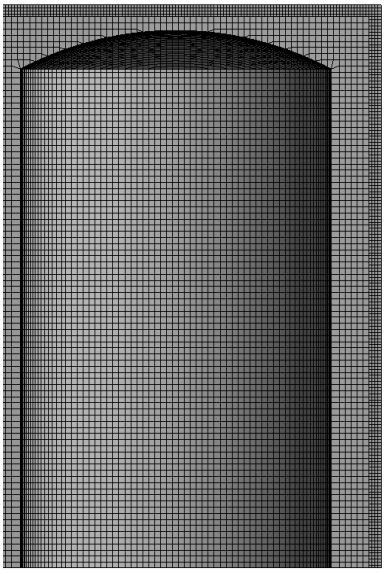

Mesh near walls

Figure 6.5: Grid generation

6.3.4 Boundary conditions

The initial information related to the annealing process was obtained from the standard operating procedure at Cogent, including the temperature, pressure and the atmospheric gas. Table 6.2 shows the important stages of the annealing process and their operating parameters. The dimensions of the furnace and inner covers were also provided for the modelling purposes.

Table 6.2: Target temperature and gas type at successive stages during the annealing process, *RT= Room Temperature

Segment	**Process type**	**Target (C^{o})**	**Gas type**
1	Heating	RT*- 640	3HN
2	Heating	900	3HN
3	Heating	1050	100% H_2
4	Heating	1190	100% H_2
5	Soaking	1190	100% H_2
6	Cooling	900	100% H_2
7	Cooling	600	75% H_2, 25% N_2
8	Cooling	500	3HN
9	Cycle End	Furnace lift	

The rotational Reynolds number was calculated based on the tangential velocity of the fluid particles attached to the cylinder surface (u_s), and the cylinder diameter (D), which represents the characteristic length in the Reynolds formula

$$Re = \frac{\rho\, u_s\, D}{\mu} \qquad 6.1$$

Table 6.3: Rotational rate, cylinder diameters and the corresponding rotational Reynolds Number, Re_r

Rotational rate		**Re_r**		
rad/sec	**rpm**	**D=100 mm**	**D=150 mm**	**D=200 mm**
100	954.93	308	692	1230
150	1432.39	461	1038	1854
200	1909.86	615	1384	2461
250	2387.32	796	1730	3076

Constant wall temperature boundary condition was applied to the furnace and the inner covers walls. The thermal and physical properties of the H_2 gas are varied through the furnace due to the variation in temperature. Therefore, the initial properties were set at the temperature of the annealing process onset (~1000 C) which were taken from the literature [16], whilst no reactions were assumed. The effect of the injected gas on the fluid domain under the furnace was not considered in this model to examine only the effect of the rotational flows induced by the proposed technique.

The rotating wall boundary condition was used to model the cylinders' rotation. A right-hand rule was used to identify the rotation-axis direction depending on how the cylinder was installed, i.e. vertically or horizontally. No-slip velocity boundary conditions were applied to all the solid walls of the furnace, inner covers and the rotating cylinders with standard wall functions to solve the near-wall flow. A constant temperature boundary condition was applied on the furnace walls. This is to avoid using transient boundary conditions in the present basic model which develops only steady state calculations.

Therefore, the steady state calculations focused on modelling the furnace when operating with 100% hydrogen as the atmospheric gas and at high temperature of 1190 ^{o}C. Some basic transient simulations were also performed to identify trends and will be discussed in the following section.

6.3.5 Development of a transient model

The CFD transient simulations are used to capture some particular data of time-varying flow features that cannot be obtained from the time-averaged solution. Therefore, a transient model was developed to capture the transient fluctuations of the flow velocity in order to measure the strength of the turbulence generated by the rotating cylinders.

When selecting the time step, one must always consider the trade-off between accuracy and computational cost. Smaller time steps will typically yield more accuracy and stability, at the expense of longer run-time and increased computational cost. The time step was selected carefully in order to extracts the data necessary for turbulence intensity calculations. The solution converged at each time step and the approximate computational running time of each case was 200 hrs.

In the transient simulation, unlike the steady state case, the data output/sampling need to be configured before performing iterations. Therefore, data of velocity fluctuations at five different locations were set in advance and saved separately. The development and successful output from a transient model for this problem is an order of magnitude more complicated than for the steady-state case. Hence, it is the intention to provide indicative trends of the transient solution characteristics, and future studies will be required for a more thorough study.

6.4 Results and Discussion

Comparison criteria based on temperature contours and velocity charts in five locations across the model was used to select the optimal cylinder configuration that can generate flow recirculation in a wide space within the fluid domain. Figure 6.7 shows planes and line locations in the absence of the cylinders.

For a reliable comparison, plane (3) which is marked in red in Figure 6.7 was chosen to examine the temperature distribution contours for the cases under investigation. Thus the comparison was from plane to plane rather than the position of the cylinders.

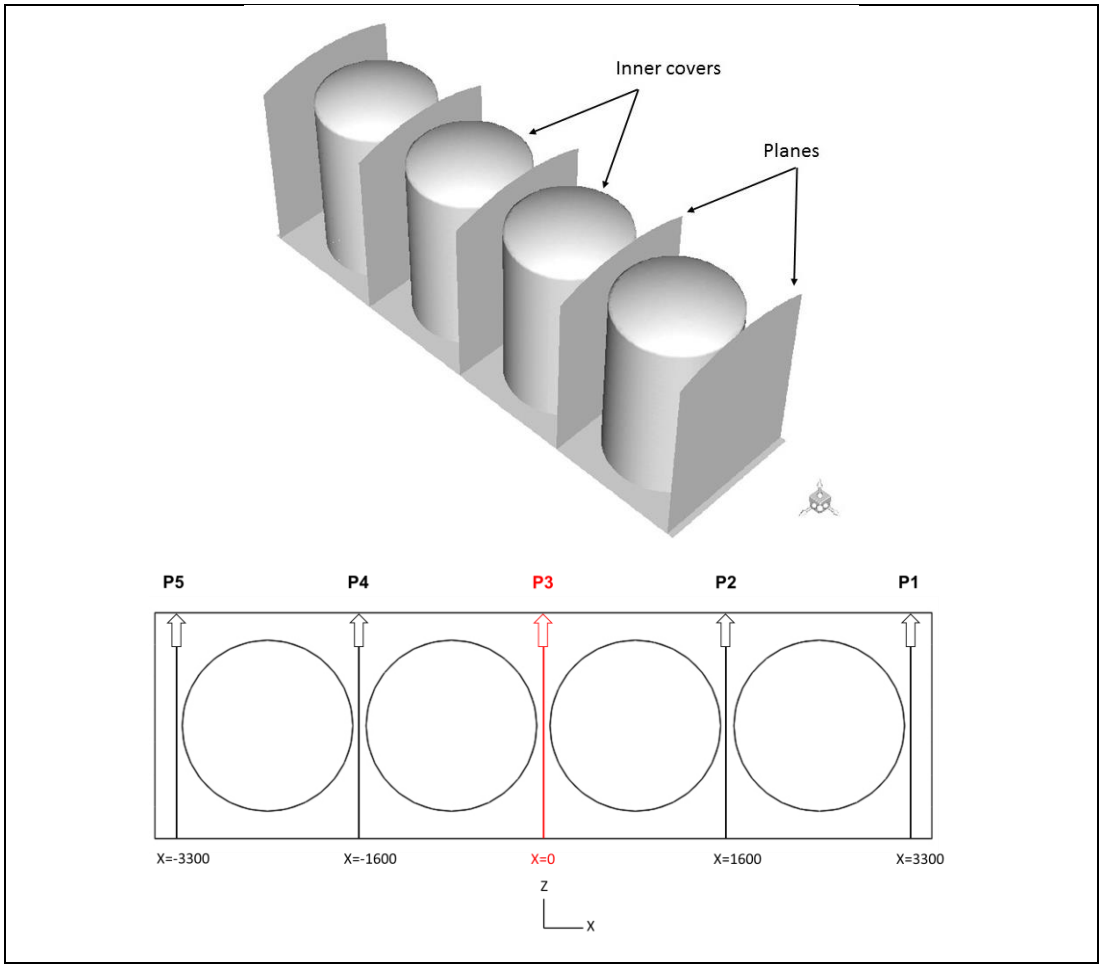

Figure 6.6: Location of planes and lines through the furnace geometry in the absence of the rotating cylinders

6.4.1 Without using the proposed technique

During the early stages of the annealing cycle, the atmospheric gas enters in a turbulent state, i.e. Re > 10,000, because of the high flow rate (1060 $ft^3/hr \sim 0.008 m^3/sec$) at which the flow is injected through the pipes located under the inner covers. However, the flow quickly becomes transitional as its temperature increases, density starts falling, and its velocity decreases as it exits the pipe and expands into the spaces under the inner covers and the furnace. The gas velocity continues to fall as it moves through the fluid domain inside the furnace cavity, (Figure 2.12). The combination of low gas velocity, high temperature and high hydrogen concentration produces a laminar flow for the majority of the annealing cycle.

First, the furnace was simulated when the rotating cylinder technique was not employed. Velocity profiles and temperature contours were obtained for evaluating the gas behaviour under these benchmark conditions.

The temperature contour and the velocity profiles shown in Figure 6.8 and 6.9 respectively, demonstrate the static nature of the atmospheric gas inside the furnace cavity. The temperature gradients between the centre of the furnace and the furnace wall are high which caused by, aside from the domination of radiant heat transfer mode, the stagnant nature of the process and devoid of fluid motion. Whereas the process requires low differences in temperature through the furnace, to avoid undesirable properties of the final product.

The velocity profiles show zero velocity magnitude at the selected locations, which indicates the lack of fluid motion and the absence of the turbulent flow. The lack of fluid motion contributes to increase in hotspot formation, especially during long operation conditions or the failure of one of the heating elements.

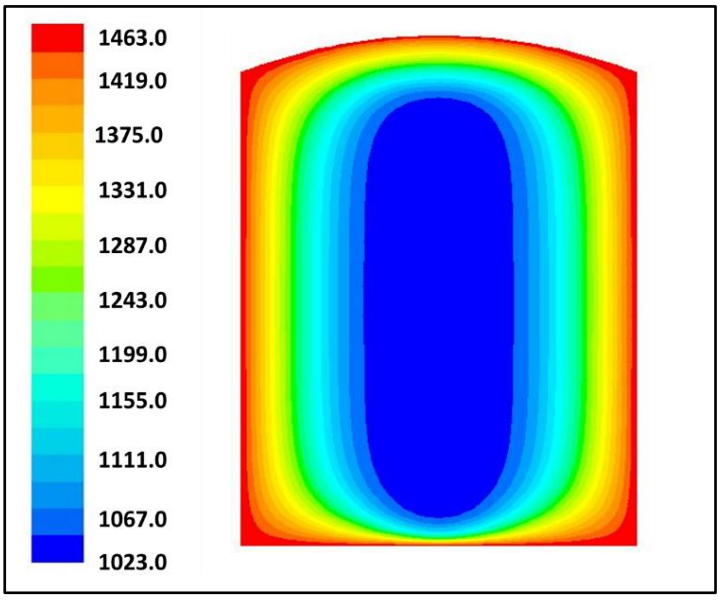

Figure 6.7: Temperature contour (shown in Kelvin) at plane 3

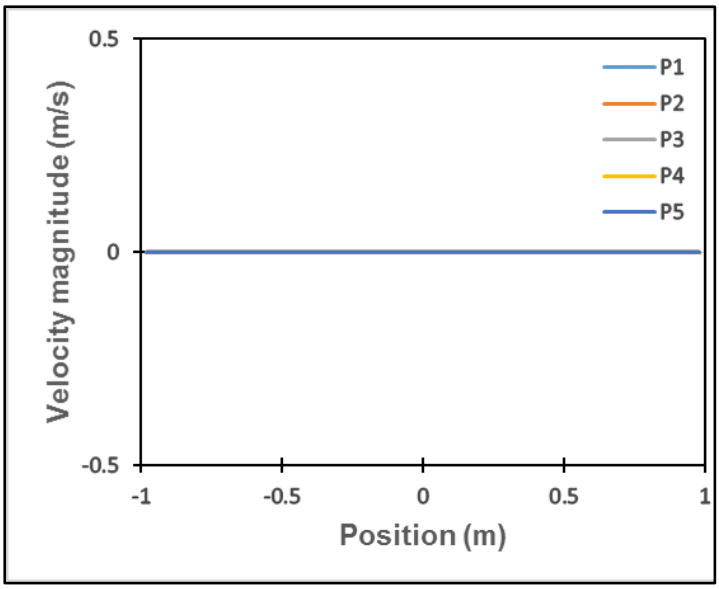

Figure 6.8: Velocity profiles at five different locations across the geometry

6.4.2 Implementing the proposed rotating cylinder technique

The aim of using the rotating cylinder is to generate fluid flow inside the annealing furnace during the annealing process, thus introducing forced convection. This would help in minimising the thermal inefficiencies that are usually experienced during the electrical failure of one of the heating elements. Velocity vectors, velocity charts, temperature contours and turbulence intensity were used to set appropriate comparison criteria to evaluate the performance of the proposed technique.

Turbulence in fluid mechanics is characterised by velocity fluctuations of the fluid flow [48], caused by the formation of eddies or vortices. These vortices mix the fluid and enhance convection. The vortices occur due to the continuous growth of the fluid layer around the cylinder under the effect of its rotation. The vortices at various scales develop continuously within the fluid domain and travel to the surrounding areas [17]. Figure 6.10, shows velocity vectors of fluid particles at cylinders rotational rates of 100, 150, 200 and 250 rad/sec.

Figure 6.10 shows the fluid flow induced by the cylinder rotation and the generation of vortices at different scales. At low rotational rate 100 rad/sec, i.e. low rotational Re, the turbulence was very weak in the remote areas near the furnace roof, unlike the case

of high rotational rate where the turbulence, characterised by the vortices, was observed at the same referred area.

Turbulent motion decay is influenced by several processes, including; the removal of the agitation that initially set the fluid in motion, low Reynolds number, and the growth of the spatial structure of the turbulence to the size of its container [139]. The turbulence decay occurs when the unstable eddies break down to eddies of small size, which in turn, also break down to even smaller eddies, until eddies small enough to be dominated by viscous actions are produced; this phenomenon is known as energy cascade. The smallest eddies are hydrodynamically stable, and their kinetic energy is dissipated by friction with other eddies and converted into internal energy.

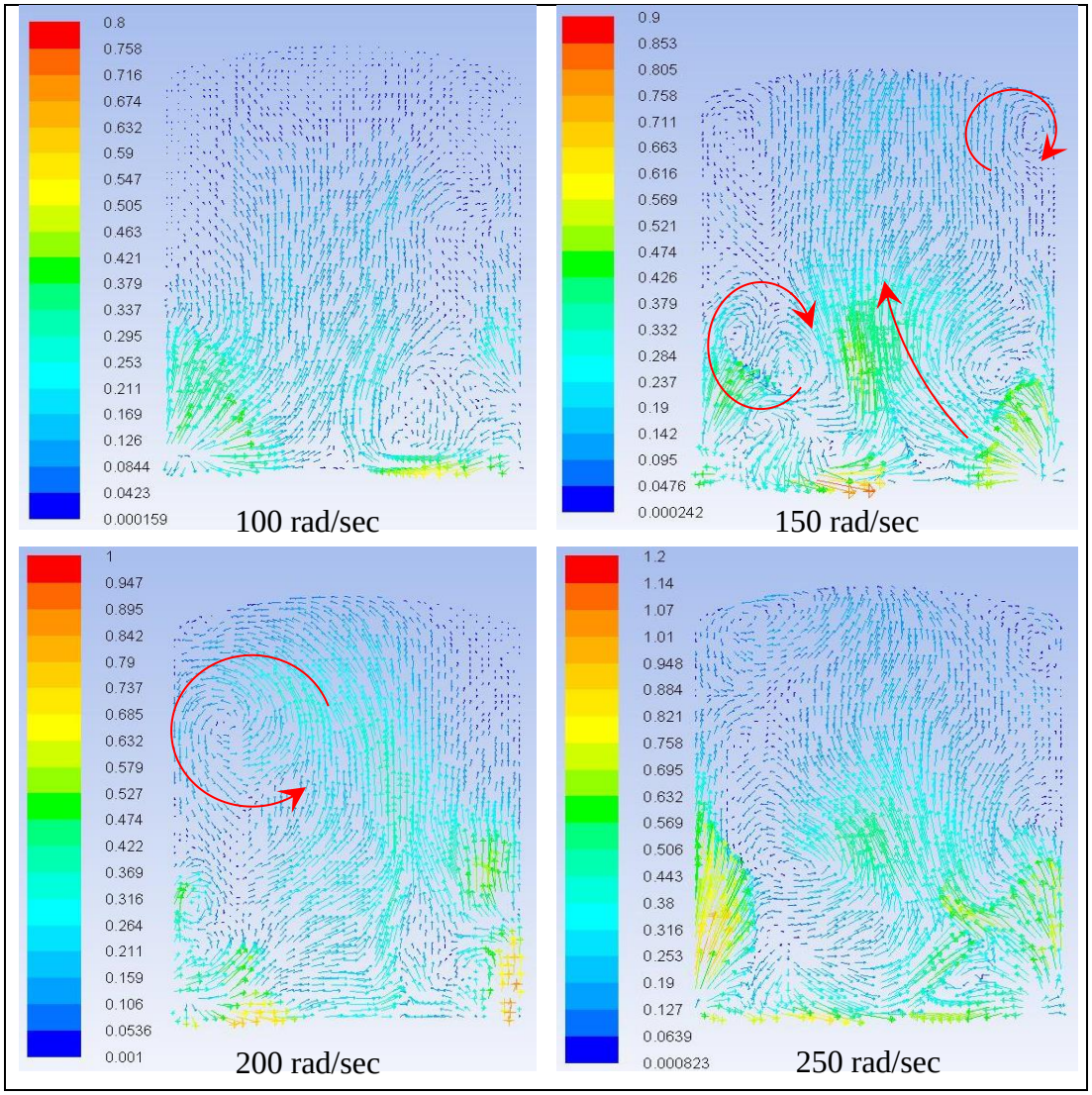

Figure 6.9: Velocity vectors coloured by velocity magnitude (m/s)

Therefore, a source of kinetic energy such as; non-uniform mean flow velocity, buoyancy due to density differences, and centrifugal actions due to rotation of the fluid, needs to be provided to ensure turbulence sustainability. The proposed technique of cylinder rotation offers sustained turbulence that can continuously mix the atmosphere gas inside the furnace cavity.

Velocity charts, Figures 6.11-6.14, show fluctuations in velocity magnitude at five different locations across the geometry when using the rotating cylinders. The variation between velocity charts are associated with vortex boundaries. The greatest part of the turbulent kinetic energy is carried by the largest eddies, which characterise the velocity fluctuations and the most active turbulent motions. This means that at a particular location the variation in velocity magnitude depends on the size of the vortex formed at that location due to the amount of stored energy that is proportional to the vortex size. The velocity fluctuations act to transport momentum and heat efficiently [24]. Figures 6.10 and 6.11-14 confirm that turbulence can be sustained within the furnace fluid domain via the technique of rotating cylinders.

It was observed that the resultant velocity increases with increasing rotational speeds due to higher tangential velocity. At the highest rotational rate, inertial forces become dominant to viscous forces, and hydrodynamic turbulence is evident, although using the high rotational velocity rate, the velocity magnitudes seem low. This is due to the low density of the hydrogen at high temperatures, also the large furnace size and the flow constraints imposed by the furnace wall and the inner covers, which slow down the gas velocity and dissipate the turbulence. However, from a practical standpoint, the minimum value of 0.4 m/s seems acceptable in the presence of sustained turbulent fluctuations all around the gas domain.

It was noticed that for those layouts where the cylinders are located vertically on the furnace base, the velocity is higher than those cases where the cylinders are installed horizontally on the furnace. This can be attributed to the cylinder locations near the inner covers and the furnace walls, which hinder the development and the distribution of the vortices and suppress the turbulence, even at high rotational rates. Density fluctuations across the profile also affect this phenomenon, with lower density at the top of the confinement, hence less fluid mass movement around the cylinders. Due to

the adapted feature in Layout 5 and cylinders locations, gas recirculation was weak near the walls at locations P1 & P5. Therefore, Layout 1 seems to be the best regarding mixing enhancement, although Layout 2 is simpler to implement from a practical standpoint.

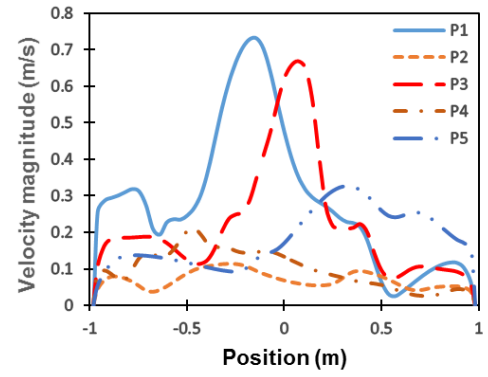

Layout 1

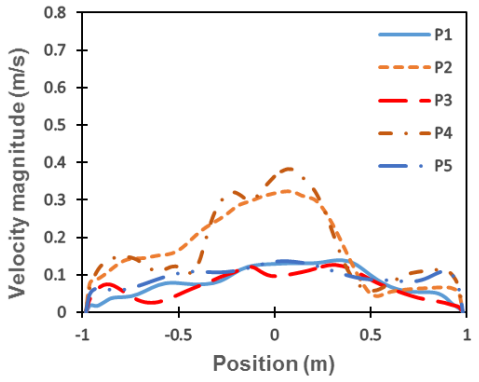

Layout 2

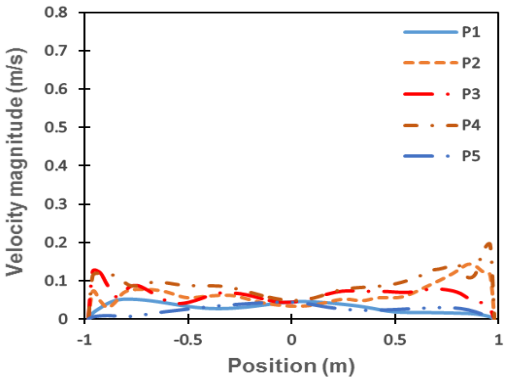

Layout 3

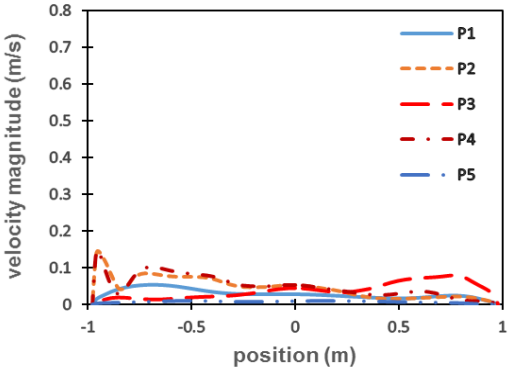

Layout 4

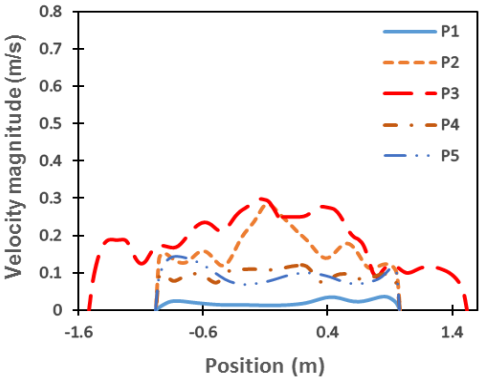

Layout 5

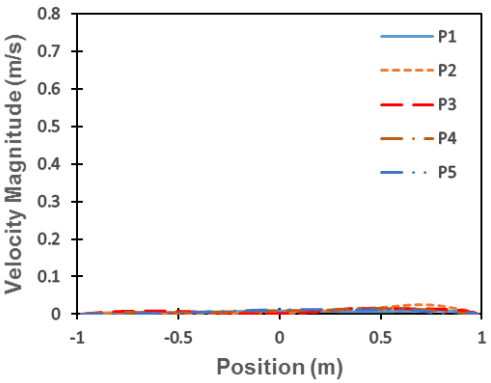

Layout 6

Figure 6.10: Velocity profiles at rotational rate 100 rad/ sec at locations P1 to P5

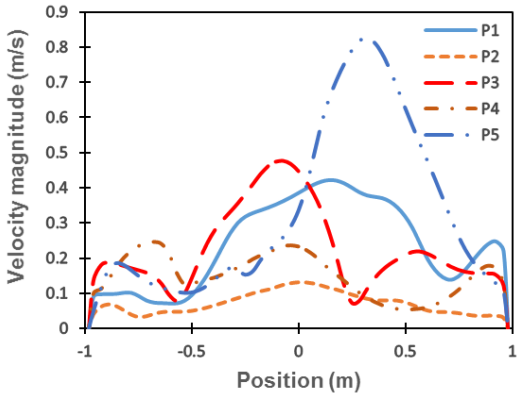

Layout 1

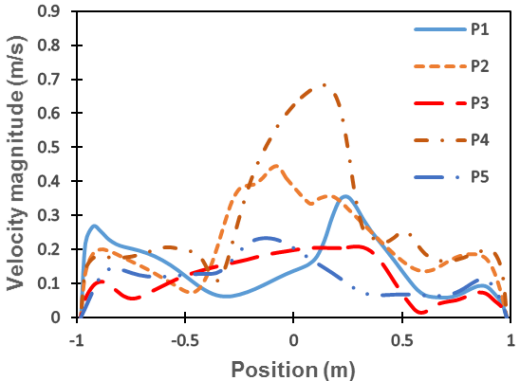

Layout 2

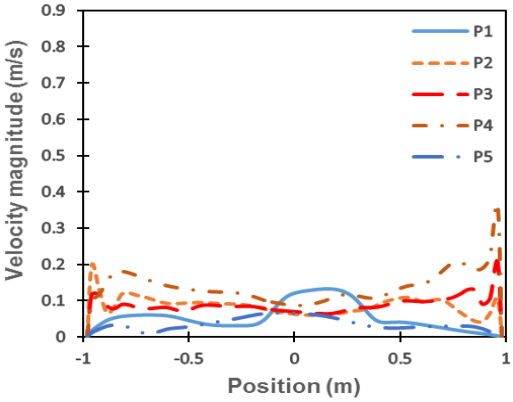

Layout 3

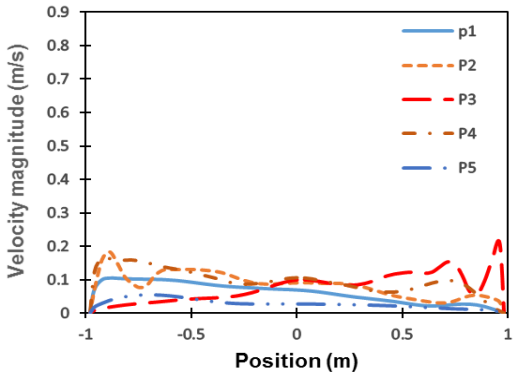

Layout 4

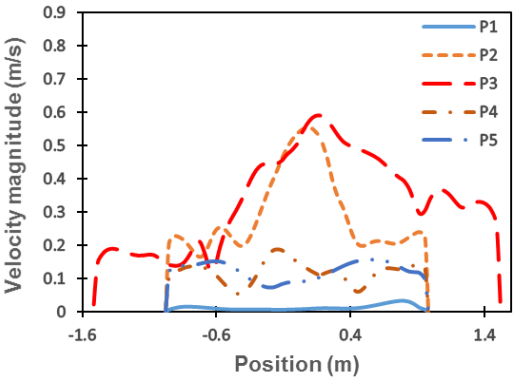

Layout 5

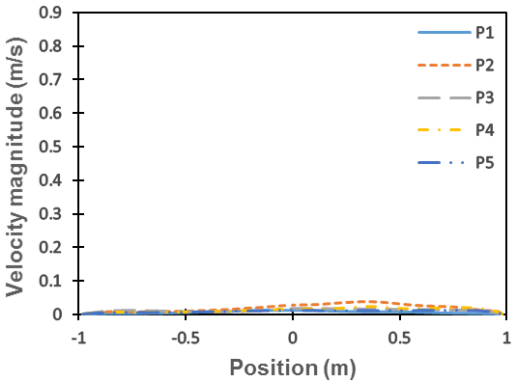

Layout 6

Figure 6.11: Velocity profiles at rotational rate 150 rad/ sec at locations P1 to P5

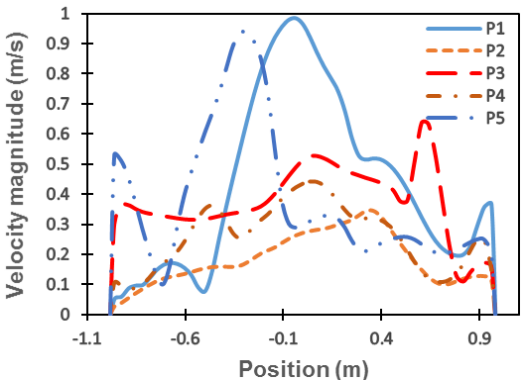

Layout 1

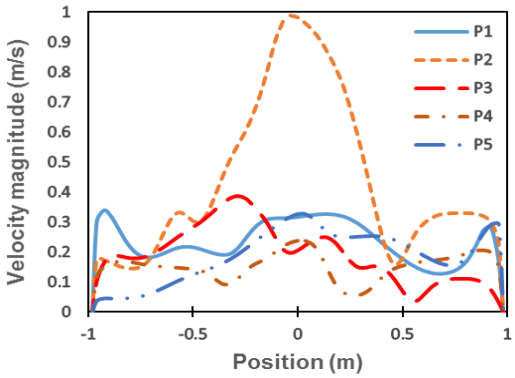

Layout 2

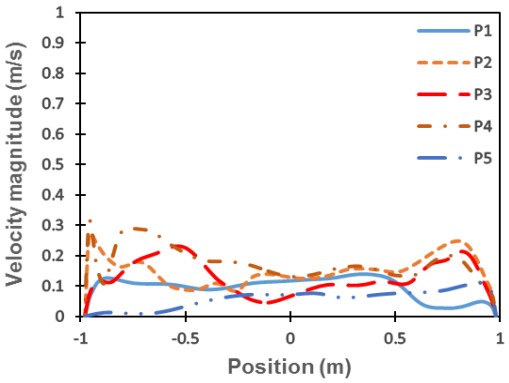

Layout 3

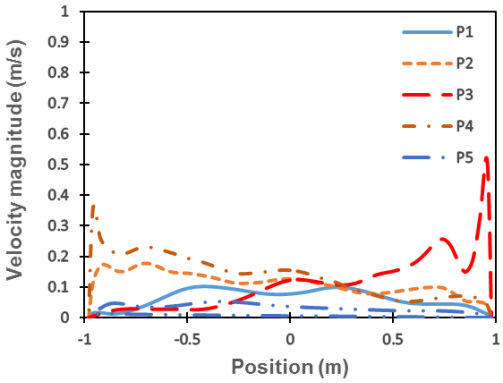

Layout 4

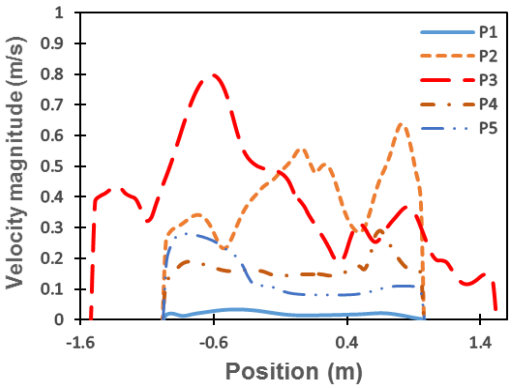

Layout 5

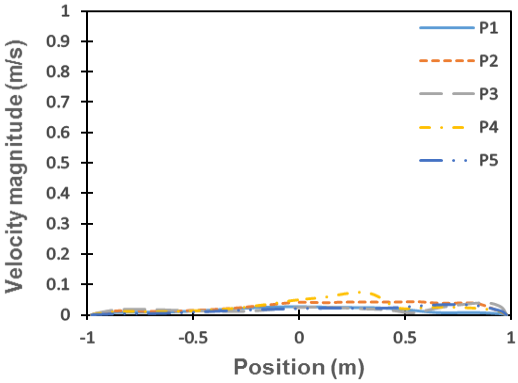

Layout 6

Figure 6.12: Velocity profiles at rotational rate 200 rad/ sec at locations P1 to P5

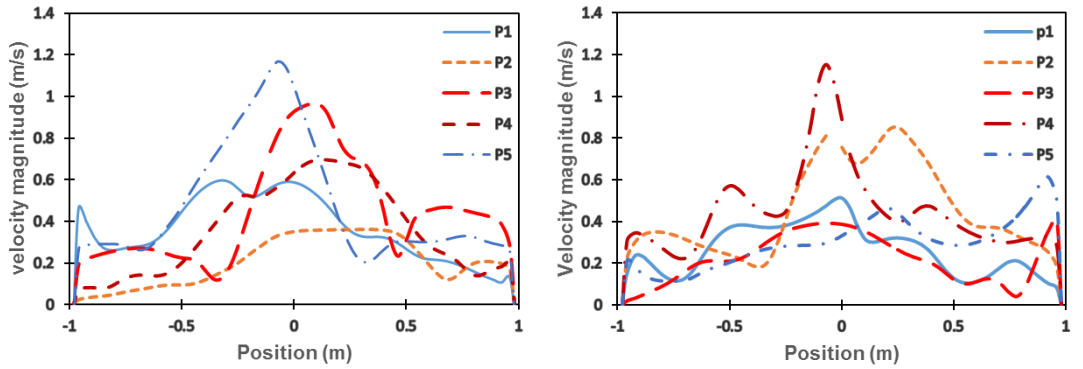

Layout 1

Layout 2

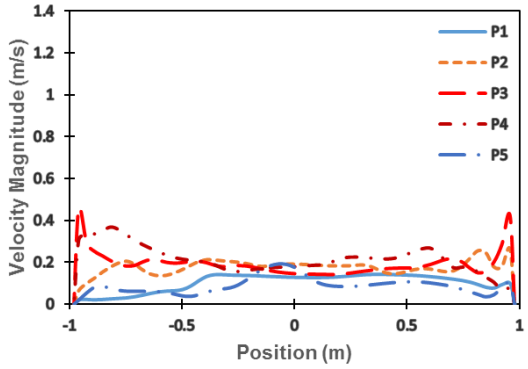

Layout 3

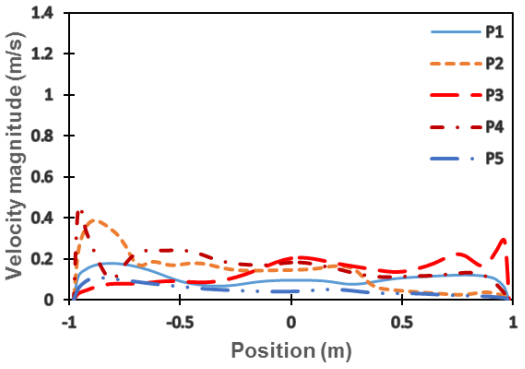

Layout 4

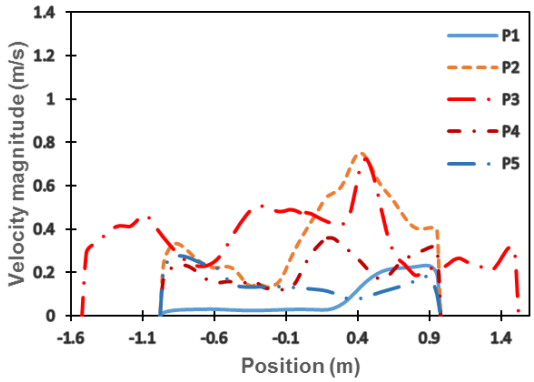

Layout 5

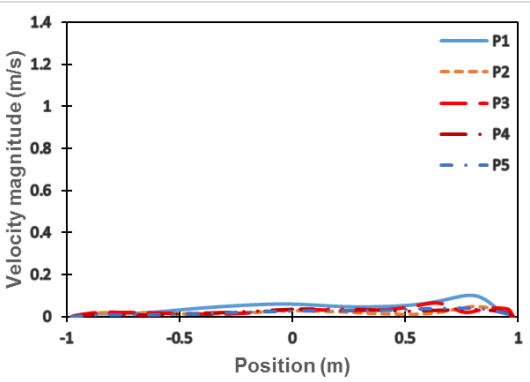

Layout 6

Figure 6.13: Velocity profiles at rotational rate 250 rad/ sec at locations P1 to P5

A typical furnace is designed to deliver an appropriate thermal cycle to the steel charge. However, thermal inefficiencies sometimes occur due to the failure in one of the heating zones, leading to low energy transfers by radiation to the charge and the need for the enhanced convection becomes indispensable.

Figures 6.15 to 6.20 show the temperature distribution contours for the six different layouts at plane 3, (marked in red in Figure 6.7), when using the rotating cylinder technique. The temperature profile was affected noticeably by the rotational flow induced by the rotation of the cylinders, in comparison with the same temperature profile for a case when the technique was not involved, Figure 6.8.

In turbulent flow, particles of fluid which are initially separated by a long distance can be brought close together by the eddying motions. As a consequence, heat, mass and momentum are, very effectively, exchanged. Therefore, turbulent flow promotes diffusivity which is a signature of a mixing. Mixing results from fluctuations interaction of the transport parameters [111, 140].

The convective heat transfer and fluid mechanics are strongly connected. Temperature contours show that the hot gas is going towards the cylinders owing to the action of inertial forces produced by the stirring device movement. Cylinder rotation creates an enhanced thermal profile (i.e. continuously re-distributed) inside the furnace by mixing the gas with different densities due to temperature differences. The redistribution of the atmospheric gas, thus the heat, can be sustained by the rotating cylinders technique even under the long operation conditions of the cycle. Thus, the technique can help in preventing the formation of hotspots.

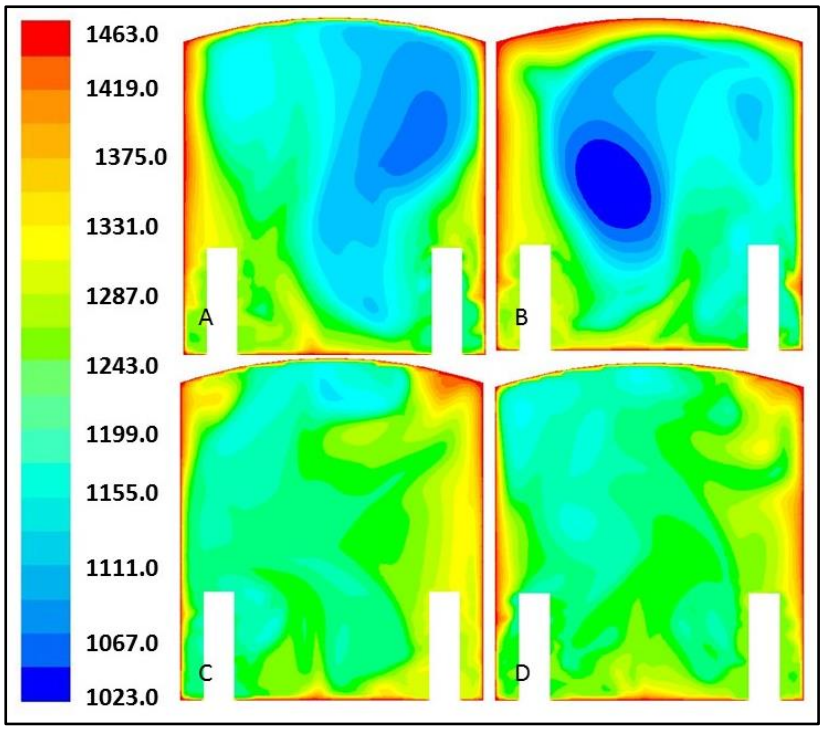

Figure 6.14: Temperature distribution contours (shown in Kelvin) for Layout 1 at, A. 100 rad/sec, B. 150 rad/sec, C. 200 rad/sec and D. 250 rad/sec

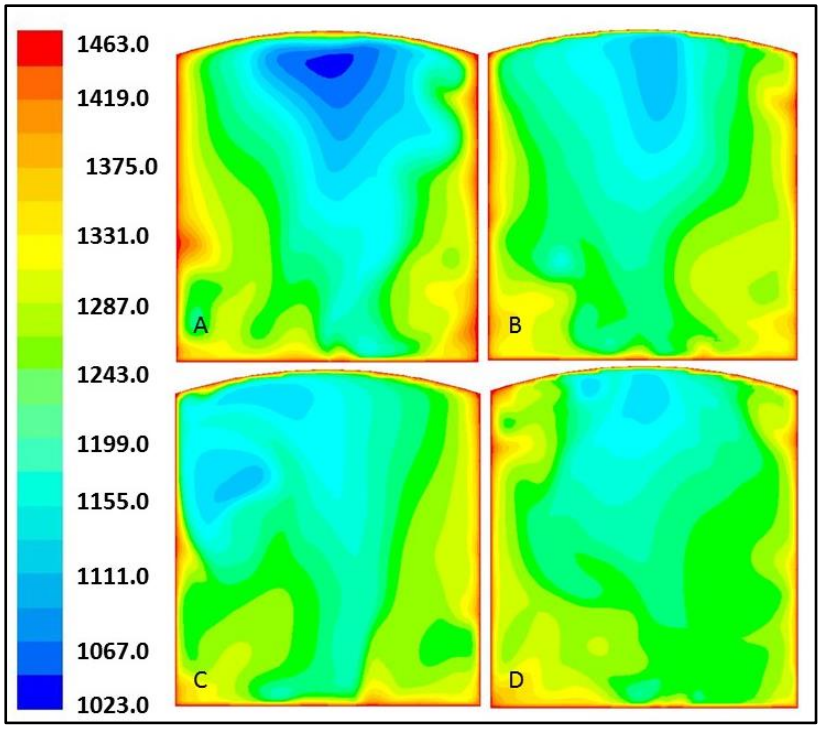

Figure 6.15: Temperature distribution contours (shown in Kelvin) for Layout 2 at, A. 100 rad/sec, B. 150 rad/sec, C. 200 rad/sec and D. 250 rad/sec

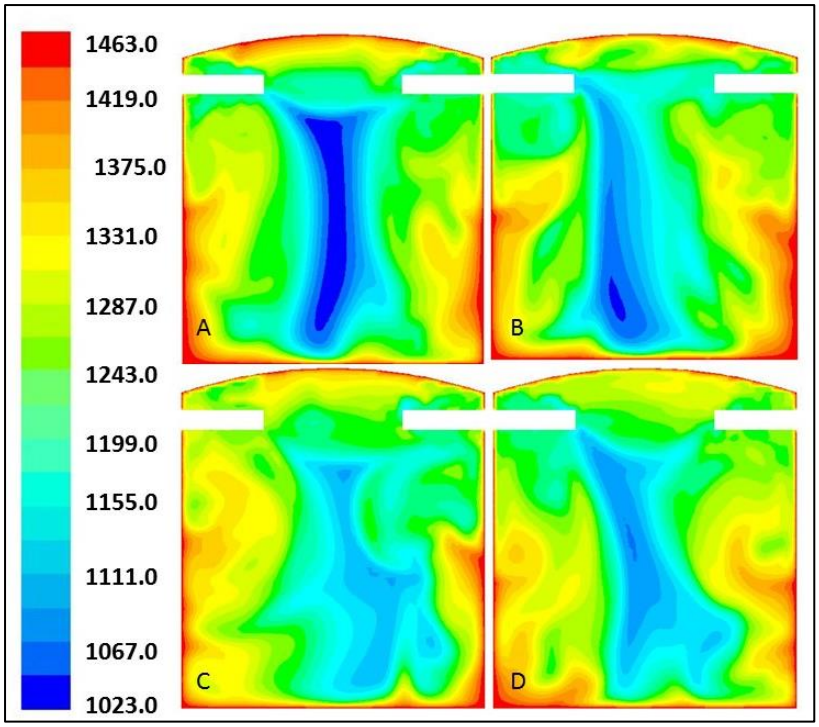

Figure 6.16: Temperature distribution contours (shown in Kelvin) for Layout 3 at, A. 100 rad/sec, B. 150 rad/sec, C. 200 rad/sec and D. 250 rad/sec

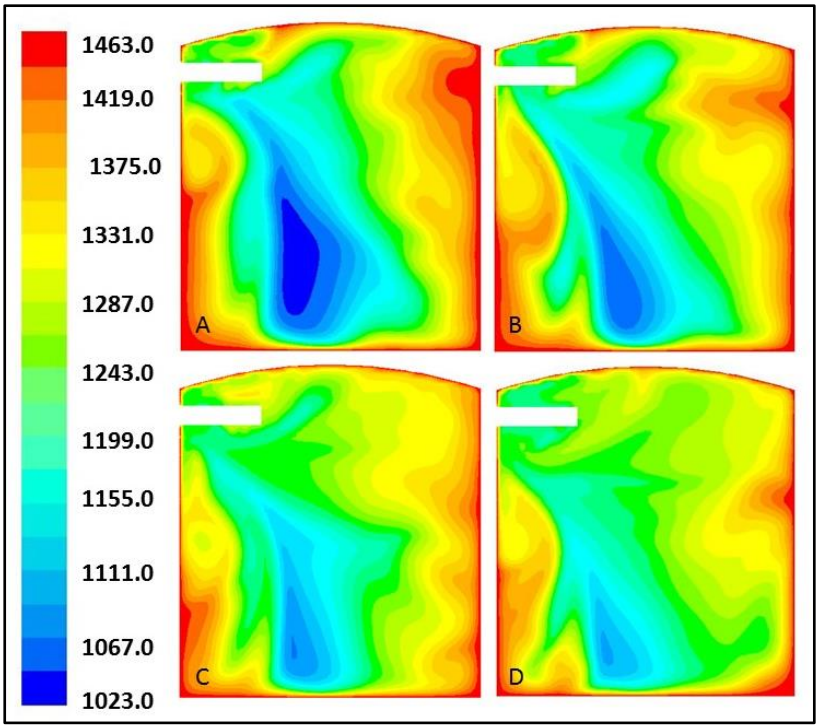

Figure 6.17: Temperature distribution contours (shown in Kelvin) for Layout 4 at, A. 100 rad/sec, B. 150 rad/sec, C. 200 rad/sec and D. 250 rad/sec

It can also be observed that for a particular layout the temperature gradients between the furnace wall and the furnace centre decrease with increasing the rotational speed, because of the generation of turbulent flow and the increase in fluid velocity. Turbulent flow is highly diffusive causing rapid mixing and increases rates of mass and heat transfer. This enhances the energy transfer quality by promoting forced convection.

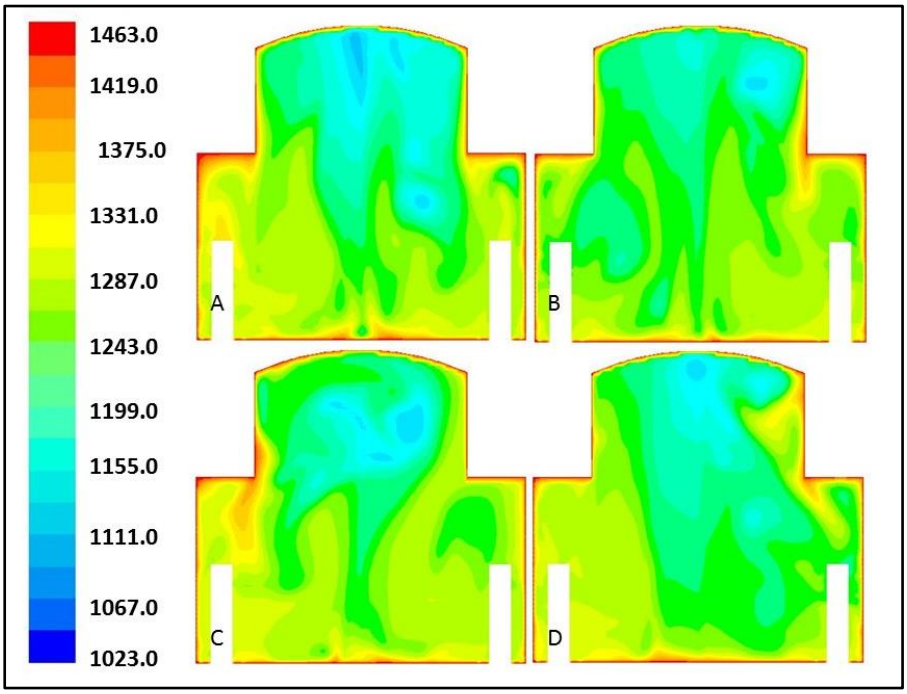

Figure 6.18: Temperature distribution contours (shown in Kelvin) for Layout 5 at, A. 100 rad/sec, B. 150 rad/sec, C. 200 rad/sec and D. 250 rad/sec

However, vortex formation in Layout 6 is confined to the top of the furnace, due to the cylinders proximity to the inner cover and the furnace top wall, Figure 6.4, which restrains the development and propagation of the vortex. Consequently, the rotation has a weak influence on the fluid structure in this layout.

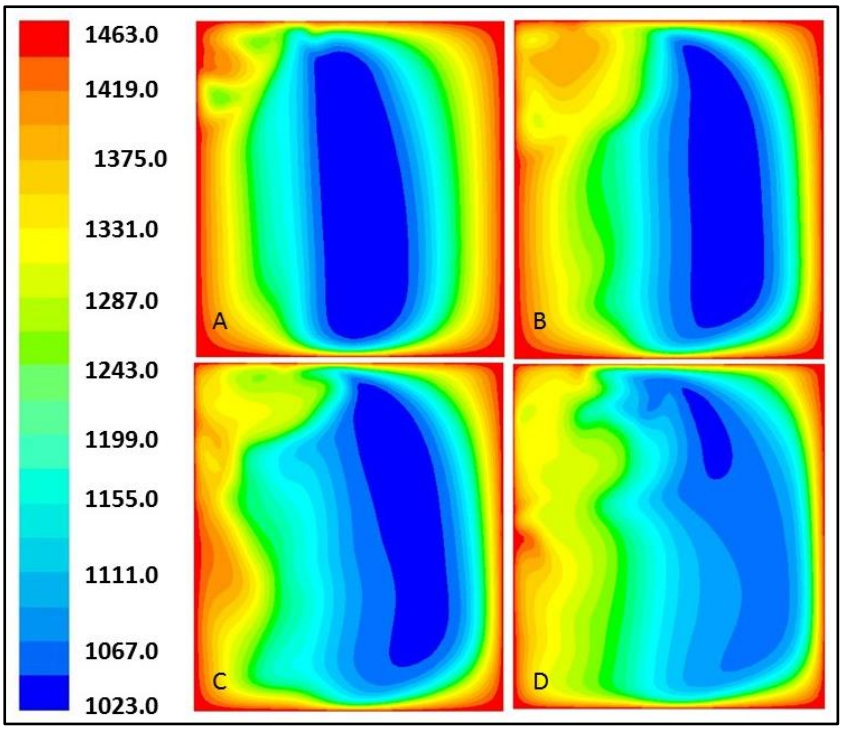

Figure 6.19: Temperature distribution contours (shown in Kelvin) for Layout 6 at, A. 100 rad/sec, B. 150 rad/sec, C. 200 rad/sec and D. 250 rad/sec

Turbulence intensity was calculated in the same way that was described in Chapter 5, using the transient velocity fluctuations data that was obtained from the transient solution for the specific time-interval using Layout 2.

Turbulence intensity values give a clear insight into the level of the turbulence strength. This uniform measurement scale would vary from 0% for an idealised flow with absolutely no fluctuations in fluid speed or direction to 100% for the fully turbulent flows. Turbulence intensity values greater than 100% are possible and can happen when the average fluid speed is small, and there are large fluctuations presented [141].

The turbulence intensity values are varied at the selected locations shown in Figure 6.7. However, the general trend shows that the turbulence intensity increases with increasing the cylinders rotational rate, i.e. with increasing rotational Reynolds number, Figure 6.20.

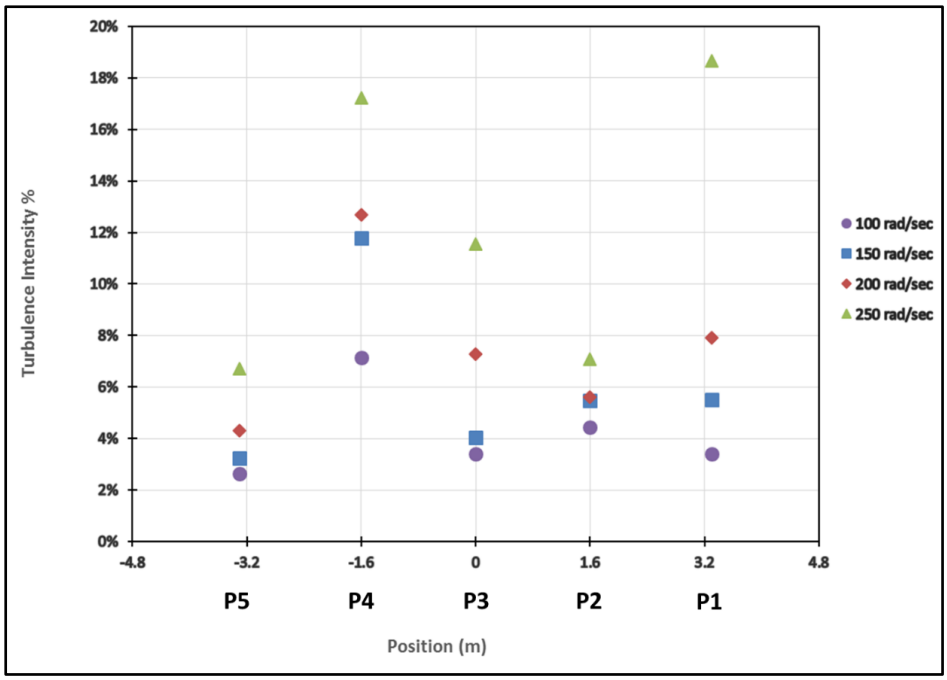

Figure 6.20: Turbulence intensity values at the selected locations of layout 2

6.4.3 Rating of the proposed layouts

The layouts were rated based on the CFD results presented in this Chapter, as shown in Table 6.4. The classification was conducting after examination of the velocity charts at various locations and the temperature contours. The layout with highest fluid velocity and best thermal mixing was classified as very good and vice versa. The optimised cylinder configuration is of Layout 1, and further transient analysis concerning the cycle duration of this particular layout is presented in the following Chapter.

Table 6.4: Performance rating of the suggested layouts

Layout	Very good	Good	Acceptable	Poor	Very poor
1	☑				
2		☑			
3			☑		
4			☑		
5				☑	
6					☑

6.5 Summary

A numerical investigation was performed using ANSYS Fluent V18.2 to explore the use of rotating cylinder technique in the High-Temperature Coil Annealing (HTCA) furnaces. The aim was to generate fluid flow during the annealing process which would eliminate the formation of the hotspots which occur during the HTCA process.

The technique was appraised empirically by first suggesting six different arrangement, at which the cylinders were installed vertically and horizontally inside the furnace cavity in order to prioritise the best arrangement that can generate fluid recirculation. Four rotational rates were investigated 100, 150, 200 and 250 rad/sec.

The simulations involved steady-state and transient solutions. The presentation of the results was via velocity charts, velocity vectors, temperature distribution contours and turbulence intensity chart.

The results were considered promising as they showed the capability of the technique to produce turbulent flow and generate gas recirculation in the HTCA furnaces. The results also showed that the layouts where the cylinders were installed vertically produced relatively higher turbulence than those layouts where the cylinders were installed horizontally.

The rotational rates of the cylinders have an influential effect on the fluid domain and the turbulence generated. It was noted that the speed of the fluid particles increases with increasing the rotational speed due to the high inertial forces applied to the fluid domain by the rotating cylinders. The turbulence intensity also increases with increasing the rotational rates due to the increase in rotational Re.

The temperature profile presented by the temperature distribution contours showed a noticeable response to both the generated flow and the increase in rotational rates. Therefore, it is shown that the proposed technique can help in generating recirculation and thus help in reducing the formation of the hotspots in batch annealing furnaces. In the following chapter, the potential enhancement is explored further through a bespoke transient model developed for this purpose.

CHAPTER 7:

TRANSIENT MODELLING OF RAPID HEATING PROCESS

Chapter 7

Transient Modelling for Rapid Heating Process

7.1 Introduction

In this chapter a transient modelling of the heating-up segment is presented. The transient analysis was performed using Layout 1 which was found to be the optimised cylinder configuration in terms of generating better fluid mixing based on the outcomes of the steady state analysis presented in Chapter 6. The objective is to explore the potential enhancement of the proposed technique represented by reducing the cycle duration.

7.2 Heat Transfer Mechanisms in The HTCA Furnace

The predominant heat transfer mechanism in the HTCA furnaces is the thermal radiation emitted from electrically heated wall elements. Natural convection is also present due to the density difference of the atmospheric gas. The inner covers receive heat from the electrical elements and re-radiate it to the coil surface; heat is then conducted through the coil wall to the bore.

Heat transfer in the furnace during heating process is described by the following mechanisms, Figure 7.1:

1. Radiation from the heating elements to the inner cover and base plate
2. Inner cover to coil's outer diameter by radiation
3. Atmosphere to expose surfaces by convection
4. Outer coil surface to interior by conduction
5. Inlet furnace gas cools expose surfaces by convection
6. Base heating element to bottom coil by conduction

The present research focuses on promoting forced convection in the furnace chamber, i.e. between the inner covers and the heating elements using the proposed technique

of the rotating cylinders. Thus, the heat transfer mechanisms change by introducing extra mechanism represented by the forced convection, Figure 7.2.

The surfaces that are affected by the forced convection are only the inner covers. This is because the technique is not capable of generating any fluid recirculation inside the inner covers, hence no forced convection is introduced around the steel charge. Therefore, the temperature of the inner cover surface was examined throughout the transient model in this Chapter. The examination included monitoring the inner cover temperature to check if it reaches the target temperature, dictated by the segment's requirement, in a short time. It was assumed that the time saved during heating-up the inner covers has an impact on reducing the overall cycle time as the following segment could start earlier than in a conventional cycle.

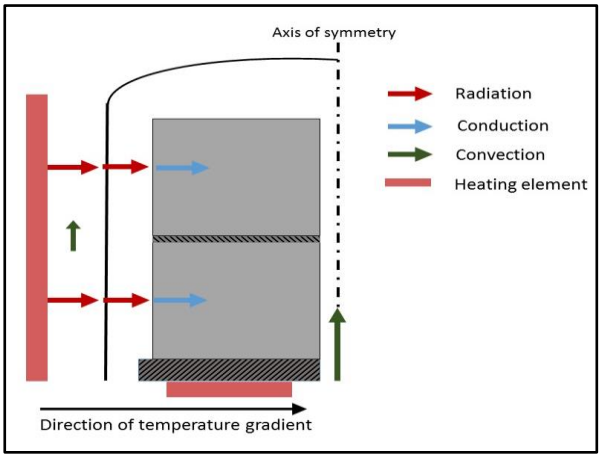

Figure 7.1: Principal heat transfer mechanisms in furnace during heating

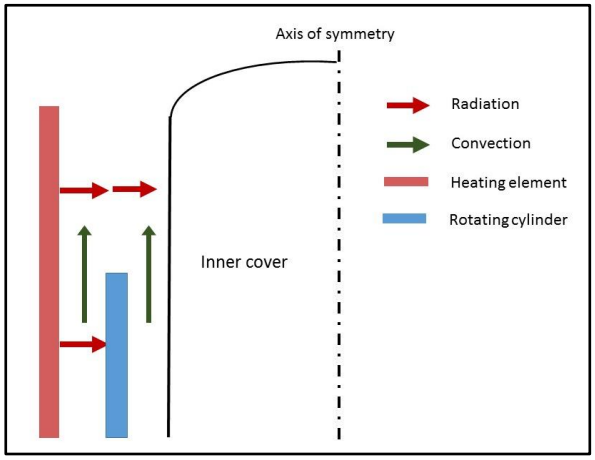

Figure 7.2: Schematic of heat transfer mechanisms when using the technique

7.3 Transient Model of The HTCA Heating-up Cycle

In this Chapter an advanced transient model of the rapid heating-up segment of the annealing process is presented. As stated in the previous section, the model focused on monitoring the transient temperature of the inner cover surface when fluid mixing is introduced. Some simplifying assumptions were made to produce simple representation of the present problem.

For instance, taking the advantage of the symmetrical distribution of the heating elements on the furnace wall and the gas inlet pipes on the base as well as the inner covers, the computational model of the present transient analysis was created as an axisymmetric section through the centre of the 3D-geometry of the furnace, Figure 7.3. This eliminates the computational-time for solving the governing equations of a full geometry. Furthermore, the effect of the radiation view factor was assumed negligible and, therefore, the temperature supplied by the furnace to the entire inner cover surface was assumed uniform. This assumption facilitates both; setting up monitoring of the average temperature on the inner cover surface and selecting less expensive radiation model, such as discrete ordinates (DO) model. The effect of the heat from the base on the inside of the inner cover surface was neglected, as most of the heating energy transfers by conduction directly to the base plate and the steel coil stacked in the bottom.

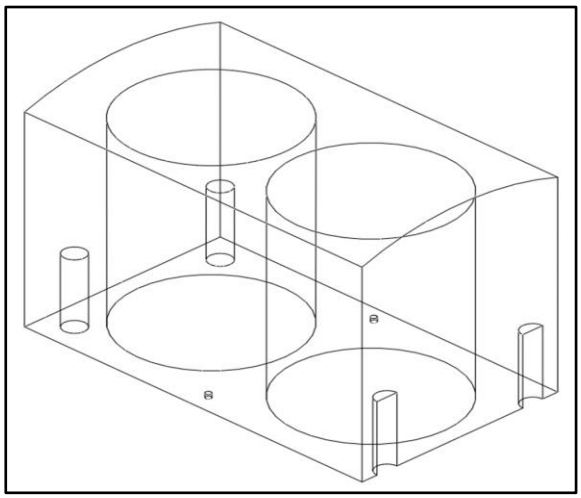

Figure 7.3: A symmetrical computational model of the HTCA furnace with the presence of the cylinders

7.3.1 Physical and boundary condition setup

The transient simulation considered the rapid heating-up segment which is the onset of the annealing process. During this segment, the furnace components and the steel load are heated from the ambient temperature (~20 ^{o}C) to a temperature of (640 ^{o}C) of total running time of approximately (~ 5 hrs). The early stage of the annealing process operates with an atmospheric gas of 3NH mixture, which is a mixture of 3% H_2 and 97% N_2. The atmospheric gas is injected to the furnace chamber at a specific mass flow rate in regular periods throughout the segment. The gas enters the furnace at the ambient temperature.

The properties of the gas mixture were calculated as the sum of the values of the corresponding properties of the individual components, multiplied by their mass fraction in the mixture, Equation 7.1,

$$\emptyset_n = \sum(x_i * \emptyset_i)_n \qquad 7.1$$

where, x_i, is the mass fraction of the component (i) in the mixture. The variations in the mixture properties throughout the process were taken in the consideration by applying a piecewise-linear function of temperature for the material properties within Fluent database.

The main boundary conditions were controlled with respect of time by User-Defined Functions (UDFs) written especially for this simulation in C++ programming language using Visual C++ 2010 Express software. The UDF is called by Fluent solver to update the boundary conditions before the next time step of the time-dependent solution. UDFs were devised to control the furnace wall temperature and the inlet gas flow rates, appendix A. The UDFs were tested thoroughly in separate solutions to ensure that they are valid and represent the process boundary conditions. The tests were done by monitoring the coded conditions at their relevant boundaries.

The gas flow rate was obtained from the standard operating procedure provided by Cogent. Data of wall temperature was obtained from thermocouples recording of an actual heating-up process at Cogent, Figure 7.4. In the actual conventional process,

the inner cover heats to the target temperature by the radiation emits from the heating elements taking approximately 5 hours and 27 minutes. The CFD model was created up to the end of the rapid heating up segment and was set to end when the temperature of the inner cover reaches the target temperature of 640 ºC. Two different rotational rates of 100 and 150 rad/sec were used.

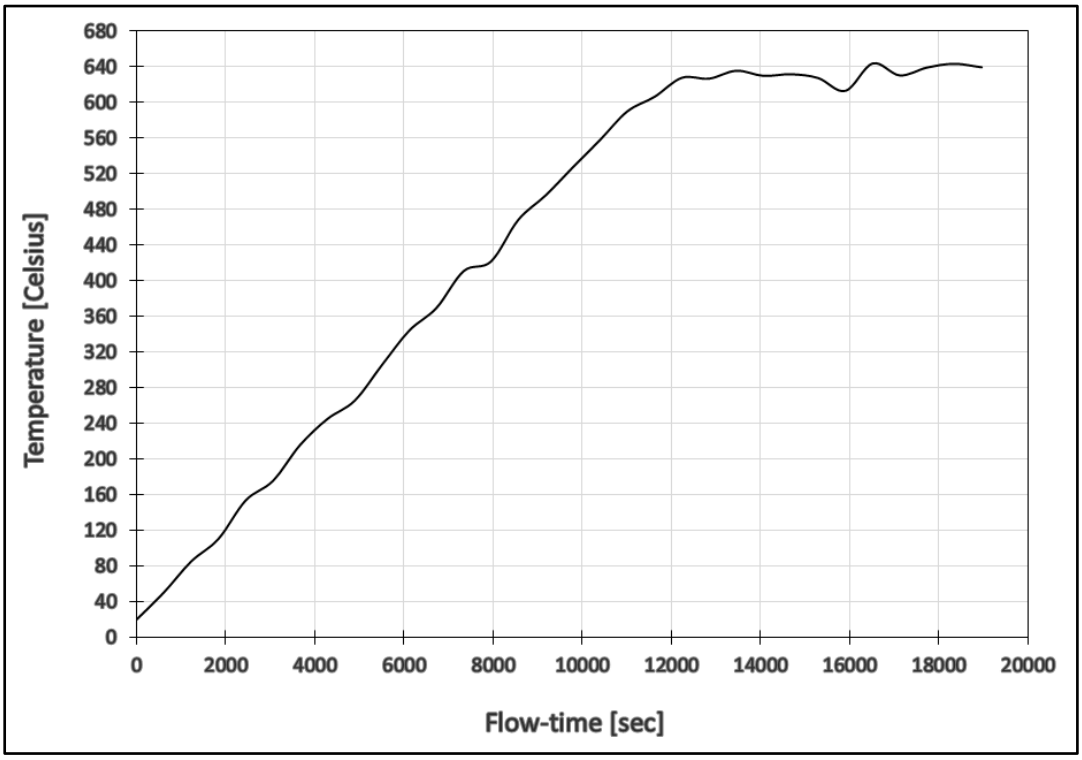

Figure 7.4: Actual temperature records on furnace wall of heating-up segment

7.4 Results and Discussion

Figure 7.5 shows temperature profiles of the inner cover surface when using the rotating cylinder at 100 and 150 rad/sec. The temperature profiles were plotted and compared with a data of actual process, Figure 7.4. Due to lack of recorded data of inner cover temperature, it was assumed that the inner cover heats at same time with the furnace wall and both have relatively same thermal profile in a conventional annealing process. This assumption was made based on data provided by Buckley [131], which showed that the temperature profiles of the inner cover at two different locations matched with the furnace wall during the rapid-heating segment, this is because of the well distribution of the heating elements inside the furnace.

It can be seen from Figure 7.5 that the inner cover temperature reached the target temperature of the segment, i.e. 640 ^{o}C, considerably earlier than in the conventional process. As stated in the previous section the solution ended when the inner cover reached the target temperature that was set through the boundary conditions using the UDF. The temperature is expected to increase further as the furnace wall temperature continuous in increasing. Therefore, the segment would need to be rescheduled to consider the savings in order not to heat the product for long time.

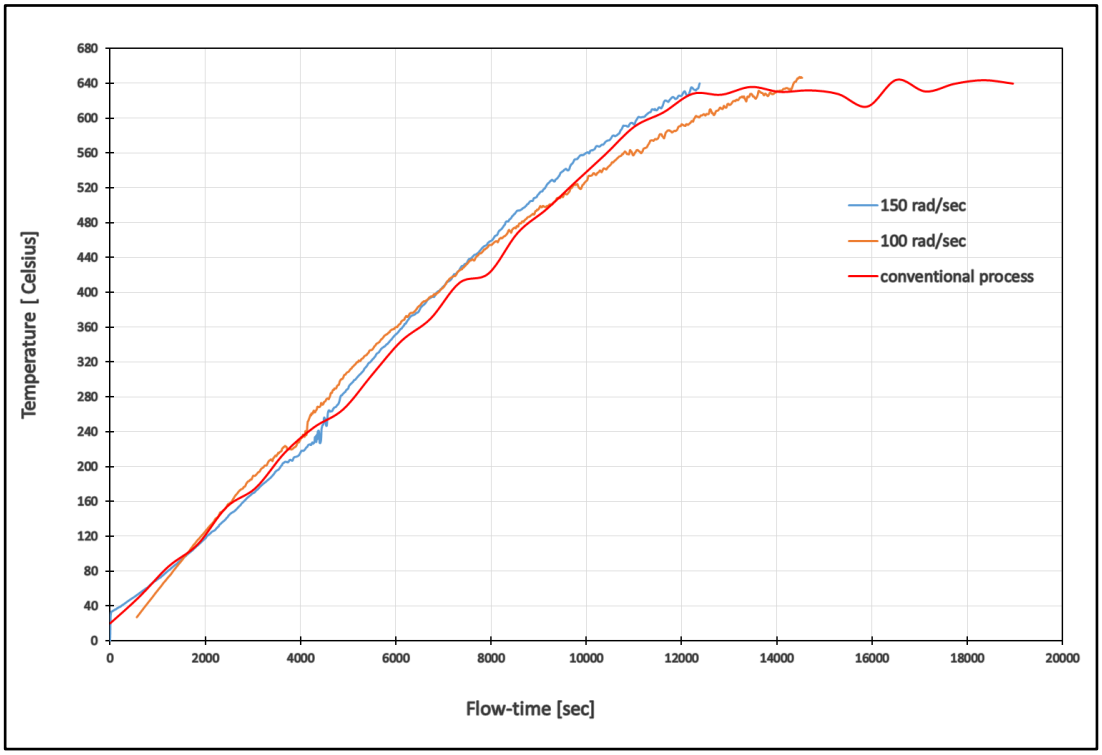

Figure 7.5: Inner cover temperature at 100 and 150 rad/sec.

There was about 1.8 hour saving when using high rotational rate of 150 rad/sec, whereas the amount of time saved when using low rotational rate of 100 rad/sec was approximately 1 hour. The higher rotational rate promoted high fluid velocity which enhanced the convective heat transfer. The convection heat transfer is strongly dependent on the flow velocity, the higher flow velocity the higher heat transfer rate, see Section 2.5. The results presented in Chapter 6 shows that the flow velocity varies through the furnace in an average of 0.43 m/sec at 100 rad/sec and 0.51 m/sec at 150 rad/sec.

Figure (7.6), shows the flow instantaneous path-lines inside the furnace coloured based on the temperature values at early stage of the heating process. The figure shows the fluid layers induced by the rotating cylinder. The stream lines at different temperatures indicates the fluid mixing and the energy transfer between the furnace wall and the fluid, and between different layers of the fluid domain itself. The heat then transfers from the fluid to the inner cover, promoting a forced convection.

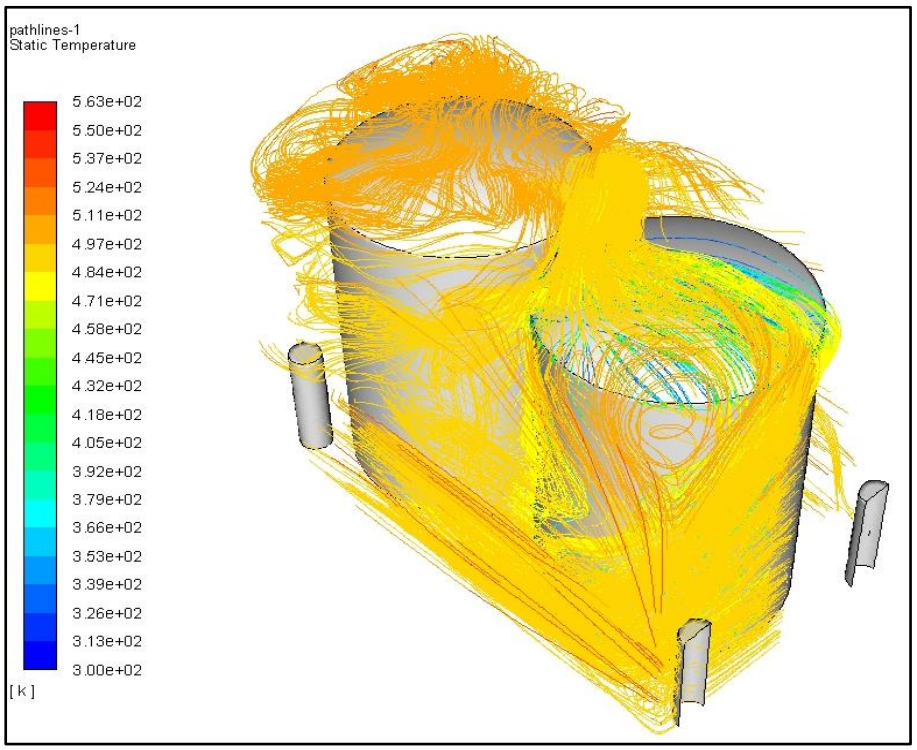

Figure 7.6: Flow path-lines coloured by the value of static temperature

7.5 Summary

A transient model of the heating-up segment of the annealing process was presented in this chapter. User-Defined Functions relevant only to this process was presented through complex data analysis and C++ coding proficiency. The model looked at the heating segment of which the target temperature is 640 ^{o}C and the process atmospheric gas is 3HN. The rotating cylinder were set at 100 and 150 rad/sec in two separate solutions and the results were compared against actual process data.

There was about 2 hours saving in the segment time when applying a high rotational rate of 150 rad/sec whereas about 1 hour saving for the low rotational rate. According to this saving the segment duration can be, therefore, re-scheduled in the actual process in order to prevent product overheating during the segment.

The predictions for time reduction and cost-saving shown in the following chapter are based on the time saving obtained when using the cylinders at the heating-up segment of the 640 ^{o}C peak in the transient model, presented in this chapter, and on a theoretical assumption of eliminating the occurrence of the electrical failure, when using the cylinders during the full annealing process.

The numerical investigation presented in this study showed that the technique is capable of both; generating fluid mixing and producing forced convection which speeds the heating time of the inner cover.

CHAPTER 8:

GENERAL DISCUSSION

Chapter 8

General Discussion

8.1 Overview

Production of electrical steel requires large amounts of energy due to processes that add high value to the basic raw material; steel sheet. Recent years have seen a worldwide change in the environmental policy towards integrated pollution prevention and energy consumption. These policies have focussed their attention on energy-intensive industry with the aim of reducing energy consumption in order to mitigate greenhouse gas emissions. Legislations to reduce energy use in the commercial sector was introduced in the UK. The impact of this legislation will affect the British industry, pushing it towards greener technologies in order to meet the government's binding targets on emission reductions.

One of the most energy-intensive processes utilised in the production of the electrical steel is the high-temperature coils annealing process. This study was devoted to investigating the opportunities of improving the thermal cycle in the high-temperature coil annealing furnaces. The study aimed at developing convection during the process by promoting fluid recirculation, thus providing better fluid mixing and reducing the process duration. An unconventional technique that has never been utilised in such application in industrial furnaces was proposed; that is the rotating cylinders technique.

8.2 General Evaluation of The Proposed Technique

In this study, a rotating cylinder technique was proposed as an alternative to the conventional techniques that are usually used to generate fluid flow, such as impellers. The limitations of using other conventional devices in the high-temperature annealing furnaces are represented by the space limitation and the high cost of using super-alloy construction materials to cope with the elevated temperatures and to be easily manufactured to a shape of blades. The simple geometry of the cylinder make its

manufacturing out of, for instance, ceramic materials less complicated. Ceramic materials have a long history of effective use in many applications due to their hardness, stiffness, strength, resistance to corrosion, resilient to oxidation and deterioration at elevated temperature. Continuous fibre ceramic composites (CFCC) [142] or ceramics such as Alumina (Al_2O_3) and Silicon Carbide (SiC) [143] are the popular material of choice , for instance in burners, because of their high melting temperatures [144].

It is a challenging task to accommodate the cylinders inside the inner covers to generate fluid recirculation due to the space limitation. Furthermore, due to the process requirement of settling the inner cover in a sand seal to maintain certain pressure inside the covers, the range of the flow circulation cannot exceed the inner covers wall. Thus, the limitation of the technique is that not providing any fluid recirculation inside the inner covers, hence there is no change in the heat transfer mechanisms (discussed in Chapter 7) inside the inner covers. This would need to be considered for further investigation on the improvement of the HTCA technology.

The technique provides sustained turbulence, thus fluid mixing, within the fluid domain. However, it cannot provide the maximum mixing in some layouts, e.g. Layout 6 and 4, unless using high rotational rates, i.e. high rotational Reynolds number. This would be of great challenge when implementing it as it will require continuous inspection and maintenance to the cylinder's shaft and motor assembly as well as building the cylinders of materials that can cope with the high-rotational rates.

In the layouts where the rotating cylinders were installed horizontally in the furnace, the effect of fluid circulation is low especially in the gaps between the inner covers. The fluid velocity was low at these locations (~ 0.4 m/sec) as shown in the velocity charts, Chapter 6. To generate better fluid mixing in the space between the inner covers a large number of cylinders must be used so that a pair of cylinders can be located between two successive covers. In this regard, and based on the fluid velocity achieved at the referred locations, Layouts 1 & 2 are the best options.

The design of Layouts (1&2) is relatively simple for implementation as they do not require any modifications in the furnace i.e. enlargement, see appendix B.

Furthermore, there is a flexibility in selecting the vertical cylinder's height, whereas in the horizontal cylinders was limited due to the inner covers location. The horizontal cylinders are less durable as the high temperature and the gravity effect can lead to bending of the cylinder's geometry.

The cylinders in the base of the furnace can be monitored more easily by the HTCA operators during the packing process of the furnace using the head crane, whereas the horizontal cylinders are more exposed to be damaged when fitting the furnace on the base with the existence of the inner covers. Furthermore, the inspection and maintenance process of the horizontal cylinders could be a cumbersome task, because of their location. This would cause a delay in the production process as the furnace cannot be used on a ready charge, as it has to cool down for the inspection purposes.

Layout 6 was suggested in order to increase the convection at the top of the furnace. This can create a thermal balance between the top of the furnace and the base, which experiences heat accumulation due to the extra heat coming from the base heating elements. However, this layout requires using, exclusively, high rotational rates to overcome the flow's restrictions represented by the inner covers and the furnace roof. Moreover, it requires some enlargement of the furnace to accommodate the cylinders above the covers. Therefore, Layout 5 and 6 would not be recommended for implementation due to the high cost and engineering difficulties associated with re-building the furnace geometry and the lining. Table 8.1 shows the criteria that were used to make the decision over the optimised cylinder configuration.

Table 8.1: Practicality rating of the suggested layouts

Criteria	**Lay. 1**	**Lay. 2**	**Lay. 3**	**Lay. 4**	**Lay. 5**	**Lay. 6**
Availability	+++	+++	+++	+++	---	---
Ease of implementation	+++	+++	+-	+-	---	---
Ease of maintaining	+++	+++	---	---	+++	---
Reliability	+-	+-	+-	+-	---	---
Temperature uniformity	+++	+-	+-	+-	---	---

(+++) High (+-) Moderate (---) Low

The reliability of the majority of the layouts was rated as moderate because of the limitations of the technique itself. Layout 1 can deliver the best benefit to the current situation. The distribution of the cylinders inside the furnace in this layout creates enhanced fluid mixing and gas flow within most of the fluid domain inside the furnace. The cylinder position close to the heating elements can eliminate the occurrence of the hotspots. This alone could save the HTCA process a two-hour extension added to each defective charge by the process computer for a zone failure.

8.2.1 Comparison of the proposed technique and other options

The fan has always been the best option to be considered for generating fluid flow, it is more reliable than any other alternatives. The current HTCA furnace is equipped with a centrifugal fan attached to the furnace and connected with a water-cooled heat exchanger. The fan is used only during cooling process when the hydrogen concentration is very low. The fan takes the hot gas out through the outlet pipes, (see Figure 2.11), and force it to pass through the heat exchanger before returning the gas to the furnace chamber through the inlet pipes. Theoretically, the fan can be used during the rapid heating stage when the temperature arises from the ambient temperature to the lower soaking temperature of 850 ºC. For several reasons the fan cannot be used beyond this limit, for example the fan material quality limitation.

Research by Buckley [131] suggested using an impeller to produce convection in the furnace and around the steel coils, however, the study focused, mainly, on radically modifying the furnace design. The furnace redesign would work at the time of Buckley's research because the coil diameter was about 60% smaller than the coil that is processed at Cogent in the present time. The proposed re-design of the HTCA furnace enables installing an impeller in the base more easily.

The present study considered the challenge at the current furnace configuration and the space limitations of the furnace and the base, thus, installing an impeller is not possible. Due to all the above challenges associated with using a fan/impeller, this option was not approved by the industrial sponsor represented by Cogent, see appendix C, and thus, it was not considered for further investigation in the present study.

8.3 Energy Analysis and The Expected Benefit

After a comprehensive evaluation of the proposed layouts based on their practicality and the results presented in Chapter 6, it was decided that the optimal cylinders design is Layout 1, a layout with six cylinders of 200 mm in diameter installed vertically in the base. Therefore, other layouts were omitted during energy analysis process presented in this section.

By preventing the occurrence of the hotspots via generating better fluid mixing, the annealing process will experience no events of electrical failure, unless other physical problems/damage exist in the heating elements themselves. Thus, the process will eliminate the extra two-hour-extension of the full cycle time for the element failure, and save about ~ 16% of the consumed energy per charge (when saving the extra kilo-watts that are consumed to overcome the electrical failure). Another potential benefit is represented by the removing purchase and maintenance costs for the inner covers when they deform due to the hotspots formation.

The results showed that with presenting forced convection around the inner cover about ~2 hour was saved out of the segment total time. Based on the standard energy consumption at Cogent, 1 hour saving in time is equal to ~ 400 kWh saving in energy. Simple payback calculation is presented in Table 8.2, the calculations are based on the time saved during the first heating segment of the annealing process.

The cost of the first implementation (£185k) is considerably expensive as it is the first ever implemented, thus further implementations are expected to be cheaper.

Table 8.2: Payback analysis

Detail	**Value**	**Description**
Electricity tariff [145]	13p/kWh	ex VAT
Target weeks/year	54	
Target cycles/week	1	Assuming one charge/week
Target hours/cycle	1.8	Saved from 1st segment
kWh saving/charge	720	
kWh saving/year	38880	
Monetary savings/year	**£5054**	
kWh added/charge	8000	During electrical failure
kWh saving/year	432000	Estimated from elimination of failure
Monetary saving/year	**£56160**	
Total estimated savings	**£61214**	
Modified unit cost	185,000	Estimated
Simple payback	3	Years

CHAPTER 9:

CONCLUSIONS AND FUTURE RECOMMENDATIONS

Chapter 9

Conclusions and Future Recommendations

9.1 Conclusions

The main conclusions of this study can be summarised as follow:

- Using a simple analysis, it was shown that the HTCA furnace with a standard performance consumed approximately 8000 kWh extra energy to compensate the thermal inefficiency during a single charge when an electrical failure occurs.

- Fluid recirculation needs to be generated in the annealing furnaces to eliminate the formation of hotspots, which are the main cause of electrical failure. Fluid recirculation promotes convection and thermal diffusivity within the atmospheric gas in the furnace chamber, thus developing better fluid mixing and energy transfer.

- A technique of rotating cylinders was proposed to generate fluid recirculation inside the HTCA furnaces. It has been shown experimentally the potential to influence the fluid structure and generation of instabilities.

- Numerically, the proposed technique of the rotating cylinders showed the capability of generating turbulence and fluid recirculation in the HTCA furnaces. The fluid recirculation is sustained as long as the cylinder is in a rotation.

- The technique has some limitations such as, it cannot generate fluid recirculation around the steel coils. Another limitation is represented by the requirement of high-rotational rates, in some layouts, to generate the desired fluid mixing.

- Furthermore, the cylinders arrangement could be sometimes a challenge from an engineering standpoint due to the nature of the HTCA technology which has limited the flexibility of installing the cylinders inside the furnace.

- The optimal cylinder configuration from the six proposed, is Layout 1, which is more practical than the others and best option to generate fluid mixing near the heating elements due to the cylinders' location near to most of the heating elements (i.e. the critical hot-spot areas).

- The transient CFD model demonstrated that the proposed technique helped reduce about 2 hours of the heating-up segment time through improved convective heat transfer.

- The estimated annual savings when using the rotating cylinders technique is £61k per annum, giving an estimated payback period of about 3 years.

9.2 Future Recommendations

The outcomes and findings of this study could open new horizons of developing the performance of the thermal cycle of the HTCA process and tackling the issue of the hotspots. Some other relevant investigations that could not be covered in this study need to be taken in the consideration. This includes:

- It is recommended conducting further transient modelling studies to cover more range of furnace operations. This requires witting very complicated C++ codes to set the transient boundary conditions, including the compositions of the atmospheric gases and their flow rates during the different segments. This is particularly important when two different gases with different flow rates are injected separately during a single heating segment.

- This study suggested using ceramic materials to build the cylinders because of their excellent performance at high temperature. However, an intensive investigation should be carried out using cylinders made of a range of materials exposed to high-temperatures and rotate at high rotational rates to select the material that has the

best durability in such environment of high stresses and elevated temperatures. This investigation was not in the scope of the present study and it is important if the rotating cylinders technique is implemented in the actual furnaces.

- Building a laboratory demonstrator that could simulate the furnace's fluid domain and the rotating cylinders technique in order to test, experimentally, the validity of the proposed technique;

  - A high-speed camera and LDV technique could be used to examine the flow topology around the cylinders and the fluid domain in the surrounded area. The demonstrator should, then, be built of Perspex sheets to allow optical access.

  - White fused alumina micro-EK micro F 1000 could be used for seeding the fluid to facilitate the examination with the LDV technique.

  - Helium can be used as the working fluid inside the demonstrator enclosure. It is a good candidate for an alternative to H_2 and 3HN because it has similar mechanical properties such as density and dynamic viscosity.

APPENDICES

Appendix A

User Defined Function (UDF); transient temperature, transient mass flow rate.

```
/*****************************************************************/
/* UDF adapted by Oula Fatla       */
/*****************************************************************/

/*****************************************************************/
/* UDF written for use with Fluent V18.2       */
/*****************************************************************/

/*****************************************************************/
/* UDF need to be compiled to create a shared library in Fluent   */
/*****************************************************************/

/*****************************************************************/
/* UDF to set the transient boundary conditions       */
/*****************************************************************/

#include "udf.h"


/*****************************************************************/
/*  UDF  for  specifying  a  transient  wall  temperature  boundary
condition*/
/*****************************************************************/


 DEFINE_PROFILE(unsteady_wall_temperature, thread, position)

 {

    face_t f;                     /* Face data type */

       real t = CURRENT_TIME;

      begin_f_loop(f, thread)

/* Loop over each face belonging to the current thread */

      {

F_PROFILE(f, thread, position) = (-1e-10*t*t*t)+(7e-07*t*t)+(0.0543*t)+289.06;

      }

    end_f_loop(f, thread)

 }

/* Finish UDF */
```

```
/*****************************************************************/
/* UDF for specifying a transient mass flow rate inlet boundary
condition*/
/*****************************************************************/

/*****************************************************************/
/* time-step size should be set to match the time value in the
function */
/*****************************************************************/


 DEFINE_PROFILE(transient_mass_flow_rate, thread, i)

{

   face_t f ;

   const real delta_t = 60;      /* seconds */


   real t = RP_Get_Real("flow-time");

/* to calculate the physical time step*/

   begin_f_loop(f, thread)

  {

       if (

       (t > 0 && t < delta_t)                /* range of t */

       ||

       (t > 3600 && t < 3600 + delta_t)

       ||

       (t > 2*3600 && t < 2*3600 + delta_t)

       ||

       (t > 3*3600 && t < 3*3600 + delta_t)

       ||

       (t > 4*3600 && t < 4*3600 + delta_t)

       ||

       (t > 5*3600 && t < 5*3600 + delta_t)

       )

       {

       F_PROFILE(f, thread, i) = 0.00046/delta_t;   /* in kg/sec */

       }

       else
```

```
        {
        F_PROFILE(f, thread, i) = 0;
        }
}
end_f_loop(f, thread)
}

/* Finish UDF */
```

Appendix B

Proposals for circulating cylinder project. HTCA furnace, Tata Orb Newport provided by Wellman Furnaces: A division of Almor Limited, December 2016

The following proposal is an abstract to the real quote provided by Wellman Furnaces LTD. It covers for the first off, prototype retrofit being carried out to be established on an existing HTCA base at the Tata Cogent Power. In these retro-fit proposals, it is assumed that 6 rotating cylinders would be included in a base. The updated base will then be lifted into pre-prepared foundations in the "C" battery position. Based on the confidentiality, all units and values a part of the cost has been removed. In basic outline, the following would include:

Material Supply:

• The supply of rotating cylinders, coupling assembly, main cooling/drive assembly, drive motors etc. to provide a completely packaged assembly (six in total) for incorporation onto an existing HTCA base assembly.

• The design and building of a variable speed drive control panel. This control panel would allow the individual drive/ speed control of the 6 of rotating cylinders. At this stage given the prototype nature of this project, the control of the variable speed is included as manual via speed increase/decrease pushbuttons in the case of each cylinder assembly. In a production model, this could be further updated to include an automated control loop based on temperature or an equally suitable input parameter. Visual indication of speed will also be included on the front door of this control panel for each cylinder.

Site Work:

• Wrecking out of the refractory local to each rotating cylinder position to allow the mounting assembly bung to be inserted into the existing refractory and maintain the thermal integrity of the existing structure.

• Steelwork modification and re-bracing of the existing furnace base casing to allow the mounting and securing of the rotating cylinder assembly to the underside of the furnace base itself.
• Installation of the variable speed-drive control panel at the workshop floor level in a suitable place close to the base position. To be agreed with Tata but assumed to be no more than an xx metre cable run between furnace base and this panel.

• Site wiring of the rotating cylinder motor assemblies back to the variable speed drive control panel.

• Initial testing of the rotating cylinder assemblies prior to a product trial run. Assumed to be up to several days attendance.

• Modifications to the sub steelwork structure of the “C” Battery to provide sufficient space underneath the furnace base for the motor drive assemblies to hang.

• Additional forced cooling under the HTCA bases if deemed necessary for the drive motor assemblies.

Although Almor Wellman has provided the quotation for rotating cylinders they are reliant on the participation of Cogent personnel to facilitate and enable the assembly and installation of rotating cylinders in Battery C. The Almor Wellman quotation is not the full cost of implementing because there would be additional services (e.g. power, water, fuel gas, process gases, etc.) which need to be installed to enable operation and protection of the rotating cylinders. Cogent will need to dispose of waste materials and if asbestos is present there will be both cost and Health and Safety considerations to address.

Appendix C

Technical Project Brief
Development of Convection in High Temprature Coil Annealing (PhD)

cogent

Introduction

In the steel industry, batch annealing of steel is carried out placing coil bore vertical into annealing furnaces, applying energy to the furnace and heating and cooling the steel in prescribed temperature and atmosphere cycles to obtain an annealed product which has totally recrystallized with appropriate mechanical properties.

In the case of carbon steels, this process is carried out in furnace temperatures of 850 deg C with convection fans applying a recirculation of the gases between inner protective covers and the outer furnace. For grain oriented silicon steels, the annealing temperatures at 1200 deg c which is too high for most convection fan materials to work at effectively.

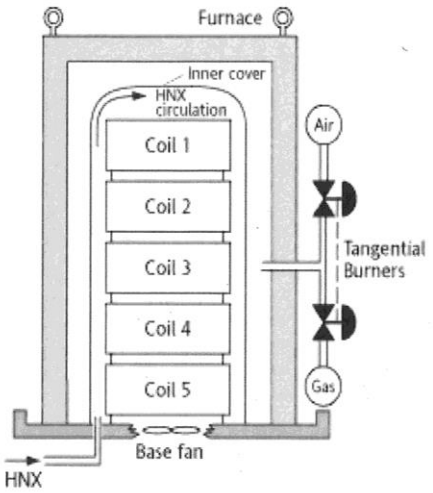

Low temperature batch annealing furnace with base fan & gas convection in cover

in the case of the Orb furnaces, space limitations, electric element heating in the outer cover and the extreme high temperatures make the process very static a number of issues result;

1. The elements operate a their operating limit and can create local hot spots which due to the lack of convection to take the excess heat away, can lead to element breakage
2. The static nature of the atmosphere in the outer cover creates temperature differentials in areas of high ratio exposure to the wall elements compared to the less direct areas. This can create metallurgical property differences in the final product.
3. The absence of convection in the inner and outer cover leads to high temperature differentials on the inner cover leading to distortion and high maintenance cost.
4. All the above are exaggerated in the case of element breakage as the remaining elements have to work harder to maintain temperature, coils experience more temperature differential and the inner covers distort more

Introduction of convection will improve all the above phenomena and by nature of more even heat distribution reduce the process cycle time by c 30% giving energy, quality and productivity improvements

The challenge

The challenge if to introduce forced convection currents in the high temperature furnace can give significant process improvements but is a significant challenge.

Design of a technology for retro fitting to 30 existing furnace would be a major improvement on the production of grain oriented electrical steels at Orb.

Approach to project (initial guide)

The focus of the project is as follows

1. Research through literature the high temperature furnace technology.
2. Research through literature and expert advice high temperature forced convection technology
3. Research through literature and "expert" contact technical aspects high temperature convection
4. Developing technical / scientific understanding of batch annealing at high temperature and influence of key parameters
5. Develop design proposals for introducing convection in the batch furnaces at Orb
6. Develop models (mathematical and / or physical) of potential designs and asses each against existing design
7. Develop recommendation from models and experience to improve batch annealing process and retro fit to existing furnaces as appropriate.

Key contributors.

The project will be undertaken within the Tata sponsored PhD programme

Technical Project Brief
Development of Convection in High Temprature Coil Annealing (PhD)

1. PhD student - TBC
2. PhD University Supervisor – TBC
3. Cogent Industrial Supervisor – Nathan Beynon
4. Expert Industrial Supervisor - TBC
5. Specialist University Supervisor - TBC

Notification - this project was not sponsored at any point throughout the time of its completion by the mentioned company (i.e. Tata Steels) as stated in the Project Brief. It was an academic project done by the author of this thesis at Cardiff University for obtaining a PhD degree.

REFERENCES

References

[1] (2015). *Strategy for losses*. Available: file:///C:/Users/c1254467/Downloads/Strategy_for_losses_17-07-15.pdf

[2] C. W. T. McLyman, *Transformer and inductor design handbook*, 2nd ed. New York: Dekker, 1988.

[3] K. Price, B. Goode, and D. Power, "Grain-oriented electrical steels for power and distribution transformers," *Ironmaking & Steelmaking*, vol. 43, pp. 636-641, 2016.

[4] R. M. Bozorth, *Ferromagnetism*: IEEE Press 1993.

[5] X. Zhaosuo, K. Yonglin, and W. Quanli, "Developments in the production of grain-oriented electrical steel. ," *Journal of Magnetism and Magnetic Materials*, vol. 320, pp. 3229-3233, 2008.

[6] J. E. Neely, *Practical Metallurgy and Materials of Industry*, 3rd ed. New York: Wiley, 1989.

[7] N. P. Goss, "Electrical sheet and method and apparatus for its manufacture and test," 1934.

[8] D. You and H. Park, "Developmental Trajectories in Electrical Steel Technology Using Patent Information," *Sustainability*, vol. 10, 2018.

[9] K. Matsumura and B. Fukuda, "Recent developments of non-oriented electrical steel sheets," *IEEE Transactions on Magnetics*, vol. 20, pp. 1533-1538, 1984.

[10] P. Beckley, *Electrical steels for rotating machines*. London: Institution of Electrical Engineers, 2002.

[11] P. Beckley, *Electrical steels : a handbook for producers and users*, 1st ed. Newport, Wales: European Electrical Steels, 2000.

[12] I. R. Uvais. (2018). *Electric Motor, Generator & Transformer Manufacturing in the UK*. Available: http://clients1.ibisworld.co.uk/reports/uk/industry/majorcompanies.aspx?entid=1730#MP8418

[13] T. Phophongviwat, "Investigation of the Influence of Magnetostriction and Magnetic Forces on Transformer Core Noise and Vibration," PhD, Cardiff University, Cardiff, United Kingdom, 2013.

[14] K. Takashina, Y. Suga, M. Fukumoto, T. Yamamoto, O. Tanaka, and K. Kuroki, "Method of producing grain oriented electromagnetic steel sheet," ed: Google Patents, 1976.

[15] R. E. Smallman and R. J. Bishop, *Modern physical metallurgy and materials engineering*, 6th ed. Oxford: Butterworth-Heinemann, 1999.

[16] F. P. Incropera and D. P. DeWitt, *Fundamentals of heat and mass transfer* 5th ed. Canada: John Wiley & Sons, 2002.

[17] R. A. Granger, *Fluid Mechanics* New York: Dover Publications, Inc, 1985.

[18] P. R. N. Childs, *Rotating flow*, 1st ed. Oxford: ELSEVIER Inc, 2011.

[19] a. s. e. blog. (2016). *On Boundary Layers: Laminar, Turbulent and Skin Friction*. Available: http://aerospaceengineeringblog.com/boundary-layers/

[20] B. S. Massey, *Mechanics of fluid* 6th ed. London: Chapman and Hall Ltd, 1989.

[21] P. A. Durbin and B. A. P. Reif, *Statistical Theory and Modeling for Turbulent Flows*, 2nd ed., 2011.

[22] N. C. Markatos, "The mathematical modelling of turbulent flows," *Applied Mthematical Modelling*, vol. 10, pp. 190 - 220, 1986.

[23] I. A. Escamilla‐Ruíz, F. Z. Sierra‐Espinosa, J. C. García, A. Valera‐Medina, and F. Carrillo, "Experimental data and numerical predictions of a single‐phase flow in a batch square stirred tank reactor with a rotating cylinder agitator," *Heat Mass Transfer*, vol. 53, pp. 2933–2949, 2017.

[24] P. J. Roberts and D. R. Webster, *Turbulent diffusion*: ASCE Press, Reston, Virginia, 2002.
[25] J. P. Holman, *Heat transfer*, 9th ed. New York: McGraw-Hill, 2002.
[26] L. Theodore, *Heat Transfer Applications for the Practicing Engineer*, 1st ed. Hoboken, New Jersey: John Wiley & Sons, Inc, 2011.
[27] M. Siddique, A. R. A. Khaled, N. I. Abdulhafiz, and A. Y. Boukhary, "Recent Advances in Heat Transfer Enhancements: A Review Report," *International Journal of Chemical Engineering*, vol. 2010, pp. 1-28, 2010.
[28] S. Chol and J. Estman, "Enhancing thermal conductivity of fluids with nanoparticles," *ASME-Publications-Fed*, vol. 231, pp. 99-106, 1995.
[29] A. E. Bergles, "The implications and challenges of enhanced heat transfer for the chemical process industries," *Trans IChemE* vol. 79, pp. 437 - 444, 2001.
[30] T. Sonawane, P. Patil, A. Chavhan, and B.M.Dusane, "A review on heat transfer enhancement by passive methods," *International Research Journal of Engineering and Technology* vol. 3, pp. 1567-1574, 2016.
[31] H.-Y. Li and J. Liu, "Mechanical engineering series- Enhanced heat transfer," vol. 1, ed, 2012, p. 6.
[32] D.V.Sabarianand, D. J. Peter, and D. Channankaiah, "Heat Transfer Enhancement in Different Corrugations – A Review," *International Journal of Innovative Research in Science, Engineering and Technology*, vol. 5, pp. 3624-3629, 2016.
[33] M. Sheikholeslami, M. Gorji-Bandpy, and D. D. Ganji, "Review of heat transfer enhancement methods: Focuse on passive methods using swirl flow devices," *Renewable and Sustainable Energy Reviews*, vol. 49, pp. 444-469, 2015.
[34] CiteSeerx. (2017). *1 ASME Fluids Engineering Division Technical Brief ACTIVE FLOW CONTROL TECHNOLOGY*. Available: http://citeseerx.ist.psu.edu/viewdoc/summary?doi=10.1.1.515.1210
[35] Y.-L. He and Y. Zhang, "Advances and Outlooks of Heat Transfer Enhancement by Longitudinal Vortex Generators," *Advances in Heat Transfer*, vol. 44, pp. 119-185, 2012.
[36] P. Deb, G. Biswas, and N. K. Mitra, "Heat transfer and flow structure in laminar and turbulent flows in a rectangular channel with longitudinal vortices," *International Journal of Heat and Mass Transfer*, vol. 38, pp. 2427-2444, 1995.
[37] M. Jadhav, R. Awari, D. Bibe, A. Bramhane, and M. Mokash, "Review on Enhancement of Heat Transfer by Active Method," *International Journal of Current Engineering and Technology* 2016.
[38] G. Mebarki, S. Rahal, and A. Hamza, "Heat Transfer Enhancement by Flow Control in a Rectangular Horizontal Channel," *International Journal of Materials, Mechanics and Manufacturing*, vol. 1, pp. 171 - 176, 2013.
[39] D. Fultz, "Films Notes - Rotating flows " pp. 1-8, 1970.
[40] H. Choi, W.-P. Jeon, and J. Kim, "Control of Flow Over a Bluff Body," *Annual Review of Fluid Mechanics*, vol. 40, pp. 113-139, 2008.
[41] Z. Han, D. Zhou, and J. Tu, "Wake-Induced Vibrations of a Circular Cylinder behind a Stationary Square Cylinder Using a Semi-Implicit Characteristic-Based Split Scheme," *Journal of Engineering Mechanics*, vol. 140, pp. 1-18, 2014.
[42] S. J. Karabelas, "Large eddy simulation of high-Reynolds number flow past a rotating cylinder," *International Journal of Heat and Fluid Flow*, vol. 31, pp. 518-527, 2010.
[43] C. F. Lange, F. Durst, and M. Breuer, "Momentum and heat transfer from cylinders in laminar crossflow at 10−4 < Re < 200," *International Journal of Heat and Mass Transfer*, vol. 41, pp. 3409-3430, 1998.
[44] A. Hemmati, D. H. Wood, and R. J. Martinuzzi, "Effect of side-edge vortices and secondary induced flow on the wake of normal thin flat plates," *International Journal of Heat and Fluid Flow*, vol. 61, pp. 197–212, 2016.
[45] S. Balachandar, R. Mittal, and F. M. Najjar, "Properties of mean recirculation region in the wakes of two-dimensional bluff bodies," *Journal of Fluid Mechanics*, vol. 351, pp. 167-199, 1997.

[46] S. Jeon and H. Choi, "Suboptimal feedback control of flow over a sphere," *International Journal of Heat and Fluid Flow,* vol. 31, pp. 208–216, 2010.
[47] J. H. Gerrard, "The mechanics of the formation region of vortices behind bluff bodies," *Journal of FLuid Mechanics,* vol. 25, pp. 401-413, 1966.
[48] P. A. Davidson, *Turbulence: An introduction for scientists and engineers*, 2nd ed., 2015.
[49] S. Kang, H. Choi, and S. Lee, "Laminar flow past a rotating circular cylinder," *Physics of Fluids,* vol. 11, pp. 3312-3321, 1999.
[50] S. C. R. Dennis and G.-Z. Chang, "Numerical solutions for steady flow past a circular cylinder at Reynolds numbers up to 100," *J. Fluid Mech.,* vol. 42, pp. 471-489, 1970.
[51] C.-W. Park and S.-J. Lee, "Free end effects on the near wake flow structure behind a finite circular cylinder," *Journal of Wind Engineering and Industrial Aerodynamics,* vol. 88, pp. 231-246, 2000.
[52] S. Kumar, C. Cantu, and B. Gonzalez, "Flow past a rotating cylinder at low and high rotation rates," *Journal of Fluids Engineering, Transactions of the ASME,* vol. 133, pp. 1-9, 2011.
[53] J. Wang and Y. Zhao, "Heat and fluid flow characteristics of a rectangular channel with small diameter circular cylinder as vortex generator," *International Journal of Thermal Sciences,* vol. 62, pp. 1-13, 2015.
[54] S. Ma, W. Chu, H. Zhang, L. Li, and J. Lang, "Impact of Vortex Produced by a Novel Curve-Micro Vortex Generator on Secondary Flow in Compressor Cascade," presented at the Turbomachinery Technical Conference and Exposition, Charlotte, North Carolina, USA, 2017.
[55] S. Ali, S. Menanteau, C. Habchi, T. Lemenand, and J.-L. Harion, "Heat transfer and mixing enhancement by using multiple freely oscillating flexible vortex generators " *Applied Thermal Engineering* vol. 105, pp. 276-289, 2016.
[56] S. B. Chen, S. Sanitjai, K. Ghosh, and R. J. Goldstein, "Three-dimensional vortex flow near the endwall of a short cylinder in crossflow: Uniform-diameter circular cylinder," *Applied Thermal Engineering,* vol. 49, pp. 73-78, 2012.
[57] E. Baban and R. M. C. So, "Aspect ratio effect on flow-induced forces on circular cylinders in a cross-flow," *Experiments in Fluids*, vol. 10, pp. 313-321, 1991.
[58] S. Rashidi, M. Hayatdavoodi, and J. A. Esfahani, "Vortex shedding suppression and wake control: A review," *Ocean Engineering,* vol. 126, pp. 57–80, 2016.
[59] M. Rosales, T. Pérez, and J. L. Nava, "Computational fluid dynamic simulations of turbulent flow in a rotating cylinder electrode reactor in continuous mode of operation," *Electrochimica Acta,* vol. 194, pp. 338–345, 2016.
[60] F. Z. Sierra-Espinosa, I. A. Escamilla-Ruiz, M. L. Rodríguez, A. Álvarez-Gallegos, F. Carrillo, and J. Teloxa, "Simulation and experimental validation of Taylor-Couette flow in square cross-section container for water treatment reactor," *Desalination and Water Treatment,* vol. 73, pp. 353–372, 2017.
[61] F. Yan, Z. Dai, G. Ruan, H. Alsaiari, N. Bhandari, Fangfu Zhanga, *et al.*, "Barite scale formation and inhibition in laminar and turbulent flow: A rotating cylinder approach," *Journal of Petroleum Science and Engineering,* vol. 149, pp. 183–192, 2017.
[62] D. Mejia, M. Bauerheim, P. Xavier, B. Ferret, L. Selle, and T. Poinsot, "Stabilization of a premixed laminar flame on a rotating cylinder," *Proceedings of the Combustion Institute,* vol. 36, pp. 1447–1455, 2017.
[63] P. Xavier, A. Ghani, D. Mejia, M. Miguel-Brebion, M. Bauerheim, L. Selle, *et al.*, "Experimental and numerical investigation of flames stabilised behind rotating cylinders: interaction of flames with a moving wall," *Journal of Fluid Mechanics,* vol. 813, pp. 127-151, 2017.
[64] D. Stojković, M. Breuer, and F. Durst, "Effect of high rotation rates on the laminar flow around a circular cylinder," *Physics of Fluids,* vol. 14, pp. 3160-3178, 2002.
[65] A. Rao, A. Radi, J. S. Leontini, M. C. Thompson, J. Sheridan, and K. Hourigan, "A review of rotating cylinder wake transitions," *Journal of Fluids and Structures,* vol. 53, pp. 2–14, 2015.

[66] S. Mittal and B. Kumar, "Flow past a rotating cylinder," *J. Fluid Mech*, vol. 476, pp. 303-334, 2003.
[67] D. E. Aljure, I. Rodríguez, O. Lehmkuhl, C. D. Pérez-Segarra, and A. Oliva, "Influence of rotation on the flow over a cylinder at Re = 5000," *International Journal of Heat and Fluid Flow*, vol. 55, pp. 76–90, 2015.
[68] H. M. Badr, M. Coutancea, S. C. R. Dennis, and C. Menard, "Unsteady flow past a rotating circular cylinder at Reynolds numbers 10^3 and 10^4," *Journal of Fluid Mechanics*, vol. 220, pp. 459-484, 1990.
[69] A. Asrokin, M. R. Ramly, and A. H. Ahmad, "Rotating cylinder design as a lifting generator," presented at the 2nd InternationalConferenceonMechanicalEngineeringResearch (ICMER2013), 2013.
[70] A. Martín-Alcántara, E. Sanmiguel-Rojas, and R. Fernandez-Feria, "On the development of lift and drag in a rotating and translating cylinder," *Journal of Fluids and Structures*, vol. 54, pp. 868-885, 2015.
[71] D. B. Ingham and T. Tang, "A numerical investigation into the steady flow past a rotating circular cylinder at low and intermediate Reynolds numbers," *Journal of Computational Physics*, vol. 87, pp. 91-107, 1990.
[72] B. Özerdem, "Measurement of convective heat transfer coefficient for a horizontal cylinder rotating in quiescent air," *International Communications in Heat and Mass Transfer*, vol. 27, pp. 389-395, 2000.
[73] G. A. Etemad and N. Y. Buffalo, "Free convection heat transfer from a rotating horizontal cylinder to ambient air: with interferometric study of flow," *Transactions of the ASME*, vol. 77, pp. 1283-1289, 1955.
[74] H. Ma, W. Lu, W. Zhou, Z. Ding, X. Lü, Y. Cao, *et al.*, "Effects of rotation on the trailing vortex and heat transfer from a horizontal rotating cylinder at higher Grashof number," *International Communications in Heat and Mass Transfer*, vol. 68, pp. 20–26, 2015.
[75] T. Takamiya, K. Hanazawa, and T. Suzuki, "Recent Development of Grain-Oriented Electrical Steel in JFE Steel," JFE Steel Corporation, Japan, JFE Technical Report 2016.
[76] K. Günther, G. Abbruzzese, S. Fortunati, and G. Ligi, "Recent Technology Developments in the Production of Grain-Oriented Electrical Steel," *Steel Research International*, vol. 76, pp. 413-421, 2005.
[77] N. Takahashi, Y. Suga, and H. Kobayashi, "Recent developments in grain-oriented silicon-steel," *Journal of Magnetism and Magnetic Materials*, vol. 160, pp. 98-101, 1996.
[78] T. Kubota, M. Fujikura, and Y. Ushigami, "Recent progress and future trend on grain-oriented silicon steel," *Journal of Magnetism and Magnetic Materials*, vol. 215-216, pp. 69-73, 2000.
[79] S. Taguchi, T. Yamamoto, and A. Sakakura, "New Grain-Oriented Silicon Steel with High Permeability "ORIENTCORE HI-B"," *IEEE Transactions on Magnetics*, vol. 10, pp. 123-127, 1974.
[80] M. Matsuo, "Texture Control in the Production of Grain Oriented Silicon Steels," *ISIJ International* vol. 29, pp. 809-927, 1989.
[81] S. Tumanski, "Magnetic Materials from: Handbook of Magnetic Measurements " in *Handbook of Magnetic Measurements* 1st ed: Routledge, 2011, pp. 117-155.
[82] C. T. Steel. (2016). *Grain oriented electrical steel*. Available: https://cogent-power.com/downloads
[83] M. B. Zirlin, "Production method for high-permeability grain-oriented electrical steel," 2015.
[84] S. Mishra, C. Därmann, and K. Lücke, "On the development of the goss texture in iron-3% silicon," *Acta Metallurgica*, vol. 32, pp. 2185-2201, 1984.
[85] Y. F. Liang, F. Ye, J. P. Lin, Y. L. Wang, and G. L. Chen, "Effect of annealing temperature on magnetic properties of cold rolled high silicon steel thin sheet," *Journal of Alloys and Compounds*, vol. 491, pp. 268–270, 2010.

[86] A. Sakakura, H. Takashima, and S. Taguchi, "Process for producing single-oriented silicon steel sheets having a high magnetic induction," 1966.
[87] M. Moghimi, M.-H. Saraee, and A. Bagheri, "Modeling of batch annealing process using data mining techniques for cold rolled steel sheets," in *Mechatronics (ICM), 2011 IEEE International Conference on Mechatronics*, 2011, pp. 277-281.
[88] Y. Zuo, W.-f. Wu, X.-x. Zhang, L. Lin, S.-h. Xiang, T.-s. Liu, *et al.*, "A Study of Heat Transfer in High-Performance Hydrogen Bell-Type Annealing Furnaces," *Heat Transfer—Asian Research*, vol. 30, pp. 615 - 623, 2001.
[89] C. H. Gur and J. Pan, *Handbook of Thermal Process Modeling Steels*: Taylor and Francis Group, 2009.
[90] D. A. Stirling, "Distributed Control of Batch Annealing Using Coil Interior Temperature Prediction," presented at the Third Conference on Control Engineering 1986: Towards a More Competitive Industry - Preprints of Papers., Sydney, Aust, 1986.
[91] T.-C. Chen, C.-H. Ho, J.-C. L. b, and L.-W. W. b, "3-D temperature and stress distributions of strip in preheating furnace of continuous annealing line," *Applied Thermal Engineering*, vol. 30, pp. 1047–1057, 2010.
[92] S. K. Sarna. (2013). *Annealing of cold rolled steel*. Available: http://ispatguru.com/annealing-of-cold-rolled-steel/#comment-733870
[93] S. Moon and A. N. Hrymak, "Scheduling of the batch annealing process—deterministic case," *Computers & Chemical Engineering*, vol. 23, pp. 1193-1208, 1999.
[94] G. Chen and M. Gu, "Simulation of steel coil heat transfer in a high performance hydrogen furnace " *Heat Transfer Engineering*, vol. 28, pp. 25-30, 2007.
[95] A. Saboonchi, S. Hassanpour, and F. Bayati, "Design of heating cycle in hydrogen annealing furnaces," *Materials and Manufacturing Processes*, vol. 24, pp. 1453-1458, 2009.
[96] A. Saboonchi and S. Hassanpour, "Prediction of H_2 Content and Inert Gas Circulation Rate Effects on Batch Annealing Process," *Materials and Manufacturing Processes*, vol. 23, pp. 277-283, 2008.
[97] U. S. A. Eurotherm. (2018). *Single and Multi-stack Batch Annealing*. Available: https://www.eurotherm.com/single-and-multi-stack-batch-annealing
[98] N. Morito, "Method of sealing an inner cover arranged in a box annealing furnace used for producing grain-oriented silicon steel sheets " US4311538 A, 1982.
[99] A. G. Dukhnov, A. M. Chernykh, V. P. Baryatinskij, and S. I. Plotnikov, "Structure formation in anisotropic electrical steel on annealing in different atmospheres," *Steel in Translation*, vol. 23, pp. 47-48, 1993.
[100] B. Hammer, C. Riediger, M. Hastenrath, and F. Bölling, "Interactions between the inhibitor phases, secondary grain growth and glass-film formation in HGO electrical steel," *Journal of Magnetism and Magnetic Materials*, vol. 112, pp. 162-164, 1992.
[101] T. Takamiya, M. Kurosawa, and M. Komatsubara, "Effect of hydrogen content in the final annealing atmosphere on secondary recrystallization of grain-oriented Si steel," *Journal of Magnetism and Magnetic Materials*, vol. 254–255, pp. 334–336, 2003.
[102] A. Buckley, A. J. Moses, and L. Trollop, "Study and redesign of high temperature batch annealing furnace for production of grain oriented electrical steel," *Ironmaking & Steelmaking*, vol. 26, pp. 477-482, 1999.
[103] T. Tang and D. B. Ingham, "On steady flow past a rotating circular cylinder at Reynolds numbers 60 and 100 " *Computers and Fluids*, vol. 19, pp. 217-230, 1991.
[104] S. B. Paramane and A. Sharma, "Numerical investigation of heat and fluid flow across a rotating circular cylinder maintained at constant temperature in 2-D laminar flow regime," *International Journal of Heat and Mass Transfer*, vol. 52, pp. 3205-3216, 2009.
[105] S. S. Ristić, J. T. Ilic, D. S. Cantrak, O. R. Ristić, and N. Z. Jankovic, "Estimation of Laser-Doppler Anemometry measuring volume displacement in cylindrical pipe flow " *Thermal Science* vol. 16, pp. 1027-1042, 2012.

[106] F. Durst, A. Melling, and J. H. Whitelaw, *Principles and practice of laser-doppler anemometry*, 2nd ed. London: Academic Press, 1981.
[107] A. Molki, L. Khezzar, and A. Goharzadeh, "Measurement of fluid velocity development in laminar pipe flow using laser Doppler velocimetry," *European Journal of Physics*, vol. 34, pp. 1127–1134, 2013.
[108] E. R. Center. (2015). *Laser Doppler Velocimetry*. Available: https://www.erc.wisc.edu/ldv.php
[109] *Phase Doppler Particle Analyzer (PDPA)/Laser Doppler Velocimeter (LDV) Operations Manual* vol. Revision D. TSI Incorporated / 500 Cardigan Road / Shoreview, MN 55126 / USA: TSI Incorporated, 2005.
[110] P. J. Roache, *Computational fluid dynamics*, 1st ed.: Albuquerque, N.M. : Hermosa Publishers 1972.
[111] H. K. Versteeg and W. Malalasekera, *An introduction to computational fluid dynamics: The finite volume method* 2nd ed.: Pearson Education Limited 2007.
[112] J. H. Ferziger and M. Peric, *Computational methods for fluid dynamics*, 3rd ed.: Springer, 2002.
[113] P. Schlatter, "Spectral methods," *Lecture Notes KTH*, 2009.
[114] S. V. Patankar, *Numerical heat transfer and fluid flow* 1st ed. United State of America: Hemisphere Publishing Corporation 1980.
[115] G. Touzot, G. Dhatt, and E. Lefrançois, *Finite element method*, 1st ed.: John Wiley & Sons, Inc., 2012.
[116] J. D. A. Jr, J. Degroot, G. Degrez, E. Dick, R. Grundmann, and J. Vierendeels, "Governing equations of fluid dynamics " in *Computational fluid dynamics: An introduction* J. F. Wendt, Ed., 3rd ed: Springer 2009.
[117] W. M. Rohsenow, J. P. Hartnett, and Y. I. Cho., *Handbook of heat transfer* 3rd ed. United States of America: The McGraw-Hill Companies, Inc., 1998.
[118] M. H. Aissa, T. Verstraete, and K. Vuik, "Use of modern GPUs in Design Optimisation," presented at the Proceedings of the 10th ASMO UK Conference Engineering Design Optimization, UK, 2014.
[119] ENVENIO. (2016). *Advantages of Structured Grids Over Unstructured Grids*. Available: http://blog.envenio.com/advantages-of-structured-grids-over-unstructured-grids
[120] *ANSYS Fluent Theory Guide*: ANSYS, Inc, 2013.
[121] FLUENT. (2003). *Overview of Numerical Schemes*. Available: http://jullio.pe.kr/fluent6.1/help/html/ug/node810.htm
[122] ANSYS. (2009, 2018). *Solver theory-Overview of flow solver* Available: http://www.afs.enea.it/project/neptunius/docs/fluent/html/th/node359.htm
[123] D. C. Wilcox, *Turbulence modelling for CFD*. California DCW Industries, Inc. , 1993.
[124] *Turbulence modeling*. Available: https://www.cfd-online.com/Wiki/Turbulence_modeling
[125] P. Chou, "On velocity correlations and the solutions of the equations of turbulent fluctuation," *Quarterly of Applied Mathematics*, vol. 3, pp. 38-54, 1945.
[126] D. Phylipsen, K. Blok, E. Worrell, and J. d. Beer, "Benchmarking the energy efficiency of Dutch industry: an assessment of the expected effect on energy consumption and CO_2 emissions," *Energy Policy*, vol. 30, pp. 663–679, 2002.
[127] E. Giacone and S. Mancò, "Energy efficiency measurement in industrial processes," *Energy*, vol. 38, 2012.
[128] P. Mullinger and B. Jenkins, *Industrial and process furnaces: principles, design and operation*, 1st ed. Oxford, UK: Elsevier, 2008.
[129] (2018). *Statistics Dictionary*. Available: http://stattrek.com/statistics/dictionary.aspx?definition=coefficient_of_determination
[130] W. Trinks, M. H. Mawhinney, R. A. Shannon, R. J. Reed, and J. R. Garvey, "Saving Energy in Industrial Furnace Systems," in *Industrial Furnaces*, 6th ed: John Wiley & Sons, Inc., 2004.

[131] A. Buckley, "Simulation and redesign of high temperature batch annealing furnaces," PhD, UWC, 1999.
[132] "Project mandate energy efficiency," Orb Woks internal reports2013.
[133] "Orb Electrical Steels, private comunication," N. Beynon, Ed., ed, 2017.
[134] S. B. Paramane and A. Sharma, "Heat and fluid flow across a rotating cylinder dissipating uniform heat flux in 2D laminar flow regime," *International Journal of Heat and Mass Transfer*, vol. 53, pp. 4672-4683, 2010.
[135] T. R. Camp and H.-W. Shin, "Turbulence Intensity and Length Scale Measurements in Multistage Compressors," *Transactions of the ASME*, vol. 117, pp. 38-46, 1995.
[136] M. Ozgoren, E. Pinar, B. Sahin, and H. Akilli, "Comparison of flow structures in the downstream region of a cylinder and sphere," *International Journal of Heat and Fluid Flow*, vol. 32, pp. 1138-1146, 2011.
[137] H. M. Badr, S. C. R. Dennis, and P. J. S. Young, "Steady and unsteady flow past a rotating circular cylinder at low Reynolds numbers," *Computers & Fluids*, vol. 17, pp. 579-609, 1989.
[138] G. F. Smaism, O. M. H. Fatla, A. Valera-Medina, A. M. Rageb, and N. Syred, "Investigation of heat transfer and fluid mechanics across a heated rotating circular cylinder in crossflow," *54th AIAA Aerospace Science Meeting*, 2016.
[139] M. Sinhuber, E. Bodenschatz, and G. P. Bewley, "Decay of Turbulence at High Reynolds Numbers," *Physical Review Letters*, vol. 114, pp. 1-5, 23 January 2015.
[140] (2018). *Chapter 3: Dispersion and mixing*. Available: https://thayer.dartmouth.edu/~d30345d/courses/engs43/Chapter3.pdf
[141] (2010). *Turbulence intensity measurements applicable instrument models: 9555, 9565, 7565, 7575, TA460, TA465, EBT730, PH730, 8715*. Available: https://assets.tequipment.net/assets/1/26/TSI-141.pdf
[142] P. A. Craig and L. Connolly, "Continuous Fiber Ceramic Composites CFCC Program for DMO Materials," Unites States2002.
[143] C. Luzzatto, A. Morgana, S. Chaudourne, T. O'Doherty, and G. Sorbie, "A new concept composit heat exchanger to be applied in high-temperature industrial processes " *Applied Thermal Engineering*, vol. 17, pp. 789-797, 1997.
[144] J. William D. Callistert, *Material Science and Engineering-An Introduction* 7th ed. United State of America John Wiley & Sones, Inc., 2007.
[145] (2019). *Gas & Electricity Tariff Prices per kWh*. Available: https://www.ukpower.co.uk/home_energy/tariffs-per-unit-kwh